

Gyration Spun Polymeric Fibres for Antibacterial Applications

A dissertation submitted in partial fulfilment of the requirements for
transfer to the degree of
Doctor of Philosophy

September 2017

Zewen Xu

Department of Mechanical Engineering
University College London
Torrington Place, London WC1E 7JE
UK

Declaration

I, Zewen Xu, confirm that the work presented in this thesis is my own. Where information has been derived from other sources, I confirm that this has been indicated in the thesis.

Your Sincerely,

Zewen Xu

Abstract

Hybrid polymeric fibres and fibrous structures have widely been used to construct porous polymer scaffolds with excellent functionality, and are of great interest in biomedical applications. In this thesis, in contrast to electrospinning, a novel approach, gyration spinning with or without pressure is reported to achieve a high production rate for hybrid nanoparticle embedded polymer fibres in the micro to nanometre scale range using either polymer solutions or melts. Polyurethane (PU), nylon, and poly(ethylene oxide) (PEO) were used as the polymers not only because of their excellent biocompatibility, but also depends on good oxidative biostability, processability of PU, good mechanical strength, spinnability and stability for nylon, and non-toxicity of PEO. In the meantime, silver nanoparticles, copper oxide nanoparticles and zinc oxide nanoparticles were used to increase the antibacterial performance to produce hybrid nanofibres using pressurised solution gyration. A pressurised melt gyration process was used for the first time to generate poly(ϵ -caprolactone) (PCL) fibres and silver coated PCL fibres in the micrometre range ($< 50 \mu\text{m}$) due to the low melting point (60°C) of PCL pellets. The formation of fibres depends on the centrifugal force, pressure blowing and evaporation. Fibre diameter is significantly reduced with a decrease in the weight percentage of the polymer in solution, and an increase in the melting temperature, rotational speed and working pressure.

Field emission scanning electron microscopy (FE-SEM) was used to study the characteristics and morphology of the fabricated polymer fibres. Incorporation of Ag nanoparticles into the polymer fibres was confirmed using a combination of advanced microscopical techniques and Raman spectrometry to study the bonding characteristics of the polymer and Ag nanoparticles. Inductively coupled plasma mass spectroscopy

(ICP-MS) showed that the substantial concentration of Ag ions in the nylon fibre matrix was producing effective antibacterial properties. Ag nanoparticles and CuO nanoparticles were successfully incorporated into polymer fibres and proved to be of higher antibacterial efficacy than virgin polymer fibres, against the Gram-negative bacteria *Escherichia coli* and *Pseudomonas aeruginosa*.

Publications

Journal Papers

1. Zewen Xu, Suntharavathanan Mahalingam, Jennifer L. Rohn, Guogang Ren, Mohan Edirisinghe. *Physio-Chemical and Antibacterial Characteristics of Ag Nanoparticles Bonded Nylon Nanofibres Prepared by Pressurised Gyration*. Materials Sciences and Engineering: C Vol. 56 (2015), p.195.
2. Suntharavathanan Mahalingam, Zewen Xu, Mohan Edirisinghe. *Antibacterial Activity and Biosensing of PVA-Lysozyme Microbubbles Formed by Pressurized Gyration*. Langmuir Vol, 31 (2015), p. 9771.
3. Zewen Xu, Suntharavathanan Mahalingam, Pooja Basnett, Bahijja Raimi-Abraham, Ipsita Roy, Duncan Craig, Mohan Edirisinghe. *Making Nonwoven Fibrous Poly(ϵ -caprolactone) Constructs for Antimicrobial and Tissue Engineering Applications by Pressurized Melt Gyration*. Macromolecular Materials and Engineering Vol. 301 (2016), p. 922.
4. Zewen Xu, Suntharavathanan Mahalingam, Guogang Ren, Mohan Edirisinghe. *Antimicrobial activity of copper oxide and silver loaded PEO-Chitosan blended gyrospon fibres (in preparation)*.

Conference Presentations

1. Zewen Xu. Oral presentation and poster. Novel preparation and antibacterial use of hybrid nylon nanofibres. Mechanical Engineering PhD Students' Conference, UCL, London, UK, 18th July 2014.

2. Zewen Xu. Oral presentation and poster. Melt gyration and Antibacterial use of Hybrid PCL fibres. Mechanical Engineering PhD Students' Conference, UCL, London, UK, 25th June 2015.
3. Zewen Xu. Poster presentation. Pressurised Gyration and Antibacterial use of Hybrid Micro/Nanofibres. 7th APS International PharmSci Conference, Technology and Innovation Centre, Glasgow, UK, 5-7th September 2015.
4. Zewen Xu. Oral presentation. Gyration Spun Hybrid Fibres for Anti-microbial Applications. 5th International Conference on Material Science and Engineering Technology. Tokyo, Japan, 29-31st, October 2016.
5. Zewen Xu. Poster presentation. Pressurised Gyration and Antibacterial use of Hybrid Micro/Nanofibres. 2nd International PharmTech Conference 2017. London, UK, 14th July 2017.

Acknowledgements

I would like to thank my supervisor Professor Mohan Edirisinghe. His inspiring guidance and timely encouragement have helped me to gain confidence and to develop as a good researcher. This work has also been continuously supported and insightfully guided by my second supervisor Dr. Suntharavathanan Mahalingam, who invented the pressurised gyration process. I am lucky to have this precious opportunity to study with these two excellent supervisors.

Thanks are due to Kevin Reeves and Tom Gregory from the Archaeology Department in UCL and Steve Firth from the Department of Chemistry in UCL, for their training and assistance in SEM and Raman spectroscopy. I gratefully thank Dr. Jennifer L. Rohn and Harry Horsley for their supervision and assistance with antibacterial testing in the School of Life & Medical Sciences at UCL. The advice of Dr. Guogang Ren (School of Engineering and Technology, University of Hertfordshire) was greatly appreciated during the initial stages of my work.

I would also like to thank my research colleagues for their help and suggestions throughout my research; it has been a great pleasure to work and live with the whole lab.

Last but not least, I am grateful to my parents who taught me to be strong, supported my studies throughout, and showed unconditional love for me. I truly appreciate that I have them in my life.

Dedication

To

My parents

And my teachers

Table of Contents

Declaration	1
Abstract	2
Publications	4
Acknowledgements	6
Dedication	7
List of Tables	13
List of Figures	14
List of Abbreviations	20
Chapter 1 - Introduction and Background	21
1.1 Background	21
1.2 Aims and Objectives	26
1.3 Thesis Structure.....	29
Chapter 2 - Literature Review	31
2.1 Introduction	31
2.2 Fibres and Fibrous Structure	31
2.2.1 Nanofibres	32
2.2.2 Applications of Nanofibres	32
2.2.2.1 <i>Tissue Engineering</i>	34
2.2.2.2 <i>Drug Delivery</i>	34
2.3 Fibre Production Methods.....	35
2.3.1 Electrospinning	35
2.3.1.1 <i>Electrohydrodynamic Process</i>	35
2.3.1.2 <i>Process Parameters which Effect Electrospinning</i>	38

2.3.2 Solution Spinning.....	40
2.3.2.1 <i>Wet Spinning</i>	41
2.3.2.2 <i>Dry Spinning</i>	41
2.3.2.3 <i>Flash Spinning</i>	41
2.3.2.4 <i>Gel Spinning and Liquid Crystal Spinning</i>	42
2.3.3 Emulsion Spinning.....	43
2.3.4 Rotary Jet Spinning.....	43
2.3.5 Melt Spinning.....	46
2.3.6 Blowing.....	48
2.3.7 Self-Assembly.....	51
2.4 Pressurised Gyration	53
2.5 Characteristics of silver nanoparticles	55
2.5.1 Silver ion release	55
2.5.2 Antibacterial ability.....	57
2.6 Summary	58
Chapter 3 - Experimental Details	59
3.1 Materials for Polymer Fibre Fabrication.....	59
3.1.1 Polymer	59
3.1.1.1 <i>Polyurethane</i>	59
3.1.1.2 <i>Nylon</i>	60
3.1.1.3 <i>Poly(ϵ-caprolactone)</i>	61
3.1.1.4 <i>Chitossan</i>	62
3.1.1.5 <i>Poly(ethylene oxide)</i>	64
3.1.2 Metal Nanoparticles	65
3.1.2.1 <i>Silver Nanoparticles</i>	65

3.1.2.2 Copper Oxide Nanoparticles	66
3.1.3 Solvents for Metal Nanoparticles.....	67
3.2 Preparation of Solutions.....	68
3.2.1 Polyurethane Solutions	68
3.2.2 Nylon Solutions.....	68
3.2.3 Poly(ϵ -caprolactone)	69
3.2.4 Poly(ethylene oxide) Solutions	69
3.2.5 Chitosan-Poly(ethylene oxide) Blend Solutions	69
3.3 Gyration Set up and Materials for Polymer Fibre Fabrication.....	70
3.3.1 Pressurised Gyration	70
3.3.2 Pressurised Melt Gyration.....	71
3.4 Preparation of Solutions for the Fabrication of Hybrid Fibres	72
3.4.1 Polyurethane, Copper Oxide and Zinc Oxide Loaded Polyurethane Nanofibres	72
3.4.2 Nylon Solutions and Silver Loaded Nylon Nanofibres	73
3.4.3 Poly(ϵ -caprolactone) and Silver Coated Poly(ϵ -caprolactone) Fibres	73
3.4.4 Poly(ethylene oxide), Silver and Copper Oxide Embedded Poly(ethylene oxide) Nanofibres.....	74
3.4.5 Chitosan-Poly(ethylene oxide) Blend, Silver and Copper Oxide Embedded Chitosan-Poly(ethylene oxide) Blend Nanofibres	75
3.5 Characterisation of Polymer Solutions.....	75
3.5.1 Physical Properties	75
3.5.2 Scanning Electronic Microscopy	76
3.5.3 Raman Spectra	77
3.5.4 Inductively Coupled Plasma Mass Spectroscopy (ICP-MS)	77

3.5.5 Differential Scanning Calorimetry	78
3.5.6 UV/vis Spectroscopy.....	79
3.5.7 Antibacterial Testing.....	79
Chapter 4 - Fabrication of Polyurethane and Nylon Nanofibres Using Pressurised Gyration	81
4.1 Introduction	81
4.2 Analysis of the Polyurethane System.....	82
4.3 Physical properties of nylon solutions	85
4.4 Fibre diameter analysis	86
4.5 Raman spectra	94
4.6 Silver ion release	96
4.7 Antibacterial activity	99
4.8 Summary	106
Chapter 5 - Making Poly(ϵ-caprolactone) fibres by Pressurised Melt Gyration	108
5.1 Introduction	108
5.2 Physical Properties of Poly(ϵ -caprolactone) pellets.....	108
5.3 Fibre diameter analysis	109
5.4 Raman spectra	115
5.5 Differential scanning calorimetry	118
5.6 UV/vis spectroscopy	120
5.7 Antibacterial studies.....	123
5.8 Summary	125
Chapter 6 - Making Pure poly(ethylene oxide) Chitosan-Poly(ethylene oxide) Nanofibres by Pressurised Gyration	126
6.1 Introduction	126

6.2 Formation of Poly(ethylene oxide) Nanofibres.....	127
6.2.1 Physical Properties of Poly(ethylene oxide) Solutions	127
6.2.2 Fibre Diameter Analysis	128
6.2.3 Fibre Diameter Analysis	131
6.3 Formation of Chitosan-Poly(ethylene oxide) Blend Nanofibres	134
6.3.1 Physical Properties of Chitosan-Poly(ethylene oxide) Blend Solutions...	134
6.3.2 Fibre diameter analysis	135
6.4 Antibacterial Activity.....	141
6.4.1 Antibacterial activity of gram-negative <i>E.coli</i> cells.....	142
6.4.2 Antibacterial activity of gram-negative <i>P. aeruginosa</i> cells.....	145
6.4.3 Time-Dependent Antibacterial Activity Against <i>E. coli</i>	152
6.4.4 Time-Dependent Antibacterial Activity Against <i>P. aeruginosa</i>	155
6.5 Discussion	158
6.6 Summary	161
Chapter 7 - Conclusions and Future Work	162
7.1 Conclusions	162
7.1.1 Material Selection	163
7.1.2 Influence of Process Parameters	163
7.1.3 Antibacterial Activities	164
7.2 Future Work	165
References	169

List of Tables

Table 4.1: Measured values of surface tension and viscosity for nylon solutions.....	85
Table 4.2: Fibre diameter variation for different conditions of pressurised gyration ...	89
Table 5.1: Thermal properties of scaffolds prepared by PMG. ΔH_m , ΔH_c , T_m , T_c and X represent melting enthalpy, crystallization enthalpy, melting temperature, crystallization temperature and crystallinity, respectively.....	109
Table 5.2: PCL fibre diameter variations at various melt temperatures, rotating speeds and working pressures (a) 24000, 36000 rpm (b) 0.01, 0.02 MPa.....	111
Table 5.3: Release quantity of Ag^+ ions from various PCL-Ag mats.....	122
Table 6.1: Measured values of surface tension and viscosity for PEO solutions and nanoparticle loaded PEO solutions	127
Table 6.2: Fibre diameter variation for different conditions of pressurised gyration.	129
Table 6.3: Measured values of surface tension and viscosity	134
Table 6.4: Fibre diameter variation for different conditions of pressurised gyration .	140
Table 6.5: Antibacterial rates	150

List of Figures

Figure 1.1: The pressurised gyration process.....	23
Figure 1.2: The pressurised melt gyration process.....	24
Figure 2.1: The diverse areas of applications identified for polymer nanofibres	33
Figure 2.2: Typical laboratory scale electrospinning set-up	37
Figure 2.3: Rotary jet-spinning set-up	44
Figure 2.4: Fibre formation mechanisms in the rotary jey-spinning system.....	45
Figure 2.5: Solution blowing set-up.....	49
Figure 2.6: Jet blowing process.....	50
Figure 2.7: Template approach to well-dispersed polymer/nanofibre composites	52
Figure 3.1: Chemical structure of polyurethane.....	60
Figure 3.2: Chemical structure of nylon	60
Figure 3.3: Chemical structure of poly(ϵ -caprolactone)	61
Figure 3.4: Chemical structure of chitosan	64
Figure 3.5: Chemical structure of poly(ethylene oxide)	64
Figure 3.6: Copper oxide particles observed by transmission electron microscopy	67
Figure 3.7: Chemical structure of formic acid and acetic acid.	68
Figure 3.8: Experimental set-up of the pressurised gyration process	71
Figure 3.9: Experimental set-up of the melt-pressurised gyration process.....	72
Figure 4.1: Analysis of polyurethane fibres fabricated by pressurised gyration.....	83

Figure 4.2: EDX analyses for PU and zinc oxide fibres	84
Figure 4.3: Fibre diameter variation for 5 wt.%, 10 wt.%, 15 wt.% and 20 wt.% of nylon and nylon with Ag nanoparticle incorporation (a), (b) varying rotating speed at a constant working pressure of 0.1MPa. (c), (d) varying working pressure at a fixed rotating speed of 36000 rpm.	87
Figure 4.4: (a)-(h) SEM images of nanofibres generated with 20 wt.%, 15 wt.%, 10 wt.% and 5 wt.% nylon solutions under different working pressure and maximum rotating speed (36000 rpm) and corresponding fibre diameter distributions.....	92
Figure 4.5: (a) FE-SEM (FIB-SEM inset) micrograph showing that the Ag nanoparticles (see arrows) were distributed on nanofibers made using the 20 wt.% nylon – 1 wt.% Ag suspension, and (b) the corresponding EDX analysis.....	93
Figure 4.6: Raman spectra for nanofibres (a) nylon (b) lower concentration (1 wt.%) of Ag-loaded nylon (c) higher concentration (4 wt.%) of Ag-loaded nylon.....	95
Figure 4.7: Silver ion concentration in various nylon nanofibre mats after 24, 48 and 72 hr of washing. Sample numbers are shown in brackets.	96
Figure 4.8: Bacterial colonies (a), (b) <i>E. coli</i> co-cultured with 20 wt.% nylon nanofibre for 2 hr and for 24 hr; (c), (d) <i>E. coli</i> co-cultured with Ag-loaded 20 wt.% nylon nanofibre for 2 hr and for 24 hr; (e), (f) <i>E. coli</i> control group for 2 hr and for 24 hr; (g), (h) <i>P. aeruginosa</i> co-cultured with 20 wt.% nylon nanofibre for 2 hr and for 24 hr; (i), (j) <i>P. aeruginosa</i> co-cultured with Ag-loaded 20 wt.% nylon nanofibre for 2 hr and for 24 hr; (k), (l) <i>P. aeruginosa</i> control group for 2 hr and for 24 hr. ..	101
Figure 4.9: Antibacterial rates of (a) <i>E. coli</i> at two time points; (b) <i>P. aeruginosa</i> at two time points; (c) Graph of antibacterial rate versus co-cultured time for nylon nanofibres and Ag-loaded nylon nanofibres on <i>E. coli</i> and <i>P. aeruginosa</i>	103

Figure 4.10: Optical micrographs showing <i>E. coli</i> bacterial cells cultured in media (a) Glass slide control; (b) Nylon nanofibres after 2 hr; (c) Nylon nanofibres after 24 hr; (d) Ag-loaded Nylon nanofibres after 2 hr.	104
Figure 5.1: Fibre diameter variation of PCL fibres processed at various temperatures under different rotating speeds and working pressure (a) 24000 rpm (b) 36000 rpm (c) 0.01 MPa (d) 0.02 MPa.....	111
Figure 5.2: Scanning electron micrographs of PCL fibres obtained at various temperatures at 36000 rpm (a) 95°C (b) 105°C, 0.01 MPa working pressure (c) 125°C (d) 155°C (e) 200°C, 0.01 MPa working pressure. Scale bars in the in-set images are 20 µm.	114
Figure 5.3: (a) Raman spectra of PCL fibres made at various temperatures at 36000 rpm and 0.01 MPa working pressure and raw PCL pellets. (b) Microanalysis of Raman band of (a) in the range 1700-1760 cm ⁻¹ . (c) Raman spectra of Ag-coated PCL fibres and raw PCL pellets. (d) Microanalysis of Raman band of (c) in the range 1700-1760 cm ⁻¹	117
Figure 5.4: MTDSC results (heat-cool-heat cycle) of (a) PCL pellets, fibres spun at different temperatures (b) 95°C (c) 125°C (d) 155°C (e) 200°C.	119
Figure 5.5: (a) Silver ion (Ag ⁺) release from scaffolds in de-ionised water at the ambient temperature (23°C) for various PCL fibrous scaffolds (b) Log (Ag ion concentration) vs Log (time) graphs.	122
Figure 5.6: Antibacterial rates against (a) <i>E. coli</i> after 2 hours (b) <i>P. aeruginosa</i> after 2 hours for different types of fibre mats prepared in this work.	124

Figure 6.1: Fibre diameter under varying concentrations and working pressures at a fixed rotating speed of 36000 rpm (a) Pure PEO solutions; (b) Ag nanoparticle loaded PEO solutions; (c) CuO nanoparticle loaded PEO solutions.	131
Figure 6.2: SEM images of PEO and Ag and CuO loaded PEO fibres (a) 15 wt.% PEO (b) 10 wt.% PEO (c) 5 wt.% Ag loaded 15 wt.% PEO (d) 2 wt.% Ag loaded 15 wt.% PEO (e) 2 wt.% Ag loaded 10 wt.% PEO (f) 5 wt.% CuO loaded 15 wt.% PEO (g) 2 wt.% CuO loaded 15 wt.% PEO.	133
Figure 6.3: SEM images of the 20wt.% PEO/chitosan fibres obtained at 36000 rpm and 0.2 MPa working pressure (a) 1wt.% chitosan; (b) 2wt.% chitosan.	136
Figure 6.4: (a) SEM micrograph showing that the CuO nanoparticles were distributed on nanofibers made using the 20 wt.% PEO with 1 wt.% Chitosan – 1 wt.% CuO nanoparticle, and (b) the corresponding EDX analysis.....	137
Figure 6.5: (a) SEM micrograph showing that the Ag nanoparticles were distributed on nanofibers made using the 20 wt.% PEO with 1 wt.% Chitosan – 1 wt.% Ag nanoparticle, and (b) the corresponding EDX analysis.....	138
Figure 6.6: Fiber diameter for 20 wt.% PEO with Chitosan under varying working pressure at a fixed rotating speed of 36000 rpm (a) 1 wt.% and 2 wt.% of Chitosan. (b) 0.5 wt.% CuO nanoparticles and 0.5 wt.% Ag nanoparticles.....	140
Figure 6.7: Antibacterial rate for 20wt.%PEO/1wt.%chitosan, 20wt.%PEO/2wt.%chitosan, 20wt.%PEO/1wt.%chitosan/0.5wt.%CuO, 20wt.%PEO/1wt.%chitosan/1wt.%CuO, 20wt.%PEO/1wt.%chitosan/0.5wt.%Ag and 20wt.%PEO/1wt.%chitosan/1wt.%Ag nanofibre mats after 30, 60, 120 and 180 minutes incubation with <i>E-coli</i> suspension ($\sim 0.5 \times 10^6$ CFU/ml).	144

Figure 6.8: Antibacterial rate for 20wt.%PEO/1wt.%chitosan, 20wt.%PEO/2wt.%chitosan, 20wt.%PEO/1wt.%chitosan/0.5wt.%CuO, 20wt.%PEO/1wt.%chitosan/1wt.%CuO, 20wt.%PEO/1wt.%chitosan/0.5wt.%Ag and 20wt.%PEO/1wt.%chitosan/1wt.%Ag nanofibre mats after 30, 60, 120 and 180 minutes incubating with *P. aeruginosa* suspension ($\sim 0.5 \times 10^6$ CFU/ml)..... 146

Figure 6.9: Antibacterial rate for 20wt.%PEO/1wt.%chitosan, 20wt.%PEO/2wt.%chitosan, 20wt.%PEO/1wt.%chitosan/0.5wt.%Ag, 20wt.%PEO/1wt.%chitosan/1wt.%Ag, 20wt.%PEO/1wt.%chitosan/0.5wt.%CuO, and 20wt.%PEO/1wt.%chitosan/1wt.%CuO, nanofibre mats after 30, 60, and 120 minutes incubation with (a) *E. coli* ($\sim 1 \times 10^6$ CFU/ml); (b) *P. aeruginosa* ($\sim 1 \times 10^6$ CFU/ml). 149

Figure 6.10: Time dependent antibacterial activity against *E.coli* (a) Time-dependent antibacterial activity of PEO/chitosan, PEO/chitosan/CuO and PEO/chitosan/Ag nanofibre mats after incubating with *E-coli* suspension. (b) Time-dependent antibacterial activity for 20wt.%PEO/1wt.%chitosan and 20wt.%PEO/1wt.%chitosan /1wt.%CuO suspension incubated after 30, 60, 120 and 180 minutes. (c) Time-dependent *E. Coli* cell inactivation rates for 20wt.%PEO/1wt.%chitosan and 20wt.%PEO/1wt.%chitosan /1wt.%CuO suspensions extracted from Figure 6.10 (b) with unit of d(%) /d(min). (d) Time-dependent antibacterial activity for 20wt.%PEO/1wt.%chitosan and 20wt.%PEO/1wt.%chitosan /1wt.%Ag suspension incubated after 30, 60, 120 and 180 minutes. (e) Time-dependent *E. Coli* cell inactivation rates for 20wt.%PEO/1wt.%chitosan and 20wt.%PEO/1wt.%chitosan /1wt.%Ag suspensions extracted from Figure 6.10 (d) with unit of d(%) /d(min). 154

Figure 6.11: Time dependent antibacterial activity against *P. aeruginosa* (a) Time-dependent antibacterial activity of PEO/chitosan, PEO/chitosan/CuO and PEO/chitosan/Ag nanofibre mats after incubating with *P. aeruginosa* suspension. (b) Time-dependent antibacterial activity for 20wt.%PEO/1wt.%chitosan and 20wt.%PEO/1wt.%chitosan /1wt.%CuO suspension incubated after 30, 60, 120 and 180 minutes. (c) Time-dependent *P. aeruginosa* cell inactivation rates for 20wt.%PEO/1wt.%chitosan and 20wt.%PEO/1wt.%chitosan/1wt.%CuO suspensions extracted from Figure 6.11 (b) with unit of d(%) /d(min). (d) Time-dependent antibacterial activity for 20wt.%PEO/1wt.%chitosan and 20wt.%PEO/1wt.%chitosan /1wt.%Ag suspension incubated after 30, 60, 120 and 180 minutes. (e) Time-dependent *P. aeruginosa* cell inactivation rates for 20wt.%PEO/1wt.%chitosan and 20wt.%PEO/1wt.%chitosan/1wt.%Ag suspensions extracted from Figure 6.11 (d) with unit of d(%) /d(min). 156

List of Abbreviations

CFU	Colony-Forming Units
DCM	Dichloromethane
DMF	Dimethyl Formamide
DSC	Differential Scanning Calorimetry
EDX	Energy Dispersive X-Ray Spectroscopy
EHD	Electrohydrodynamic
FE-SEM	Field Emission Scanning Electron Microscopy
ICP-MS	Inductively Coupled Plasma Mass Spectroscopy
LB	Luria-Bertani
PCL	Poly(E-Caprolactone)
PEO	Poly(Ethylene Oxide)
PTFE	Polytetrafluoroethylene
PU	Polyurethane
PVA	Polyvinyl Alcohol
PVC	Polyvinyl Chloride
PVP	polyvinylpyrrolidone
RJS	Rotary Jet-Spinning
TCM	Trichloromethane
TEM	Transmission Electron Microscopy
TFA	Trifluoroacetic Acid
TFEA	Trifluoroethanol
TSB	Tryptic Soy Broth

Chapter 1 - Introduction and Background

1.1 Background

Hybrid fibres are an interesting class of materials which are currently receiving significant attention in many areas compared to bulk materials due to their unique chemical, electrical, optical and mechanical properties, which can be achieved by combining the advantages of nanoparticles and polymer fibres (Bayle-Guillemaud, Jouneau & Chandezon et al., 2013; Bosworth L., Turner & Cartmell 2013; Erisken C., Bellan & Craighead, 2006; Li M. et al., 2007; Kalyon & Wang, 2008; Liu H., Edel, Lopez-Haro M., Jiu, Qiao L. et al., 2013). These properties enable these materials to be used in a wide range of applications, including biomedical, energy storage, catalysis and sensors. The properties of hybrid fibres not only depend on their high surface area to volume ratio but also the content, size and spatial distribution of the nanoparticles (Amna T. et al., 2013; Montazer M. & Malekzadeh, 2012; Vitichuli N. et al., 2011).

The development of hybrid fibres is of tremendous interest for the biomedical research community because scaffolds prepared from these materials resemble natural extracellular matrices with very good mechanical strength, biocompatibility and biodegradability with respect to various human cells and tissues (Catauro M., Bollino, Papale, Marciano & Pacifico., 2015; Yazdimamaghani M. et al., 2014). Fibrous structures as an antimicrobial scaffold have been found to result in greater cell adhesion

than other structures (Amna T. et al., 2013). In addition, they have been used in wound dressings and in healing, where these scaffolds enable better homogeneity and oxygen penetration, whilst preventing infections and dehydration (Ranjbar-Mohammaddi M., Bahrami & Joghataei, 2013).

Of the various techniques used to process hybrid fibres, electrospinning is a well-known and a versatile method in which fibres are extruded from a nozzle carrying a polymer solution via high voltage (Feng B. Tu, Yuan, Peng & Zhang, 2012; Patel P., Eckart, Advincula, Goldberg & Mather, 2009). A hybrid method consisting of electrospinning and electrospraying is an alternative attractive technique whereby simultaneous spinning and spraying is used to process composite fibres (Vitchuli N. et al., 2011). Despite its simplicity and flexibility, electrospinning has major challenges, such as the mass production capability associated with a single needle set-up and the high voltage required, which may be detrimental to some materials (Luo C., Stoyanov, Stride, Pelan & Edirisinghe, 2012). Considering all these issues, a new way of incorporating and reinforcing inorganic and organic materials into polymer fibres is still in its infancy and attracting more and more attention and this is one of the investigating facets of my work presented here.

Pressurised gyration, which involves rotating a perforated pot containing a polymer solution at high speed, is a promising alternative method of spinning fibres and fibrous structures with a controllable fibre size in a nano- to micro-range and fibre size distribution (Mahalingam S. & Edirisinghe, 2013; Raimi-Abraham B., Mahalingam, Edirisinghe & Craig, 2014). This technique has attracted wide interest in the research community because it overcomes the limitations of other spinning methodologies, and it has already been exploited to generate fibres, microbubbles and capsules using

polymer and protein solutions (Mahalingam S. & Edirisinghe, 2013; Raimi-Abraham B., Mahalingam, Edirisinghe & Craig, 2014; Mahalingam S., Ren & Edirisinghe, 2014; Mahalingam S., Raimi-Abraham, Craig & Edirisinghe, 2015). The high production rate, ease of production and highly controlled fibre morphology are salient features of this technique (Mahalingam S. & Edirisinghe, 2013).

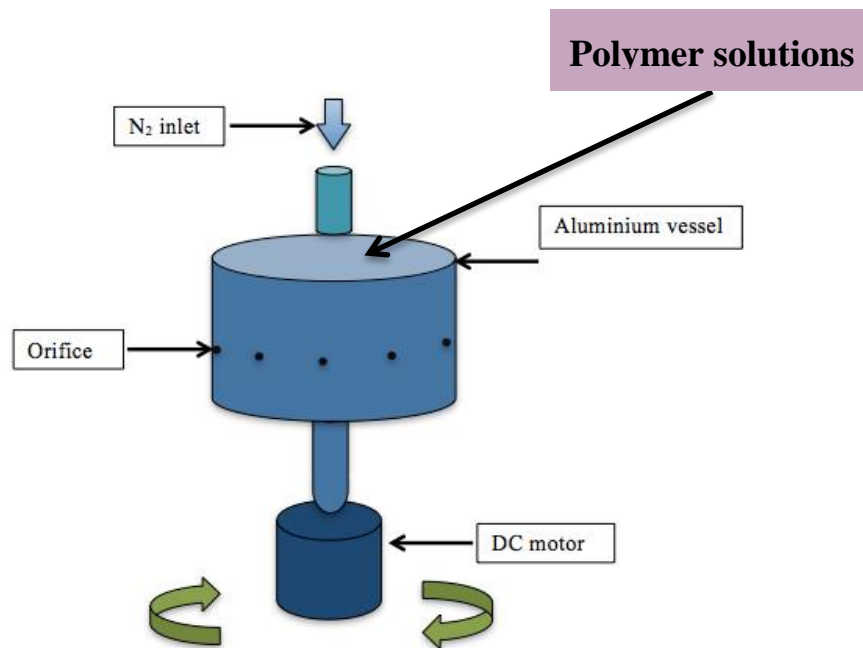


Figure 1.1: The pressurised gyration process

A schematic of the pressurised gyration process is shown in Figure 1.1. The technique consists of a vessel containing a polymer solution which is subjected simultaneously to a centrifugal force and dynamic fluid flow in order to extrude fibres with tailored morphologies and functionality (Mahalingam S. & Edirisinghe, 2013). The nanofibres produced via this technique depend on the high rotating speed of the vessel, the air pressure, and the concentration of the polymer solution. Indeed, unlike electrospinning it is a nozzle free method which is independent of electrical conductivity and the dielectric constant of the polymer solution. This process enables the production of fine,

long continuous fibres in a well oriented direction. The highly oriented fibres produced can provide mechanically strong fibres with remarkable surface active areas (Mahalingam S. & Edirisinghe, 2013; Raimi-Abraham B., Mahalingam, Edirisinghe & Craig, 2014).

Generally, non-woven polymer fibrous scaffolds are made with spinning techniques either using polymer solutions or melts (Narayanan G., Gupta & Tonelli, 2014; Ren J. et al., 2014). Although there has been much research on solution spinning to form fibrous polymer scaffolds for tissue engineering and wound healing applications, little has been reported on melt spinning to fabricate non-woven scaffolds (Brown T. et al., 2014; Ko J. et al., 2014).

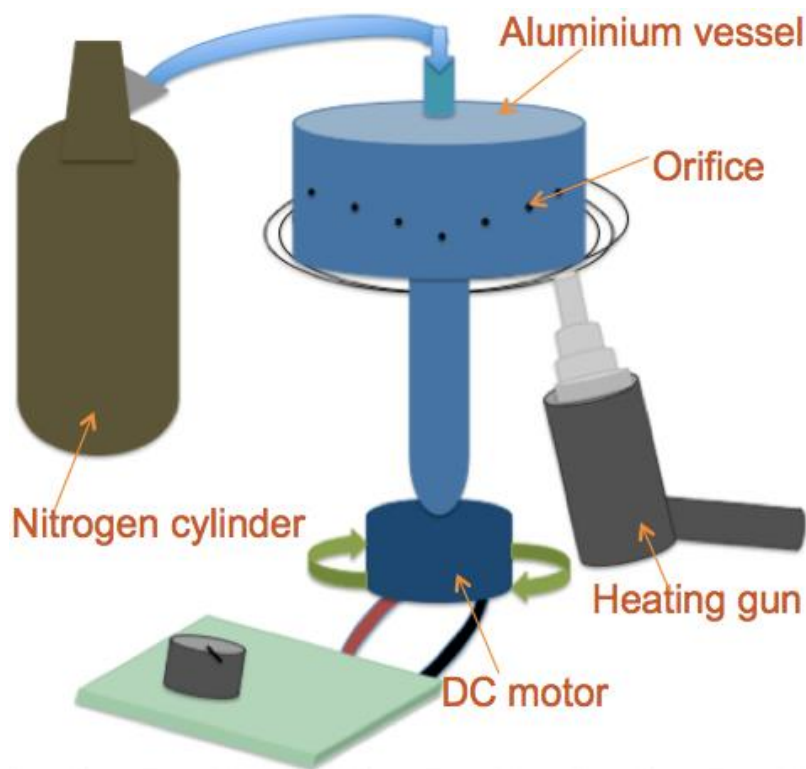


Figure 1.2: The pressurised melt gyration process

Typical pressurised gyration consists of simultaneous centrifugal spinning and solution blowing, whereby the combination of centrifugal and dynamic fluid flow forces act against the surface tension force to generate fibres. The process control parameters, such as rotation speed and working pressure, influence the fibre size, fibre size distribution, and morphology (Mahalingam S. & Edirisingh, 2013; Mahalingam S., Ren & Edirisinghe, 2014). The yield and the quality of the fibres are primarily influenced by polymer concentration and the evaporation rate of the solvent utilised. However, conventional pressurised gyration is dependent upon solvent usage and this can be a disadvantage in forming bioconstructs due to toxicity issues. In contrast, pressurised melt gyration, (Figure 1.2), which is reported for the first time in this study, does not require solvents as it forms a polymer melt in a gyrating pot which has orifices on its surface. The pot temperature can be controlled and the surface roughness of the micrometre size fibres can be tailored in order to investigate their use in typical bioengineering applications, such as antibacterial resistance and tissue engineering.

Bactericidal materials, metallic and metal oxides nanoparticles such as silver (Ag) nanoparticles, copper oxide (CuO), and zinc oxide (ZnO) have been used to fill nanofibres where they have been demonstrated to possess a high degree of antibacterial properties in some studies (Amna T. et al., 2012; Brayner R. et al., 2006; Ghule K., Ghule, Chen & Ling, 2006; Ruparelia J. Chatterjee, Duttagupta, Mukherji, 2008). According to both size and high surface area to volume ratio of metal nanoparticles, they can interact with the bacterial surface and intracellular components closely (Salata O., 2004). Similarly, the metal ions from heavy metals and metal oxides play an important role on bactericidal effect (Feng Q. et al., 2000; Jung W. et al., 2008; Pal S., Tak & Song, 2007). Vargas-Reus tested the antimicrobial activity of different nanoparticles that

showed in a descending order 'Ag > Ag + CuO > Cu₂O > CuO > Ag + ZnO > ZnO' (Vargas-Reus M., Memarzadeh, Huang, Ren & Allakeret al., 2012).

In this project the pressurised gyration of nylon and Ag-loaded nylon solutions, poly(ethylene oxide) (PEO)/chitosan and CuO or Ag loaded PEO/chitosan blend solutions to fabricate nanofibres is investigated. The pressurised melt gyration process is used to generate poly(ϵ -caprolactone) (PCL) and Ag-doped PCL fibres for the very first time. The influence of processing parameters, such as the rotating speed of the vessel, air pressure, polymer concentration in solution, and melt temperature, on the fibre size and the size distribution are investigated. Surface morphology studies and chemical analyses were carried out on the fibres produced, and the antibacterial properties of Ag-loaded nylon nanofibres, Ag-doped PCL fibres, and CuO or Ag embedded PEO/chitosan blend nanofibres were confirmed using the Gram-negative bacteria *Escherichia coli* and *Pseudomonas aeruginosa* which were commonly used for antibacterial studies, tested in an aerobic suspension culture. Thus, the hybrid fibres formed could be employed in a wide range of biological applications, such as antibacterial wound dressing, functional scaffolds for tissue engineering, and in antibacterial water and air filtration devices and systems.

1.2 Aims and Objectives

This study investigates the recently invented techniques, the pressurised gyration process and the pressurised melt gyration process, to produce polymer fibres with a diameter in the micro to nano range. In order to obtain this sized polymer fibres the influence of the properties of polymer solutions, spinning parameters, such as rotation speed, working pressure and temperature, were investigated. Polymers are

functionalised with metallic and metal oxides nanoparticles which render the fibrous structures produced very useful in several modern healthcare applications, such as tissue and medical engineering. The aim of the current study is to produce mats or masks containing polymer fibres plus anti-virus/anti-bacteria nanoparticles. To achieve these objectives and aim three experimental chapters are presented.

In the first part of this study pressurised gyration is used to form Ag nanoparticles embedded in nylon polymer fibres which are nanometre sized. These show high antibacterial activity against the Gram-negatives *E. coli* and *P. aeruginosa*. The nylon polymer was dissolved in formic acid and aqueous silver nanoparticles (particle size < 150 nm) were used to prepare the solutions. The influence of polymer solution concentration, vessel rotary speed and working speed for pressurised gyration on fibre diameter and morphology were investigated.

However, some solvents have toxicity issues which are not suitable for *in vivo* applications. Pressurised melt gyration was used to form micrometre PCL fibres without any solvents due to the low melting point of PCL pellets. Silver nanoparticles (30-35 wt.%, particle size \leq 50 nm) suspended in the organic solvent triethylene glycol monomethyl were coated onto PCL fibres. An assessment of their antibacterial performance showed a significant effect on bacterial viability. The influence of the processing parameters on fibre diameter and morphology, including the rotating speed of vessel, working pressure and temperature, were investigated.

The water-soluble polymer PEO was utilised in the production of nanofibres using pressurised gyration. PEO solutions were blended with 0.1M chitosan solution, which can decrease the water solubility rate of pure PEO fibres. Antibacterial properties were

provided by the addition of Ag nanoparticles (30-35% wt.%, particle size ≤ 50 nm) suspended in triethylene glycol monomethyl and also through the incorporation of CuO nanoparticles into PEO/chitosan nanofibres, demonstrating high antibacterial activity.

Table 1.1 Processing parameters for Pressurised gyration and Pressurised melt gyration.

Materials combinations	Concentrations	Rotating speed (rpm)	Working pressure (MPa)	Melting temperature ($^{\circ}$ C)
Nylon \pm Ag	Nylon: 5, 10, 15 and 20 wt.% Ag: 1 wt.%	1000, 24000 and 36000	0.1, 0.2 and 0.3	–
PCL \pm Ag	–	24000 and 36000	0, 0.01 and 0.02	95, 105, 125, 150, 155 and 200
PEO \pm Ag/CuO	PEO: 10 and 15 wt.% Ag: 2 wt.% CuO: 2 and 5 wt.%	36000	0, 0.1 and 0.2	–
PEO + Chitson \pm Ag/CuO	PEO: 20 wt.% Chitosan: 1 and 2 wt.% Ag/CuO: 0.5 and 1 wt.%	36000	0, 0.1 and 0.2	–

1.3 Thesis Structure

This dissertation focuses on the pressurised gyration process and pressurised melt gyration to produce polymer fibres and the antibacterial activity of metallic nanoparticles, silver and copper oxide.

Chapter 1 introduces the background to pressurised gyration processing. It briefly describes hybrid fibres and the advantages of combining nanoparticles and polymer fibres for use in a wide range of biomedical applications. An overview of this thesis, together with the aims and objectives are also detailed.

Chapter 2 presents the literature review of the investigations that have been conducted over recent decades in the area of fibre spinning processing, and the various types of fibre spinning processes are introduced. This chapter describes the properties of the polymers and metallic nanoparticles used in this study. These properties influence the pressurised gyration process, and include the polymer solutions, physical properties, and processing parameters. Finally, this chapter describes characterisation studies of these fibres.

Chapter 3 describes the experimental details and provides the materials and the preparation of solutions. The novel processing pressurised gyration and pressurised melt gyration used for fibre fabrication are also clearly explained. In addition, the principles of the various characterisation techniques utilized for the fibre analysis are stated.

Chapter 4 analyses the incorporation of metallic nanoparticles (CuO nanoparticles and ZnO nanoparticles) into polymer (polyurethane) fibres. An investigation of nylon and Ag-loaded nylon nanofibres was undertaken. The physical properties of the polymer

solution, together with the processing parameters exerted a significant influence on the fibre diameter and morphology. Raman spectrometry was used to study the bonding characteristics of nylon and the Ag nanoparticles, and inductively coupled plasma mass spectroscopy showed Ag ion release. Ag-loaded nanofibres showed high antibacterial activity against Gram-negative microorganisms.

Chapter 5 discusses the PCL fibres fabricated by pressurised melt gyration. The microstructural characterisation of the PCL fibres and Ag-loaded PCL fibres were investigated using a scanning electron microscope, Raman spectroscopy, differential scanning calorimetry, UV/vis spectroscopy, antibacterial studies and *in vitro* biocompatibility studies.

Chapter 6 details the characterisation of PEO nanofibres and PEO/chitosan nanofibres produced using the pressurised gyration process. Due to the high solubility of PEO in water, the PEO fibres produced were not suitable for antibacterial testing. Hence, chitosan was added to the PEO solution to form chitosan-PEO blend. A comparison of the antibacterial activities between Ag nanoparticles and CuO nanoparticles against Gram-negative microorganisms is reported.

Chapter 7 summarises the results and discusses the conclusions of the study. The future works that should be undertaken into to develop the fibres for use in biomedical applications are also presents. And the References section is listed in the end.

Chapter 2 - Literature Review

2.1 Introduction

Polymer fibres had been extensively researched by a number of biological applications in last several decades. The pressurised gyration process used for producing nanofibres in this study is similar to the rotary jet-spinning process, but is combined with pressure. The properties of Ag nanoparticles result in a high bactericidal effect for Ag-loaded nanofibres. This chapter illustrates the advantages of nanofibres, some alternative methods of fabrication and the antibacterial properties of silver nanoparticles.

2.2 Fibres and Fibrous Structure

Fibres are divided into natural and artificial synthetic materials. In 1890 the first factory commenced synthetic fibre production, with nitrocellulose artificial silk being produced by the Chardonnet company in France (Taussig, 1921). Later in 1935, DuPont patented for an invention - the artificial synthetic textile Nylon 66, acquired purely from petrochemicals as a replacement of silk in 1935 (Carothers W., 1935; Luo C., Stoyanov, Stride, Pelan & Edirisinghe, 2012; Morris P., 2005). More and more artificial fibres have been developed after that.

2.2.1 Nanofibres

Nanofibres are one-dimensional nanostructures with unique mechanical and electronic properties (Theron A., Zussman & Yarin, 2001). They have a large surface area and a small diameter (Baba R. & Jayaram, 2010; Hassan M. et al., 2013; Teo W. & Ramakrishna, 2006), with protection of the interior of nanofibres determined by the molecules, particles and biological structures (Reneker D. & Yarin, 2008).

There are many types of nanofibres, such as hydrocarbon nanofibres which can be made via low temperature oxidation and heating in an inert atmosphere, while ceramic nanofibres are formed by heating electrospun organometallic nanofibres in an oxidizing atmosphere, and metal nanofibres are made by heating a metal loaded with nanofibres in a reducing atmosphere. Spinnable and non-spinnable but conductive polymers are used to produce polymer nanofibres via the electrospinning process, solution blowing methods etc. (Bognitzki M. et al., 2006; Reneker D. & Yarin, 2008; Theron A., Zussman & Yarin, 2001; Wu H., Zhang, Liu, Lin & Pan, 2007). The morphology of nanofibres can be controlled through solvent/solution composition and operating parameters (Deitzel, Kleinmeyer, Harris & Tan, 2001). Nanofibres have small diameters and specialised techniques are required for their formation and collection (Xu S., Shi & Kim, 2006). There are several popular methods used to produce nanofibres and these are discussed in Section 2.3.

2.2.2 Applications of Nanofibres

Nanofibres and nanocomposites have been investigated extensively and play an important role in nanoscience and technology (Chik H. & Xu 2004). They are available

for many applications, such as tissue engineering scaffolds, drug delivery, filtration media, energy storage, catalysis and sensors (Huang, Zhang, Kotaki & Ramakrishna, 2003) due to their unique mechanical and electronic properties according to the recent researches (Theron A., Zussman & Yarin, 2001). Figure 2.1 shows the diverse areas of application possible for electrospun fibres (Huang, Zhang, Kotaki & Ramakrishna, 2003). The most highly researched application area for nanofibres is in the field of biomedicine; three-dimensional nanofibrous scaffolds for tissue engineering, and the design of nanofibrous devices for controlled drug delivery and wound dressings (Pham Q., Sharma & Mikos, 2006).

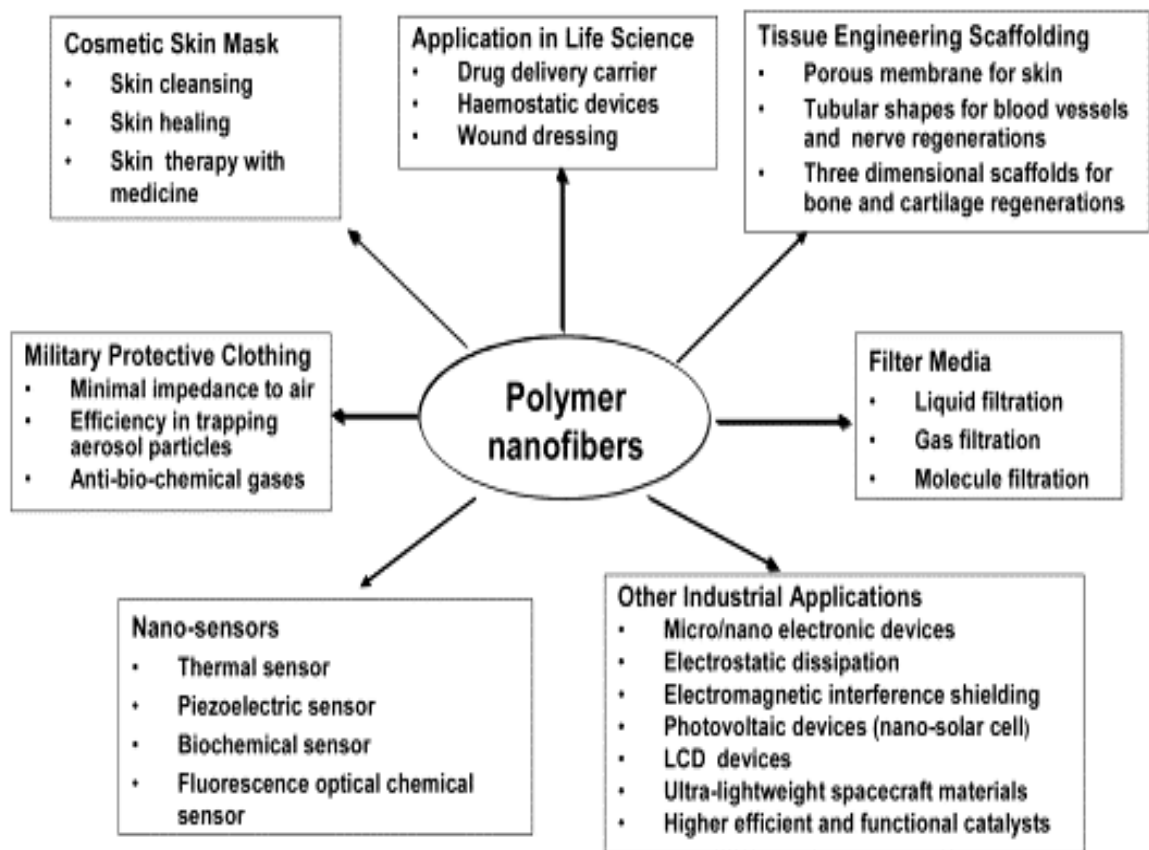


Figure 2.1: The diverse areas of applications identified for polymer nanofibres

(Huang, Zhang, Kotaki & Ramakrishna, 2003)

2.2.2.1 Tissue Engineering

Generally, non-woven biodegradable, biocompatible polymer fibrous scaffolds in the nano- to micro- range have a very similar structure to the native extracellular matrix (Sankar D., Shalumon, Chennazhi, Menon & Jayakumar, 2014; Liu W., Thomopoulos & Xia, 2012). This acts to support a cell by providing a three-dimensional network structure that consists of sequentially overlapped nanofibres which surround the outside surface of tissue (Katti D., Robinson, Ko & Laurencun et al., 2004). The large surface area and good porous property of nanofibres are beneficial for adhesion and growth of cell (Gupta A. et al., 2007). An electrospun gelatin/trifluoroethanol (TFEA) fibres investigated which has a similar structure as synthesized ECM in 2003 (Huang, Zhang, Kotaki & Ramakrishna, 2003).

2.2.2.2 Drug Delivery

For drug delivery, controlled drug release devices, such as nanofibres carrying pharmaceutical agents due to their high porosity, a high degree of uniformity and high length to diameter ratio allows polymer carriers to release the drugs gradually and also maintains the activity of the agent. The advantage of this controlled drug delivery technique comes before the associated higher costs and potential discomfort as implants are needed (Andrady A., 2008).

2.3 Fibre Production Methods

2.3.1 Electrospinning

Electrospinning and Electrospraying are part of the electrohydrodynamic (EHD) technique and have been investigated for micro-/nano-size polymeric particles and fibre processing for tissue engineering and drug delivery applications. Recently, a portable EHD device was designed by Professor Mohan Edirisinghe and co-workers to create controllable micrometre sized polymer fibres that could be used for wound dressings on human skin.

2.3.1.1 Electrohydrodynamic Process

EHD processing depends on a high electric field to form droplets. A high voltage elongates the meniscus of liquid jet that stretches from a needle exit. Hence, the electrical force results in the charged droplets formation from a liquid (Mora J. & Loscertales, 1994).

The first study of EHD processing was recorded by Bose in 1745 (Ganan-Calvo, 1999), and the instability of the EHD process and the analysis of the action of jets and drops was later explained by Rayleigh (1879). According to Rayleigh, the formation of droplet under EHD process is the work of two forces, outward electrical stress and counteracting surface tension forces. The electrical stress play a role of tearing the droplet apart while surface tension forces are trying to hold the droplet together, once the balance is reached, a droplet is formed (Rayleigh, 1882).

The stability of a drop is dependent upon the balance of forces between the outward electrical stress, which tends to disrupt a drop, and the counteracting surface tension forces, which try to hold a droplet together (Rayleigh, 1882).

The electrospinning process for fabricating textile fibres described by Formhals in 1934 is widely recognised as the first significant study. In recent decades electrospinning has become a simple and flexible method for polymer-based composites, ceramic and metal nanofibre fabrication at the micro to nanometre scale (Huang, Zhang, Kotaki & Ramakrishna, 2003; Luo C., Nangrejo & Edirisinghe, 2010; Luo C., Stoyanov, Stride, Pelan & Edirisinghe, 2012; Patra et al., 2009; Teo W. & Ramakrishna, 2006). Electrospinning is widely used in electrical, chemical, and especially biomedical applications (i.e. tissue engineering, filtration, wound dressings, drug delivery, enzyme immobilisation, etc.) (Deitzel J., Kleinmeyer, Hirvonen & Tan, 2001; Fong H., Liu, Wang & Vaia, 2002; Kenawy R. et al., 2002; Reneker D. & Yarin, 2008).

At the laboratory scale, Figure 2.2 shows typical electrospinning set-up, requires a high voltage power supply (up to 30 kV), a syringe pump, a flat tip needle and a collection platform only (Teo W. & Ramakrishna, 2006). The nanofibres produced by electrospinning are based on the electrostatic force which acts on the polymer solution as it is ejected and sprayed from a nozzle spinneret (Luo C., Nangrejo & Edirisinghe, 2010). An electrified jet of polymer solution can be produced and elongated by high voltage and as the solvent evaporates nanofibres are formed (Baba R. & Jayaram, 2010). Previous studies have highlighted that the processing parameters (such as applied voltage, flow rate, nozzle tip polarity, and etc.), characteristics of the polymer solution (e.g. concentration, solvent and solution properties, etc.), and the size of the orifice can affect the production of polymer nanofibres by electrospinning.

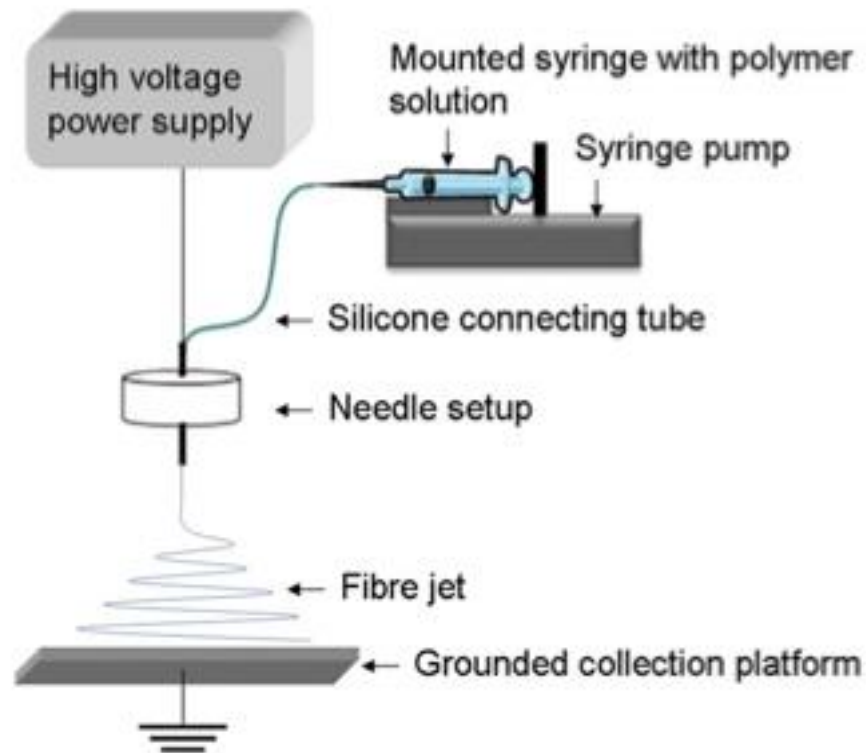


Figure 2.2: Typical laboratory scale electrospinning set-up

(Luo et al., 2010)

In 1990s, electrospinning was firstly put into research and starting to be consistently and detailed studied. And Cloupeau and Prunet-Foch (1990) presented classification of several functional modes of EHD processing under varied system operating conditions (applied voltage, flow rate, etc.), but since this technique is new at that time, most of their investigation results are based on visual observations, still, they were successfully build up approaches of measurable differences of EHD process (Cloupeau M. & Prunet-Foch, 1990).

With the deeper investigation of EHD processing, more controllable parameters are found by researchers. Meesters et al. (1992) present a way to increase the quantity of droplets

in con-jet mode atomisation, which is by increase the flow rates. And in 2002, Jayasinghe and Edirisinghe find that the viscosity had a significant effect on the product size distribution of EHD processing, and suggested the range of 1-1340 mPa is the best range to keep the solution viscosity within (Jayasinghe S. & Edirisinghe, 2002).

2.3.1.2 Process Parameters which Effect Electrospinning

The most important factor which has an influence on the diameter and morphology of spun fibres is the concentration of the polymer solution. The minimum concentration for beaded nanofibre production is termed the critical minimum concentration c_e , and this is required for molecular chain entanglements. In practise, this means that if the polymer solution concentration is below the c_e , then only droplets are formed, whereas fibres are formed if the concentration of the polymer solution is above the c_e (Colby R., Fetters, Funk & Graessley, 1991; Luo C., Nangrejo & Edirisinghe, 2010; McKee M., Elkins & Long, 2004).

Surface tension and viscosity of a polymer solution are generally considered as the two main properties which affect the electrospinnability. Viscosity is also a dominant factor which determines fibre diameter (Deitzel J., Kleinmeyer, Harris & Tan, 2001; Sukigara S., Gandhi, Ayutsede, Micklus & Ko, 2003).

Electrical conductivity is a key property of the polymer solution which influences the stability of the cone-jet and the diameter of the spun fibres. Sufficient electrical conductivity within the solution is crucial to allow enough tangential stress to build up in a charged droplet at the end of the capillary tube, before deformation into a cone-shape can occur; solutions with zero conductivity cannot be electrospun (Cloupeau M.

& Prunet-Foch, 1989). However, if the conductivity of a liquid is too high, then electrical discharge will occur due to corona discharge into the surrounding air, leading to an unstable spinning jet or halting the process altogether (Hartman R., Brunner, Camelot, Mariknissen & Scarlett, 2000).

An applied voltage is required to eject a charged jet from the droplet at the nozzle, and the minimum applied voltage depends mainly on the polymer solution properties, such as surface tension and viscosity (Demir M., Yilgor, Yilgor & Eeman, 2002). Increasing the applied voltage beyond the threshold value is directly related to the degree of whipping instability and hence the elongation of the fibre jet. However, studies on the effect of the applied voltage on the as-spun fibre diameter have reported contradictory results, although many have reported a reduction in fibre diameter with the applied voltage increases (Fridrikh S., Yu, Brenner & Rutledge, 2003; Megelski, Silke, Stephens, Chase & Rabolt 2002; Shin Q. et al., 2001).

The flow rate is the rate at which a polymer solution is pumped into the nozzle to feed the spinning cone-jet. An optimum flow rate range exists for individual spinning materials, which changes with the inner diameter of the nozzle; if the flow rate higher than this range, result in an increasing fibre diameter and broadening diameter distribution, whereas at a lower flow rate electrospinning becomes discontinuous as the cone at the tip of the nozzle becomes depleted and even recedes into the nozzle. Balancing the flow rate and applied voltage is mandatory for obtaining and maintaining a stable cone-jet during electrospinning (Deitzel J., Kleinmeyer, Harris & Tan, 2001; Demir M., Yilgor, Yilgor & Eeman, 2002).

Generally, nozzles with a smaller inner orifice diameter generate fibres of smaller diameter (Katti D., Robinson, Ko & Laurencun et al., 2004). However, blockage of the capillary tip can occur when using a viscous liquid and a nozzle with a small diameter. A ratio of 4.5 of the length of the nozzle to its diameter is the best for electrospinning process 5 (Luo C., Stoyanov, Stride, Pelan & Edirisinghe, 2012; Mitchell S. & Sanders, 2006).

The collection distance is the distance from the tip of the spinneret nozzle to the grounded collector. This distance is directly related to the electrostatic field strength of the setup and the time allowed for solvent evaporation before the fibres reach the collector. Fibre diameter has been generally found to decrease with increasing collection distance (Jalili R., Hosseini & Morshed, 2005).

2.3.2 Solution Spinning

Solution spinning is a processing of extrusion of a solution jet to generate fibres. The solvent is removed during the spinning by solidification in a wet spinning or by from by vaporisation with hot gases in a dryspinning (Gupta V. & Kothari, 1997; Luo C., Stoyanov, Stride, Pelan & Edirisinghe, 2012). The pressurised gyration involved in this study extrudes polymer solution jet through the orifices on the face of vessel to form fibres as similar as solution spinning. In the meantime, the pressure is supplied for gyration spinning that helps fibre stretching.

2.3.2.1 Wet Spinning

Wet spinning method has the longest story compared with all the other fibre spinning methods. In 1960s, several studies have been involved to produce biopolymer fibres, which used to investigate the physio-chemical properties of the macromolecules using X-ray diffraction, birefringence, or dichroism (Rupprecht A., 1966). During the wet spinning process, the spinneret immersed completely into the polymer solutions that dissolved by using a suitable solvent to extruded and stretched the solutions into a liquid jet. The fibres formed due to the precipitation and solidification of the solvent based on mass transfer (Gupta B., Revagade & Hilborn, 2007; Gupta V. & Kothari, 1997).

2.3.2.2 Dry Spinning

In contrast to wet spinning, the fibre solidification of dry spinning method refer to a stream of hot air or inert gas and the solvent is removed by heating without any chemical change. The processing of dry spinning is faster than wet spinning since fibre formation is due to evaporation of polymer jet in dry spinning instead of the precipitation of solvent in wet spinning. This method suitable for some non-thermoplastic polymers but can be dissolved in some safety and environmental friendly solvents to form mass production of polymer fibres (Luo C., Nangrejo & Edirisinghe, 2010).

2.3.2.3 Flash Spinning

There is another spinning method - Flash spinning also belongs to the solution spinning by involving a high pressure to extrude the polymer solutions. It is a non-solvent usage processing because the applied high pressure helped the polymer dissolved into a liquid

for the further jet elongation (Blades H., White, White & Ford, 1962; Shin H. & Samuels, 1992).

2.3.2.4 Gel Spinning and Liquid Crystal Spinning

Gel spinning and liquid crystal spinning are also solution spinneret-extrusion wet spinning processes to generate fibres with high modulus and high tenacity (HMHT), but the solutions extruded are in a state between a conventional fluid solution and a crystalline solid. HMHT fibres as a new material demonstrate a modulus of between 50 to 600 GPa and a minimum tenacity of 3 to 6 GPa widely used in aerospace and marine engineering application (Luo C., Stoyanov, Stride, Pelan & Edirisinghe, 2012). Contrast to the conventional wet spinning, fibres formed by the material with high crystallinity show high degree of molecular orientation, thereby improving the tenacity and modulus of the as-spun product. There is still a risk of processing high tenacity high modulus fibres, because most of the process may either have critical producing requirement or be harmful to the surrounding environment. For example, when producing para-aramid fibres, dust and fibre particulates will be generated at the same time, and that composite is flammable in the air. Besides, those dusts and fibres are harmful to human exposed parts such as eyes, noses and skin (Luo C., Stoyanov, Stride, Pelan & Edirisinghe, 2012). A little exposure of these might end up with coughing, sneezing, redness and itching of the skin, and long term handling those fibrous air without essential protection may also has a damage to air-way system. (DuPont, 2008).

The easy and simple way to differentiate the liquid crystal spinning and gel spinning is by observing the gap between the spinneret and the coagulation bath. Gel spinning jets exit directly into the coagulation bath, whereas in liquid crystal spinning there is brief

exposure to the air before the extruded material is enters the coagulation bath. Liquid crystal is a processing method for long-range orientation fibre forming by using viscoelastic materials (Rey, A. 2007; Luo C., Stoyanov, Stride, Pelan & Edirisinghe, 2012). In both gel spinning and liquid crystal spinning, drawing can minimise the disturbance of molecular chain entanglements, and fibres processing under high drawing ratios with high molecular chain alignment show high crystallinity and good tensile strength (Michielsen et al., 2001; Luo C., Stoyanov, Stride, Pelan & Edirisinghe, 2012).

2.3.3 Emulsion Spinning

DuPont invented and patented the Emulsion spinning in 1956. After the following decades, the emulsion spinning was improved by comprising of two or more fibre forming components could be beneficial for the material which was originally poorly spinnable due to its insolubility, chemical or thermo-inertness to produce shaped, composite or matrix fibres (Luo C., Stoyanov, Stride, Pelan & Edirisinghe, 2012). Emulsion electrospinning of a mixture of an aqueous solution of a material emulsified in a polymer solution has been studied for producing drug encapsulated and core-sheath nanofibres, which ease the initial burst drug release remarkably (Xu X. et al., 2005; Yang Y., Li, Qi, Zhou & Weng, 2008).

2.3.4 Rotary Jet Spinning

Electrospinning has to overcome some issues during the spinning, such as poor control over fibre orientation and the low production rate at high voltages. The high curing temperature and low solution viscosity leads to the generation of nanofibrous structures,

whilst some materials are not suitable for high voltage electrospinning (Badrossamay M., McIlwee, Goss & Parker, 2010; Nijst C. et al., 2007; Weitz R., Harnau, Rauschenbach, Burghard & Kern, 2008; Yi F. & LaVan, 2008).

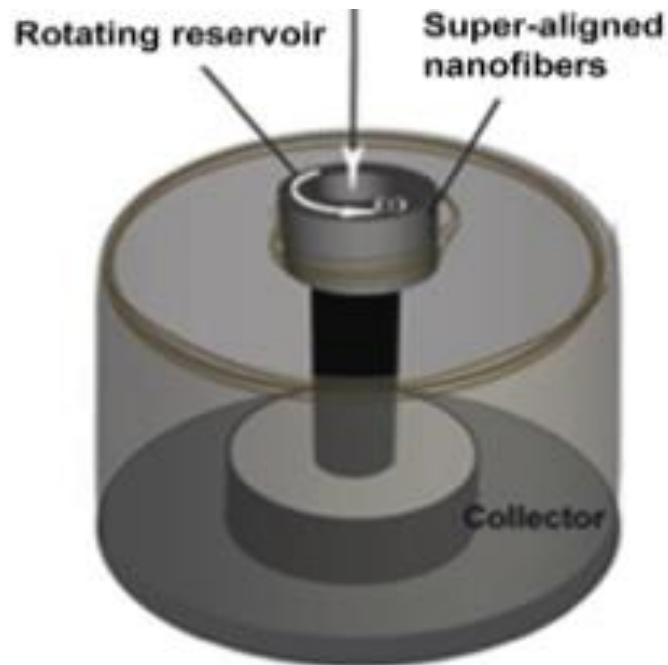


Figure 2.3: Rotary jet-spinning set-up

(Badrossamay et al., 2014)

Rotary jet-spinning (RJS) is a technique performed in a rotary mould based on high-speed rotation acting on polymer solution jets to extrude highly aligned three-dimensional nanofibre structures (Figure 2.3, Badrossamay M. et al., 2014). The ultrafine nanofibres produced by using RJS can be utilised as tissue engineering scaffolds, and in drug delivery and wound dressings (Badrossamay M., McIlwee, Goss & Parker, 2010; Mary L. et al., 2013; Senthilram T. et al., 2011). The RJS system consists of a rotating reservoir where the polymer solution continuously flows in (Badrossamay M. et al., 2014), and a motor with adjustable rotation speed, with the

nanofibres being collected in the surrounding cylindrical collector. The morphology and diameter of the nanofibres formed by RJS can be controlled by the rotating speed and properties of the polymer solution (Badrossamay M., McIlwee, Goss & Parker, 2010).

There are three stages in this process; jet initiation, jet extension and solvent evaporation (Figure 2.4). When the spinning rate of the reservoir is larger than the critical value for the balance between capillary and centrifugal forces, a viscous jet will be ejected through a small orifice. Due to the relatively high surface area of this jet, it is elongated by centrifugal forces outwards along a spiral trajectory as the solvent evaporates. The jet continues to extrude from the small orifice and solid fibres are formed as the remaining solvent evaporates (Mellado P. et al., 2011).

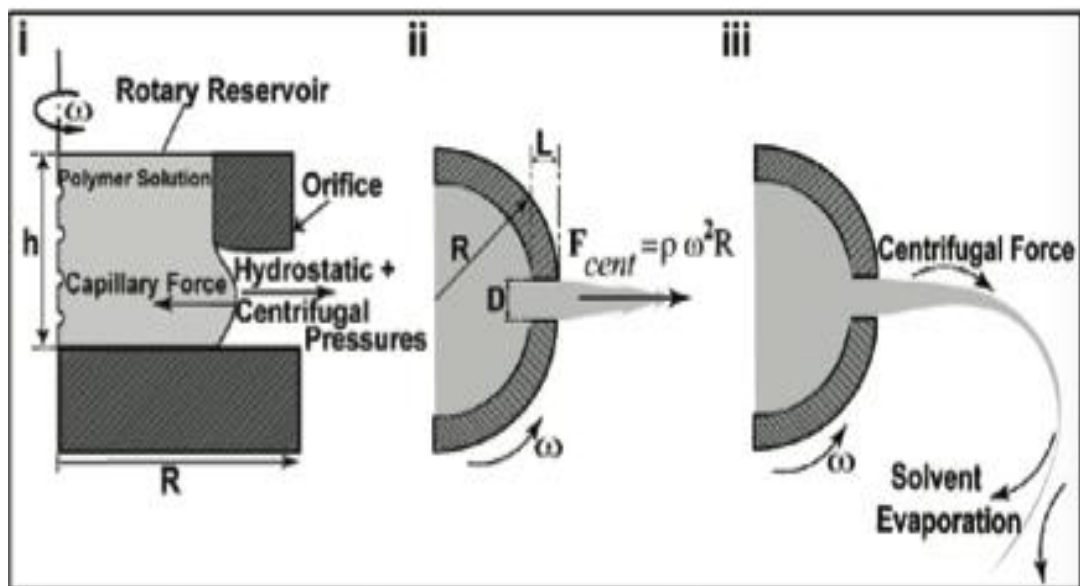


Figure 2.4: Fibre formation mechanisms in the rotary jet-spinning system

(i) jet initiation; (ii) jet extension; (iii) solvent evaporation

(Badrossamay M., McIlwee, Goss & Parker, 2010).

According to Badrossamay et al. (2010), the diameter of polymer nanofibres can be influenced by varying the rotation speed and the polymer concentration. At a lower rotation speed the fibre diameter is increased and the possibility of forming beads is higher. Similarly, if the polymer solution concentration is lower than the critical concentration value then only beads are produced, while if the concentration is above the critical concentration polymer chain entanglement produces continuous fibres (Badrossamay M., McIlwee, Goss & Parker, 2010; Shenoy S., Bates, Frisch, Wnek, 2005).

Compared to other nanofibre fabrication processes, RJS has some advantages, such as the simple set-up, the lack of a high-voltage electric field, capability for both solution and melt spinning, formation of nanofibre structures into any random distribution by changing the collector geometry, ability to alter nanofibre morphology (beaded, textured, or smooth) and diameters by varying the process parameters and fibre fabrication being independent of solution conductivity. In addition, RJS is appropriate for both polymer emulsions and suspensions, and is can achieve higher production rates contrasted to conventional electrospinning (Badrossamay M., McIlwee, Goss & Parker, 2010; Mary L. et al., 2013).

2.3.5 Melt Spinning

Conventional melt spinning is a spinneret-extrusion processing uses a polymer melt to obtain spun fibres which is stretched out by mechanical force and solidified by cooling, and also is the fastest fibre solidification processing due to one-way heat transfer (Gupta V. & Kothari, 1997; Luo C., Stoyanov, Stride, Pelan & Edirisinghe, 2012). Compared to melt spinning, solution spinning requires solvents which may cause environmental

concern, and the process has lower energy efficiency. Moreover, for the fibre solidifying process, the mass transfer in solution spinning is slower than the simple heat transfer in melt spinning. The non-solvents in melt spinning eliminates the solvent residue and solvent recovery issues. In addition, melt spinning as an environmental friendly, higher productivity process, is the more preferred method if a material is thermoplastic or can be melt-spun (Huang T. et al., 2008).

Larrondo and Manley (1981) reported a melt electrospinning technique which has drawback to produce thinner spun fibre with low conductivity and high viscosity of polymer melts by electrostatic forces (Luo C., Stoyanov, Stride, Pelan & Edirisinghe, 2012), and the surface tension instability and cohesive fractures of the spinline have significant effect on the quality of melt electrospun fibres (Larrondo L. & Manley, 1981; Lyons J., Li & Ko, 2004). The melt electrospun fibre size is influenced by material parameters, like polymer molecular weight and molecular chain conformation. A larger fibre diameter is formed by a higher molecular weight polymer due to stronger chain entanglements, higher viscosity and poor crystallisation of the melt (Luo C., Stoyanov, Stride, Pelan & Edirisinghe, 2012; Luo C., Stoyanov, Stride, Pelan & Edirisinghe, 2012).

This process incorporates convenient operation and mass productivity for rapidly spinning a molten polymer without the use of solvents into ultrafine fibres, based on the principle of solution blowing (Tang S. & Mukhopadhyay, 2006; Zhang L., Koppersta, West, Hedin & Fong, 2009). This method overcomes the limits resulting from the stiffening of some solutions due to solvent crystallisation at the ambient temperature or when a polymer is dissolved in a volatile solvent by using high-velocity hot gas to form a non-woven mat (Ellison C., Phatak, Giles, 2007; Medeiros E., Glenn, Klamczynski, Orts & Mattoso, 2009; Zhang L., Koppersta, West, Hedin & Fong, 2009).

2.3.6 Blowing

Solution blowing has recently been reported in the fabrication of micro- to nano-fibres using a high-velocity gas flow as the driving force to blow a polymer solution (Medeiros E., Glenn, Klamczynski, Orts & Mattoso, 2009; Zhuang X., Jia et al., 2014; Zhuang X., Yang et al., 2012). These fibres can widely be used in various applications, such as biomedical, tissue engineering, drug delivery, and agriculture (Chen et al., 2011). The solution blowing approach is similar to the electrospinning process but differs in the driving force for fibre production, and it also does not require a high voltage supply. Polymer solution streams are blown to solid nanofibres by utilising a high-velocity gas flow accompanied by solvent evaporation (Ellison C., Phatak, Giles, 2007; Liu R., Xu, Zhuang & Cheng, 2014; Yan G., Zhuang, Tao & Cheng, 2013; Zhuang X., Yang et al., 2012). Solution blowing is an efficient method for nanofibre non-woven mat manufacturing, and is expected to become a safe and energy saving process for mass nanofibre production (Sinha-Ray S., Zhang, Yarin, Davis & Pourdeyhimi, 2011; Liu R., Xu, Zhuang & Cheng, 2014; Zhuang X., Jia et al., 2014).

A schematic of the solution blowing set-up is shown in Figure 2.5. The single nozzle spinning die is a ringed spinning nozzle which is a coaxial surrounded by a gas cavity (Zhuang X., Yang et al., 2012). First, the polymer solution is squeezed into the single nozzle spinning die, which is under the control of a peristaltic pump. Then, a pressure regulator is used to control the compressed air transfer to the air gas cavity. The polymer solution stream is ejected from the nozzle tip and is considerably elongated by the high-velocity gas flow, with the solid fibre being formed following solvent evaporation. An exhaust blower is used to remove the evaporated solvent accompanied with air through a groove below the collector. A heated spinning cabinet is provided to heat the air

throughout the spinning process, which can accelerate the evaporation of solvent and helps to form fibres. The solution feeding rate, gas pressure provided to the gas cavity, and the air temperature of the spinning cabinet all influence the solution blowing process (; Zhuang X., Jia et al., 2014; Zhuang X., Yang et al., 2012).

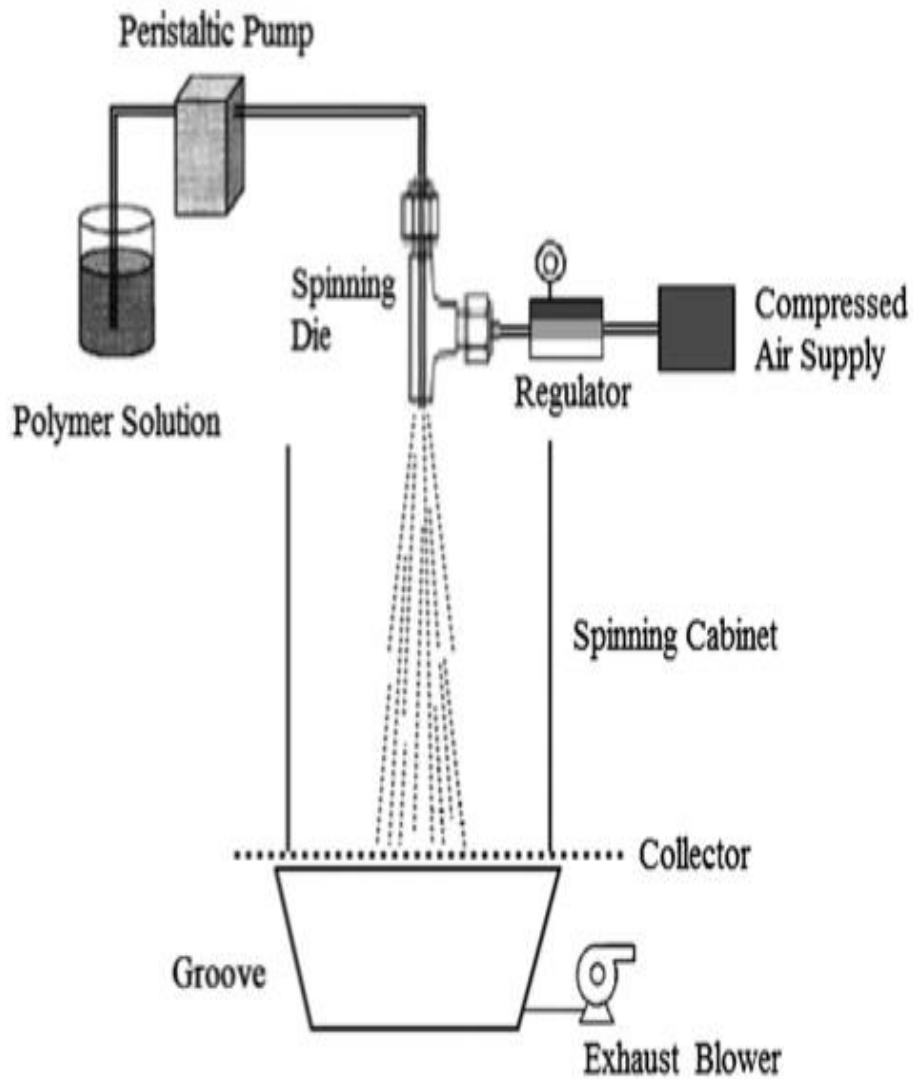


Figure 2.5: Solution blowing set-up

(Zhuang et al., 2012)

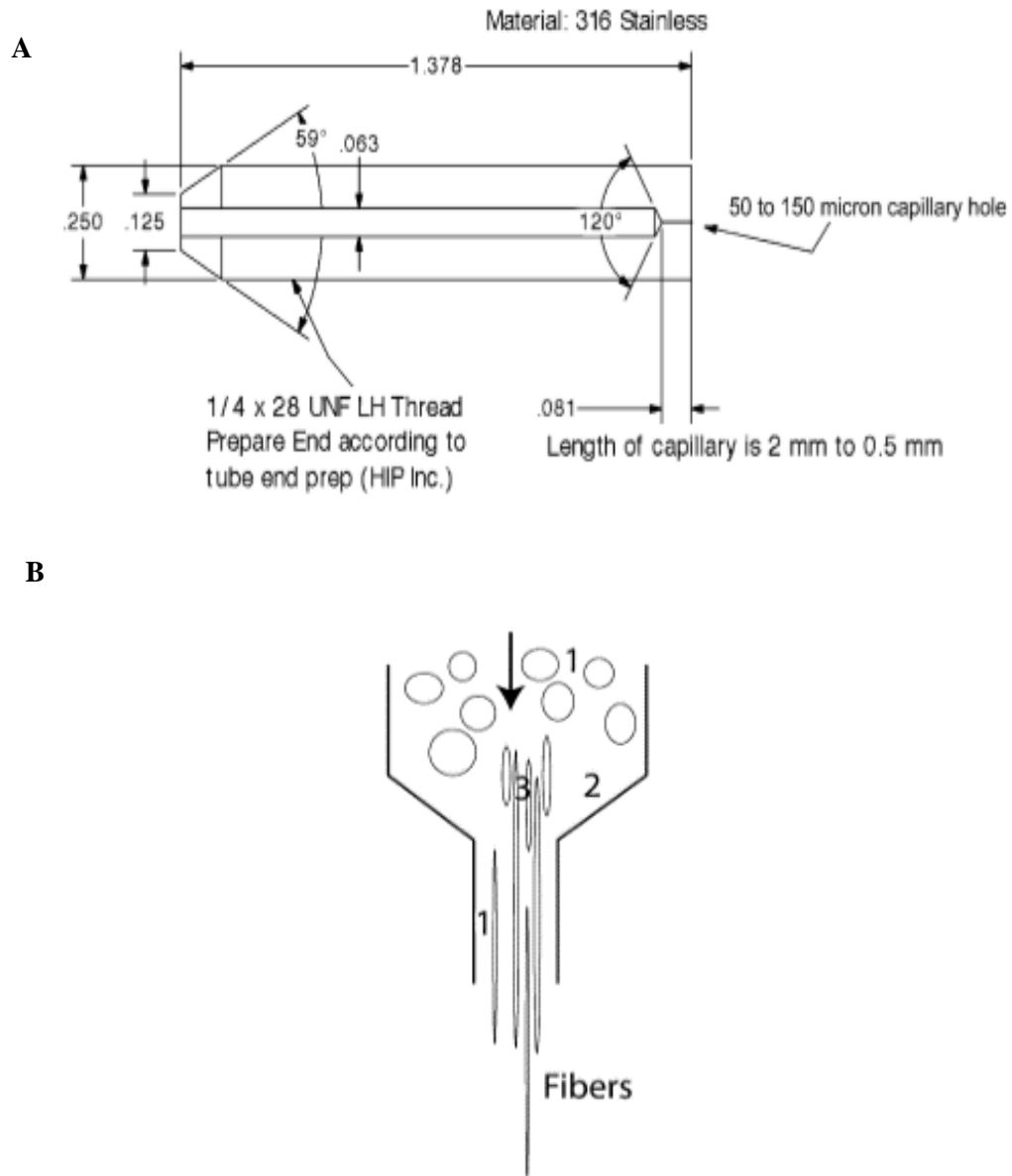


Figure 2.6: Jet blowing process

(a) Schematic drawing of the nozzle used for jet blowing. (b) Schematic showing the flow field in the nozzle of the jet-blowing process: (1) regions of principal shear flow; (2) a vertical region at the entrance of capillary; and (3) an extensional flow region just upstream of the contraction for fibre formation.

(Borkar S. et al., 2006).

Borkar et al. (2006) introduced jet blowing, a one-step, solvent-free and environmentally friendly technique to process polytetrafluoroethylene (PTFE) fibres down to a micro-/nano-metre diameter, through the use of a high pressure gas jet, even below the melting point. This method can be used to fabricate several polymers which cannot be electrospun or melt blown. High-pressure gas and a solid polymer are supplied into a stainless tube, where they are sprayed at a raised temperature and pressure via a single capillary hole (Figure 2.6a). An abrupt shrinkage in the diameter due to the large pressure drop is accompanied by high shear rates and extensional stretching at the entrance of the capillary, where the flow leads to polymer chains which are deformed, extended and reoriented, and fibres are subsequently formed (Figure 2.6b). Jet blowing can process multiple fibres in parallel within a single nozzle compared to the simple extrusion process (Borkar S. et al., 2006).

2.3.7 Self-Assembly

Self-assembly is another approach for the processing of fibres or structures which range in diameter from micrometres to nanometres, and has advantages in nanolithography compared to other methods (Kim S., Ren & Jenekhe, 2011; O'Rioradan A. et al., 2011).

Aggregation occurs when a polymer solubility is gradually modified by a solution-phase technique for the preparation of nanofibres, for example, a polymer is dissolved by a marginal solvent (such as anisole) at a raised temperature and a slow cooling process then induces aggregation (Samitsu S., Shimomura, Heike, Hashizume & Ito, 2008; Schwarz et al., 2013). Moreover, a mixed solvent can also cause aggregation (Kim S., Ren & Jenekhe, 2011). According to Schwarz et al. (2013), the self-assembly of

nanostructures is dependent on anisotropic interactions between monomers along the polymer chain, which include π - π and alkyl side chain interactions.

Nanocomposite production requires the mixing of polymer whisker and polymer solutions (Samir M., Alloin, Dufresne, 2005). However, the whisker exhibits useful mechanical properties and has a remarkable trend for aggregation (Capadona J. et al., 2007; Marchessault R., Morehead & Walter, 1959; Samir M., Alloin, Dufresne, 2005). Capadona J. et al. (2007) investigated nanocomposite fabrication by forming a 3-dimensional self-assembly nanofibre template, before adding a filled polymer into the template (Figure 2.7) The nanofibre template formed via the solution/gel process includes the following set up: (i) a non-solvent of any polymer is added into the nanofibre dispersion, (ii) self-assembly of the nanofibre gel, (iii) immersion of the gelled nanofibre containing the polymer into a polymer solution, and (iv) drying of the nanocomposite (Capadona J. et al., 2007).

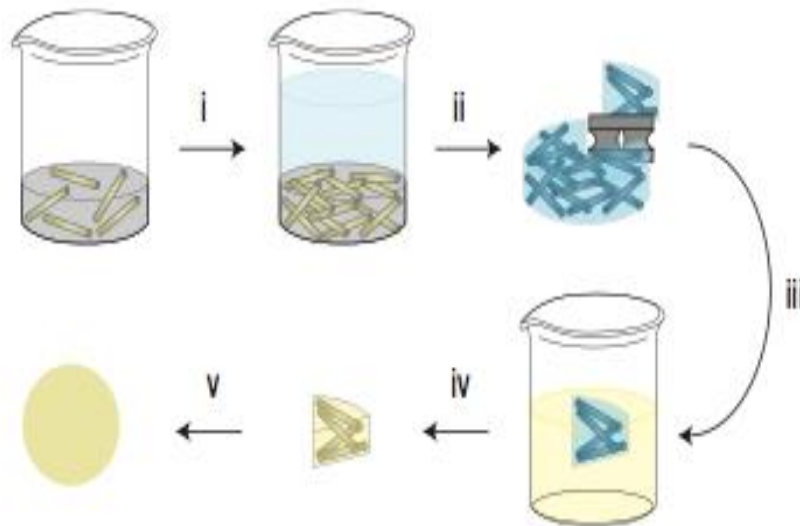


Figure 2.7: Template approach to well-dispersed polymer/nanofibre composites

(Capadona J. et al., 2007)

2.4 Pressurised Gyration

A novel and facile approach for preparing hybrid nanoparticles embedded in polymer nanofibres using pressurised gyration, has been invented by Professor Edirisinghe and co-workers. In contrast to electrospinning, the formation of nanofibres depends on centrifugal force, pressure blowing and evaporation.

The formation of polymer nanofibres in this project was achieved using pressurised gyration, which is a promising alternative to spinning nanofibres and nanofibrous structures, and consists of a perforated rotating pot, containing a polymer solution, which is spun at high speed and under high pressure (Mahalingam S. & Edirisinghe, 2013). Pressurised gyration utilises the simultaneous applications of high rotating speed and working pressure to spin nanofibres and nanofibrous structures essentially from a perforated aluminium pot containing a polymer solution. It has become a promising alternative method of fibre spinning (Mahalingam S. & Edirisinghe, 2013; Mahalingam S., Ren & Edirisinghe, 2014). This method has overcome the drawbacks of other spinning methods and attained popularity in a wide research community. Pressurised gyration has already been explored to generate fibres, microbubbles and capsules using a wide variety of polymer and protein solutions (Mahalingam S. & Edirisinghe, 2013; Mahalingam S., Ren & Edirisinghe, 2014; Raimi-Abraham B., Mahalingam, Edirisinghe & Craig, 2014; Mahalingam S., Raimi-Abraham, Craig & Edirisinghe, 2015; Amir A., et al., 2016; Mahalingam S., Raimi-Abraham, Craig & Edirisinghe, 2015; Mahalingam S., Xu & Edirisinghe, 2015; Mahalingam S., Pierin, Colombo & Edirisinghe, 2015). The benefits of the technique include simple set-up, higher rate of production, easy handling and highly controlled fibre morphology (Mahalingam S. & Edirisinghe, 2013). Concurrent use of centrifugal spinning and solution blowing in pressurised gyration

enables the drawing of nanofibres at a higher speed. In a typical pressurised gyration process the combination of centrifugal and dynamic fluid flow forces overcome the surface tension force to generate fibres. The fibre size, fibre size distribution and the morphology of generated fibres are influenced by process control parameters such as rotating speed and working pressure (Mahalingam S. & Edirisinghe, 2013; Mahalingam S., Ren & Edirisinghe, 2014; Raimi-Abraham, Mahalingam S., Edirisinghe & Craig, 2014). The centrifugal force, used as a rotational shear force and solution blowing can accelerate the air velocity to extrude the polymer solutions via a narrow orifice. The Rayleigh-Taylor instability on the jet due to the polymer solution underpins pressurised gyration technique. The external centrifugal force acts as the driving force when a polymer drop extrudes from the orifice. A flow jet is stretched to the tip of the polymer drop due to the surface tension gradient along the liquid-air interface and separated from the surrounding air subsequently. The equation for the destabilising centrifugal force per unit volume to the stabilising surface tension force per unit volume equals the instability between the liquid-gas interfaces (Mahalingam S. & Edirisinghe, 2013; Weitz R., Harnau, Rauschenbach, Burghard & Kern, 2008).

$$L = \left[\frac{h \cdot \gamma}{(\rho \omega^2 R) + \Delta p} \right]^{\frac{1}{3}} \quad (1)$$

where, L is the length of the instability, ρ is density of the polymer solution, γ is the liquid-gas surface tension, h is the distance between orifices and collector, ω is rotational speed and R is the radius of perforated vessel, Δp is the pressure difference at the orifices, and the $(\rho \omega^2 R)$ means destabilising centrifugal force.

The steps of this process for polymer fibre formation can be explained as follows.

Initially, a polymer jet is extruded through the surface orifice of the vessel, and these are stretched into homogeneous fibres due to the centrifugal force and the pressure difference at the orifice. Finally, the controllable size fibres, which are micro- to nanometre in scale, are obtained as a result of the evaporation of the solvent. The reason for only jets being formed instead of droplets in this classical surface instability is the viscoelasticity of the polymer solution used. Thus, pressurised gyration spinning is a more efficient method in contrast to electrospinning for the mass production of polymer fibres/webs.

Mahalingam et al. (2013) produced PEO nanofibres sized 60 to 1000 nm using the pressurised gyration spinning process by changing the rotation speed (from 10000 to 36000 rpm) and working pressure (from 0.1 MPa to 0.3 MPa). PEO/water solutions with different concentrations (5%, 15% and 21% wt.%) were prepared (Mahalingam et al., 2014). The main process control parameters, such as rotating speed and working pressure, which influence the fibre size, fibre size distribution and the morphology, are primarily influenced by polymer concentration, the evaporation rate of the solvent, and external environmental conditions (humidity and temperature), which effect the yield and the quality of the fibres produced.

2.5 Characteristics of silver nanoparticles

2.5.1 Silver ion release

The release characteristics of Ag ion in polypropylene was found to be influenced by crystallinity and water absorption potential of polypropylene matrix (Radheshkumar C.

& Munstedt, 2006). Soaking time, concentration of silver powder, and silver specific surface area were identified as controlling factors in Ag ion release in polyamide (Kumar R. & Munstedt, 2005). A polyamide matrix has shown greater release potential than a polypropylene matrix due to its inherent hygroscopicity (Kumar R. & Munstedt, 2005; Radheshkumar C. & Munstedt, 2006). The Ag ion release from the matrix is also influenced by the dissolution and swelling behaviour of the matrix polymer (Abdelgawad A., Hudson & Rojas, 2014). Rate of Ag ion release from the hybrid system happens through two mechanisms. Initially, Ag ion is released from the nanoparticles embedded in the surface of the nylon matrix. Secondly, when the washing or soaking time increases, the oxidation of interior Ag nanoparticles happens and subsequent Ag ion release takes place. The former is instantaneous and the latter occurs for a prolonged time where water molecules have to diffuse across many crystalline layers (Kumar R., Howdle & Munstedt, 2005). The onset of plasticisation and the equilibrium sorption would impart a degree of mobility to macromolecular chains and changes in the matrix region and in this way Ag nanoparticles embedded within the matrix get oxidised and release Ag ions over a prolonged time. In addition, polar groups in the nylon chains will be separated and thus water dipole interaction caused. This will provide a more flexible structure for Ag ion release (Radheshkumar C. & Munstedt, 2006). It is also noteworthy that the thickness of the polymer matrix barrier decreases the Ag ion release and the barrier height and the hydrophobicity of the polymer matrix influences water uptake and the diffusivity of the molecules to medium (Alissawi N. et al., 2012). Moreover, mobility and the solubility of the water molecules in the polymer has to be taken into account during the Ag ion release. Thus, for samples with a thicker barrier the water uptake is not sufficient to cause a high Ag ion release rate compared to samples with a thinner barrier height (Damm C. & Munstedt, 2008).

2.5.2 Antibacterial ability

In the presence of Gram-negative bacteria Ag nanoparticles attach to the cell walls and disturb cell wall permeability and cell respiration (Abdelgawad A., Hudson & Rojas, 2014; An J., Zhang, Zhang, Zhao & Yuan, 2009). Other studies have shown that interaction between the Ag ion and the constituents of the bacterial membrane causes the membrane structural changes and damages intracellular metabolic activity thus causing cell death (Jung W. et al., 2008). The concentration of Ag nanoparticles and the formation of “pits” in the cell wall have also been proposed as a reason for anti-bacterial activity. Here the accumulation of Ag nanoparticles in the membrane caused the permeability and the cell death (Sondi I. & Salopek-Sondi, 2004; Zhou et al., 2013). Cell death was shown not be caused directly by Ag nanoparticles but instead by Ag ion release from the Ag nanoparticles (Xiu Z., Zhang, Puppala, Colvin & Alvarez, 2012). However, the bioavailable silver ion concentration (that is the actual ions which here entered into the cells) is the most important parameter, compared with dissolution concentration of Ag nanoparticles that determines the efficiency of cell death (Ivask et al., 2014). Stronger electron storage capability of larger Ag nanoparticles are also be found be impart excellent antibacterial activity (Cao H. et al., 2013). The formation of free radicals was shown to influence cell lysis when the Ag nanoparticles were in contact with bacteria. The free radicals have the ability to destroy the cell membrane and make porous surfaces which lead to cell death (Kim J. et al., 2007). In addition, Ag ions released from the silver nanoparticles reacts with the thiol groups of vital enzymes in the bacteria and inactivate them (Matsumura Y., Yoshikata, Kunisaki & Tsuchido, 2003). Such studies have also shown that the soft acid from of Ag ion may react with soft bases in cells such as sulfur and phosphorous which can cause cell death. DNA, for example,

contain sulfur and the phosphorous, when they react with Ag, they can become damaged, ultimately leading to cell death (Morones J. et al., 2005).

2.6 Summary

A detailed literature review was illustrated in this chapter. Firstly, the applications of polymer fibres and fibrous structure in various areas have been explained, especially in biomedical field. Moreover, the different methods for fibre processing have been reviewed. Finally, the characteristics of silver nanoparticles were described for the antimicrobial application. The subsequent chapters will present the investigation for preparation and formation of hybrid polymer fibres by using pressurised gyration processing with polymer solutions or polymer melts.

Chapter 3 - Experimental Details

This chapter describes the preparation and characterisation of the polymer solutions and the materials used. The pressurised gyration device and pressurised melt gyration process experimental set up, together with the experimental procedures for the formation of polymer fibres and antibacterial testing are also described.

3.1 Materials for Polymer Fibre Fabrication

3.1.1 Polymer

3.1.1.1 Polyurethane

Polyurethane (PU) is a well-known thermoplastic polymer that is used to produce polymer nanofibres for a wide range of biomedical applications due to its good biocompatibility, oxidative biostability, processability, remarkable mechanical properties and water insolubility (Hassan M. et al., 2013; Khlystalova T., Kuraganova, Demina, Petova, Tatalannov, 1986; Kidoaki S., Kwon, Matsuda, 2006). In this study, PU solutions and PU solutions containing copper oxide and zinc oxide were obtained from the School of Engineering and Technology, University of Hertfordshire, UK.

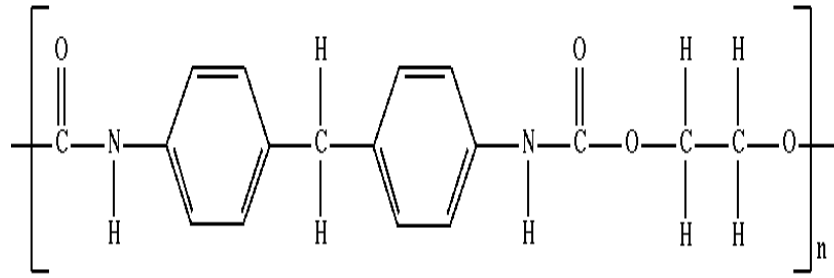


Figure 3.1: Chemical structure of polyurethane

3.1.1.2 Nylon

Nylon, a synthetic polymer, possesses excellent biocompatibility with mammalian cells and tissues and has good mechanical strength, spinnability and stability (Wang H., Li, Zuo, Li, Ma & Cheng 2007; Pant H. & Kim, 2013). Nylon nanofibres exhibit excellent mechanical properties, such as toughness and high tensile strength, and have been utilised to make various composites (Bazbouz M. & Stylios, 2012; Jiang S., Hou, Greiner & Agarwal, 2012; Sinha-Ray S., Zhang, Yarin, Davis & Pourdeyhimi, 2011; Zhang J. et al., 2012). Nylon 6/6 (pellets, molecular weight of repeat unit 262.35 g/mol, density 1.18 g/mL, laboratory grade) and formic acid (analytical grade) were purchased from Sigma-Aldrich (Poole, UK).

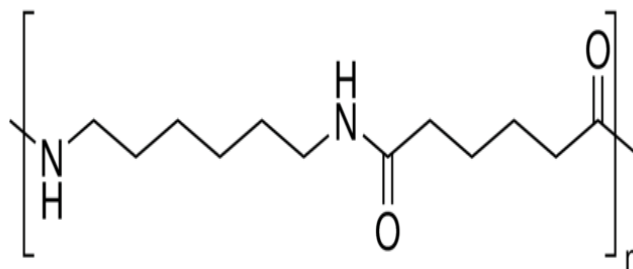


Figure 3.2: Chemical structure of nylon

3.1.1.3 Poly(ϵ -caprolactone)

PCL is one of the most promising linear aliphatic polyesters and is used extensively in the biomedical field since it is biodegradable in an aqueous medium and biocompatible in biological applications. This semi-crystalline polymer has a low melting point (60°C) and a glass transition temperature (-60°C), and therefore can be easily fabricated into any shape and size (Mohtaram N. et al., 2013; Jana S., Leung, Chang & Zhang, 2014; Catanzano O. et al., 2014). The superior rheological properties and mechanical properties of PCL has attracted interest in using this polymer in tissue engineering scaffolds, blood vessels, vascular grafts and wound healing mats (Croisier F., Atanasova, Poumay & Jerome, 2014; Wang Z. et al., 2014). The ability to blend PCL with other natural polymers, such as bacterial cellulose and cellulose acetate, makes it an excellent candidate for wound dressing scaffolds (Gea S. et al., 2010; Mi H. et al., 2014). Functionalisation of PCL with filler materials, like nanoparticles, has also shown a significant improvement in its overall properties and its flexibility in processing various architectures (Augustine R. et al., 2014). PCL ($[\text{C}_6\text{H}_{10}\text{O}_2]_n$, $M_n \sim 80000$, density = 1.145 g/ml, melt index 1g/10min) was purchased from Sigma-Aldrich (Poole, UK).

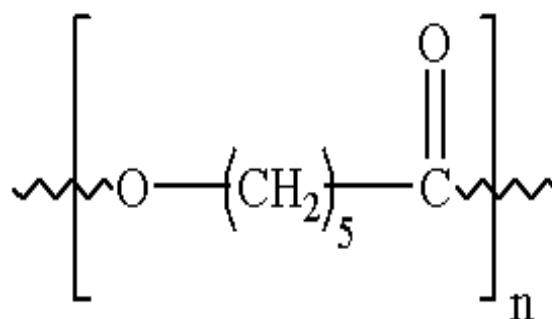


Figure 3.3: Chemical structure of poly(ϵ -caprolactone)

3.1.1.4 Chitosan

Chitosan is a special biopolymer derived from chitin and shows excellent properties besides biocompatibility and biodegradability (Pillai C. & Sharma, 2009). It is a linear and semi-crystalline polysaccharide which contains of (1→4)-2-acetamido-2-deoxy-β-D-glucan (N-acetyl D-glucosamine) and (1→4)-2-amino-2-deoxy -β-D-glucan (N-acetyl D-glucosamine) (Sun K. & Li, 2011). The degree of deacetylation of chitin to derive chitosan determines the amino groups along the polymer chain and the ratio of D-glucosamine and the sum of D-glucosamine and N-acetyl D-glucosamine (Croisier F. & Jerome, 2013). The protonation of the –NH₂ group to the main chain makes chitosan attractive for antimicrobial applications where they can inhibit the growth of a wide variety of fungi, bacteria and yeasts (Madihally S. & Matthew, 1999; Angelova et al., 1995). In addition, they can also bind and retain toxic metal ions which can be used in air cleaning and water purification applications (Sun K. & Li, 2011). chitosan is determined by the amino groups along the polymer chain and the ratio of D-glucosamine, and the sum of D-glucosamine and N-acetyl D-glucosamine. The protonation of a –NH₂ group on the main chain renders this polymer useful in antimicrobial applications, where it can inhibit the growth of wide variety of fungi, bacteria and yeasts. In addition, it can also bind to toxic metal ions and so can be used in air cleaning and water purification applications (Sun K. & Li, 2011).

The formability and spinnability of chitosan to nanofibres and nanofibrous structures are very limited owing to its polycationic nature in solution, rigid chemical structure and inter- and intra-molecular interactions. The protonation of the –NH₂ group to the main chain shows repulsive forces may also restrict the formation of sufficient chain entanglement to allow formability and spinnability (Desai K., Kit, Li, & Zivanovic,

2008). The use of solvents such as trifluoroacetic acid (TFA) and its mixtures with dichloromethane (DCM) and trichloromethane (TCM) may overcome the formability and spinnability issues, however, the major concern with this approach is working with harmful and toxic solvents which can cause health and environmental problems (Ohkawa K., Minato, Kumagai, Hayashi & Yamamoto, 2006; Schiffman J. & Schauer, 2007). Moreover, nanofibres and nanofibrous structures prepared may also contain residues which might not be safe during usage. Also nanofibres prepared with these solvents were shown to be easily dissolved in neutral and weak alkali solutions (Sangsanoh P. & Supaphol, 2006).

An alternative approach to prepare chitosan based nanofibres and nanofibrous structures is to blend them with other polymers such as polyethylene oxide (PEO), polyvinyl alcohol (PVA) and polycaprolactone (PCL) (Buraidah M., Teo, Au Yong, Shah & Arof, 2016; Chuang W., Young, Yao & Chiu, 1999; Sarasam A. & Madihally, 2005). These polymers could be easily dissolved in less hazardous and environmentally friendly solvents like water and acetone. This might overcome issues like solubility, formability and spinnability of chitosan into useful nanofibres and nanofibrous structures by creating sufficient chain entanglement and physical bonds with the blended polymers. The blending of synthetic polymer to natural polymer tend to present superior mechanical properties (tensile strength and modulus) compared to natural polymers and provide ease of processing (Buraidah M., Teo, Au Yong, Shah & Arof, 2016; Chuang W., Young, Yao & Chiu, 1999; Sarasam A. & Madihally, 2005). On the other hand, natural polymers show multifunctional bioactive properties that will enable these blends with superior performance in biological environments. They provide better interaction with the human body and show significant potential in applications in the biomedical field. For example, wound healing, tissue regeneration and engineering are well-known

applications of chitosan based blended polymer structures (Chuang et al., 2005). For this study, chitosan (medium molecular weight, viscosity 200-800 cP) was obtained from Sigma-Aldrich (Poole, UK).

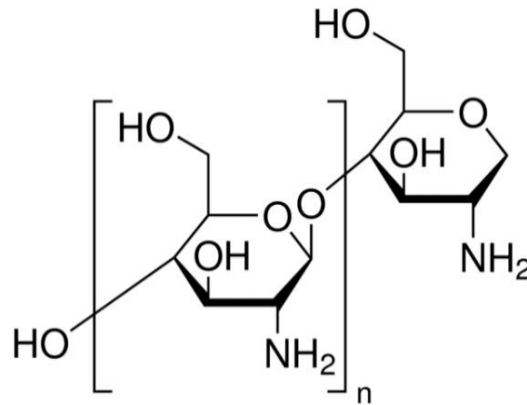


Figure 3.4: Chemical structure of chitosan

3.1.1.5 Poly(ethylene oxide)

PEO is one of the few biodegradable, biocompatible, non-toxic synthetic polymers which is soluble in both water and organic solvents and is widely used in food, cosmetics, personal care, and pharmaceutical products (Fouda M., El-Aassar & Al-Deyab, 2013). In this study, PEO (powder, M_v~200,000) was purchased from Sigma-Aldrich (Poole, UK) to produce hybrid nanofibres.

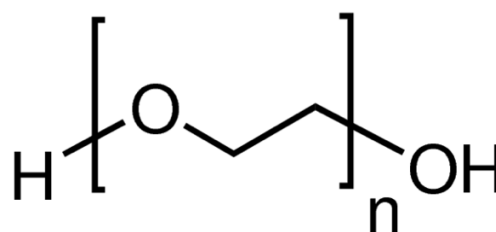


Figure 3.5: Chemical structure of poly(ethylene oxide)

3.1.2 Metal Nanoparticles

Metal nanoparticles are a class of materials which are increasingly used in many applications, including as agents for antimicrobial activity (Palza H., 2015). Such particles having a size no greater than 100 nm could impart a dramatic change in the properties of materials, for example, improved electrical conductivity, hardness, active surface area, chemical reactivity and biological activity (Mody V., Siwale, Singh & Mody, 2010). The control of infections by these antimicrobial agents primarily inhibits the growth of bacteria, viruses and fungi due to their size and the higher surface area to volume ratio. In some instances, the shape of the particles has also had an effect on the antimicrobial activity (Pal S., Tak & Song, 2007).

3.1.2.1 Silver Nanoparticles

Silver (Ag) nanoparticles show excellent antibacterial activity and have a tolerant range of cytotoxicity, with strong inhibitory and bactericidal effects (Liu Z., Zhang, Ren & Yang, 2012; Ren G., Hu, Cheng, Vargas-Reus, Reip & Allaker, 2009; Yang Z., Liu, Allaker & Reip, 2010). Ag is one of an interesting group of antimicrobials that exhibit greater thermal stability and long term activity (Williams R., Doherty, Vince, Grashoff & Williams, 1989). In addition, Ag has commanded much attention among all the antimicrobials because it not only provides intensive antimicrobial properties, but also possesses acceptable cytotoxicity towards mammalian cells and tissues (Berger T., Spadaro, Chapin & Becher, 1976). It has been reported that Ag nanoparticle embedded nanofibres showed enhanced antimicrobial efficacy against both Gram-positive and Gram-negative bacteria (Kong H. & Jang, 2008).

Ag nanoparticles have been extensively investigated as antibacterial agents (Cho K., Park, Osaka & Park, 2005; Pant H. et al., 2011; Shi Q. et al., 2011) due to the low toxicity, and strong inhibitory and bactericidal effect characteristics (Hassan et al., 2013). Aqueous silver nanoparticles (particle size < 150 nm) purchased from Sigma-Aldrich (Poole, UK) were embedded into nylon nanofibres. Silver nanoparticles (30-35% wt.%, particle size \leq 50 nm) were suspended in the organic solvent triethylene glycol monomethyl ether, which was obtained from Sigma-Aldrich (Poole, UK).

3.1.2.2 Copper Oxide Nanoparticles

Copper oxide (CuO) is a semiconducting compound with a monolithic structure and has attracted a huge interest, as it exhibits high temperature superconductivity, electron correlation effects and spin dynamics (Tranquada J. et al., 1995). Due to their narrow band gap they have been used in photocatalytic, photovoltaic and photoconductivity functions (Oku T. et al., 2011). CuO shows stable chemical and physical properties and could be prepared with unusual crystal morphologies with extremely high surface area and has shown to be an effective antimicrobial agent (Ren et al., 2009). The ease of mixing and preparation with other materials like polymers make them an ideal candidate for an antimicrobial agent. The antibacterial effect of copper oxide and zinc oxide has been previously investigated (Amna et al., 2012; Brayner et al., 2006).

CuO nanoparticles (TesimaTM) were obtained from QinetiQ Nanomaterials Ltd, Farnborough, England. Physical characterisation found that nano-scale CuO generated by thermal plasma technology, contains traces of pure Cu and Cu₂O nanoparticles. Transmission electron microscopy (TEM) demonstrated particle sizes in the range 20–95 nm (Figure 3.6). TEM energy dispersive spectroscopy gave the ratio of copper to

oxygen elements as 54.18% to 45.26%, while the mean surface area was determined to be $15.69 \text{ m}^2/\text{g}$ by Brunau–Emmet–Teller analysis (Ren et al., 2008).

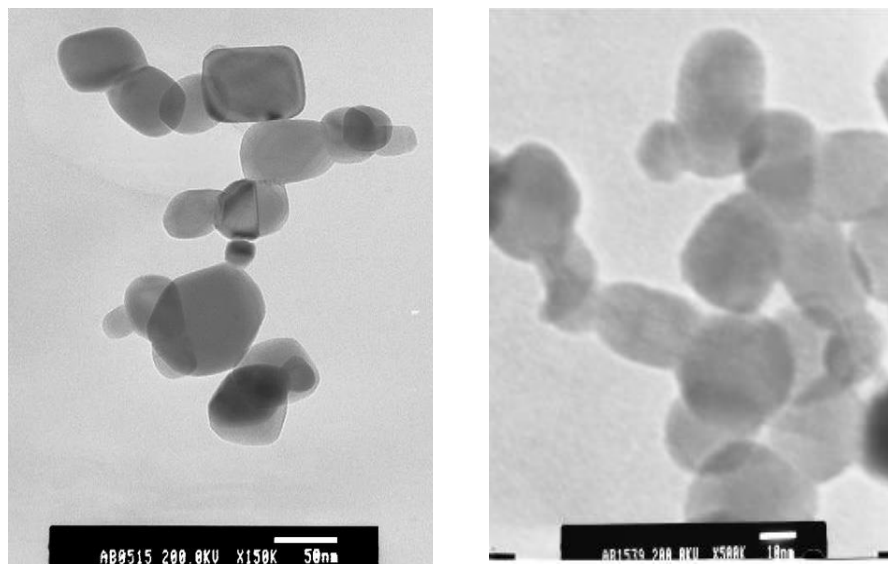


Figure 3.6: Copper oxide particles observed by transmission electron microscopy

(Ren et al., 2008)

3.1.3 Solvents for Metal Nanoparticles

Formic acid (ACS reagent, $\geq 96.0\%$) and acetic acid (99.8-100.5%) purchased from Sigma-Aldrich (Poole, UK), were used as solvents for dissolving nylon pellets and chitosan, respectively. All the reagents were used without further purification. De-ionised water (laboratory grade) was used to dissolve PEO.

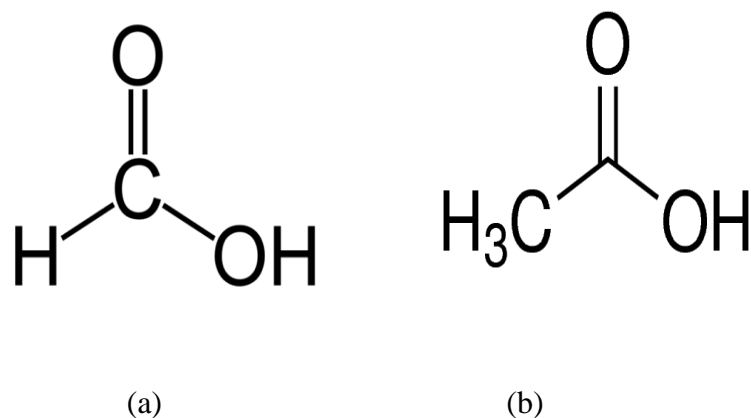


Figure 3.7: Chemical structure of (a) formic acid and (b) acetic acid.

3.2 Preparation of Solutions

3.2.1 Polyurethane Solutions

PU (5 and 10 wt.%) was dissolved in the dimethyl formamide (DMF). PU solutions containing metal oxide were also prepared: CuO (2 and 5 wt.%) and ZnO (5 wt.%) were added separately to the 10% wt.% PU solution. All of the solutions were prepared in an air-tight bottle with magnetic stirring overnight at ambient temperature ($\sim 23 \pm 1$ °C).

3.2.2 Nylon Solutions

Nylon solutions modified with functional Ag nanoparticles were prepared and used in conjunction with nylon only solutions for comparison. The polymer solutions were prepared in an air-tight bottle using formic acid as solvent to dissolve the nylon pellets under magnetic stirring for ~ 24 hours at ambient temperature (~ 20 °C). Four different concentrations of nylon (5, 10, 15, and 20 wt.%) were prepared.

Ag containing nylon solutions were prepared by adding 1wt.% of aqueous silver nanoparticle suspension to the nylon solutions. These were also prepared using a magnetic stirrer in an air-tight bottle at the ambient temperature. Similarly, 2wt.% and 4wt.% Ag nanoparticle containing nylon solutions were prepared for making nanofibers and these were only tested for Ag-ion release in aqueous solution.

3.2.3 Poly(ϵ -caprolactone)

PCL pellets and Ag coated PCL pellets were used directly because fibres produced by pressurised melt gyration do not require solvents as they form a polymer melt in a gyrating pot. Ag coated PCL pellets were obtained by immersing and soaking in Ag nanoparticle solution using the organic solvent triethylene glycol monomethyl ether at ambient temperature for 5 hours.

3.2.4 Poly(ethylene oxide) Solutions

PEO powder was dissolved in de-ionised water to obtain 10 and 15 wt.% PEO solutions with magnetic stirring for ~24 hours at ambient temperature (~20°C). Ag nanoparticles (2 and 5 wt.%) and CuO nanoparticles (5 wt.%) were mixed into the PEO solutions and stirred overnight.

3.2.5 Chitosan-Poly(ethylene oxide) Blend Solutions

Chitosan-PEO blend solutions were prepared by mixing 1 wt.% or 2 wt.% chitosan solution with 20 wt.% PEO solution. 0.1 M acetic acid solution was used as the solvent to dissolve the chitosan under magnetic stirring while heating at 60°C for 5 hours. PEO

powder was dissolved in de-ionised water in an air-tight bottle under magnetic stirring for ~24 hours at ambient temperature (~20°C) to make the PEO solutions. The PEO/chitosan solutions were mixed with a ratio of 4:1 by weight. Ag and CuO containing PEO/chitosan solutions were prepared by adding aqueous silver nanoparticle suspension (0.5 and 1 wt.%) and CuO nanopowder (1 wt.%) to the 20 wt.% PEO-1 wt.% chitosan solutions, respectively.

3.3 Gyration Set up and Materials for Polymer Fibre Fabrication

3.3.1 Pressurised Gyration

The experimental set up of the pressurised gyration process is shown in Figure 3.8. It consisted of a rotary aluminium cylindrical vessel containing 20 small round orifices on the surface. The dimensions of the vessel were diameter 60 mm, height 25 mm, and the orifices have a diameter of 0.5 mm. One end of the vessel was joined to a pressurised nitrogen cylinder through a rotary joint which can provide an inlet pressure of up to 0.6 MPa. The base of the vessel was connected to a DC motor which could produce variable speeds of up to 36,000 rpm. Because of the centrifugal force and the dynamic fluid flow through the orifices, the jet formed by the high rotation speed was elongated when it came out via the orifices and subsequently the solvent evaporated to form solid nanofibres. The device was placed in a transparent plastic container in order to conveniently collect the polymer fibres. The polymer nanofibres were collected using stationary aluminium foil within the container.

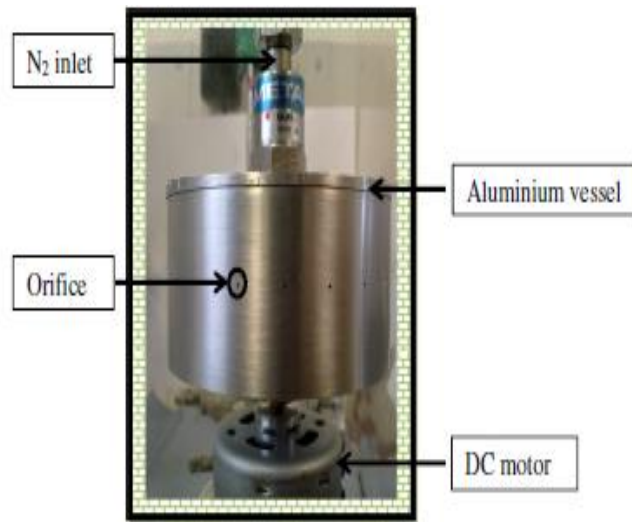


Figure 3.8: Experimental set-up of the pressurised gyration process

3.3.2 Pressurised Melt Gyration

Pressurised melt gyration is a novel process that could provide a new pathway for solvent-less spinning of polymer fibres with high throughput. As shown in Figure 3.9 which was captured using a high-speed camera, it involves melting a polymer in a rotating vessel and forcing the polymer melt through narrow orifices under the influence of centrifugal force and dynamic fluid flow. The rotating aluminium vessel had 20 orifices (each orifice had a diameter of 0.5 mm) on its face and had heating elements built into it. The temperature of the gyration vessel could be elevated up to 600°C and was monitored and controlled using an *in situ* thermocouple; the accuracy of the temperature measurement was $\pm 5^{\circ}\text{C}$.

The molten polymer was subjected to a high vortex during the rotation causing liquid jets to eject from the orifices. When the withholding surface tension force that tends to

restrict molten polymer flow is overcome by centrifugal force and dynamic fluid flow forces (due to pressurised gas), ejection of the jets occurs. The stretching of liquid jets was attenuated by the centrifugal force in the rotating axis before rapid solidification of the fibres occurred at the collector around the vessel. The solidification of the fibres was also assisted by the dynamic fluid flow through the orifices.

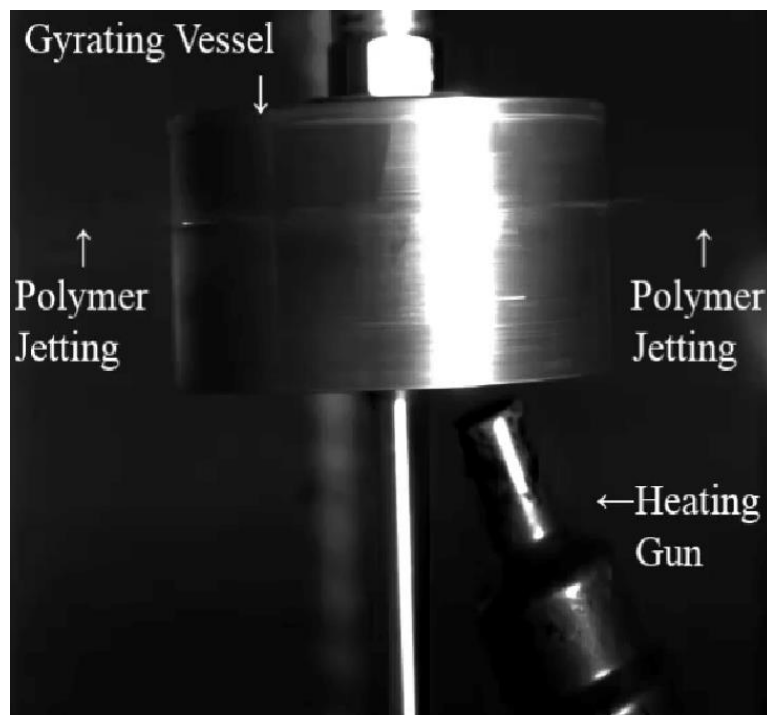


Figure 3.9: Experimental set-up of the melt-pressurised gyration process

3.4 Preparation of Solutions for the Fabrication of Hybrid Fibres

3.4.1 Polyurethane, Copper Oxide and Zinc Oxide Loaded

Polyurethane Nanofibres

CuO (2 and 5% wt.), and ZnO (5 and 10 wt.%) solutions were added to 10 wt.% PU solution and used to fabricate PU system nanofibres using the pressurised gyration

process at a rotating speed of 36,000 rpm and an added working pressure of 0.1 MPa at ambient temperature (22-24°C).

3.4.2 Nylon Solutions and Silver Loaded Nylon Nanofibres

Pressurised gyration was used to produce nylon and Ag-loaded nylon nanofibres. In order to investigate the nanofibre diameter and size distribution under different conditions, prepared polymer solutions were spun at three different rotating speeds (36,000 rpm, 24,000 rpm and 10,000 rpm) under a constant working pressure (0.1 MPa), and also at 0.2 MPa and 0.3 MPa working pressure under a constant rotating speed (36,000 rpm) at ambient temperature (22-24°C).

3.4.3 Poly(ϵ -caprolactone) and Silver Coated Poly(ϵ -caprolactone)

Fibres

PCL fibres were created using a custom-made melt pressurised gyration apparatus contained within a perspex enclosure. The rotating aluminium vessel has 20 orifices (each orifice is 0.5 mm diameter in size) on its face and has heating elements built on it. The temperature of the gyration vessel can be elevated upto 600°C. The temperature is monitored and controlled using an *in-situ* thermocouple. The accuracy of the temperature measurement was $\pm 5^\circ\text{C}$. Before loading the PCL pellets on to the vessel a stable temperature was attained by heating the gyration vessel for five minutes at a specified temperature. This facilitated up keep of temperature homogeneity across the vessel and stable spinning of PCL scaffolds. The maximum rotating speed and the working pressure of the melt pressurised gyration is 36000 rpm and 0.3 MPa,

respectively. In this work PCL scaffolds were obtained at four different temperatures (95, 125, 155 and 200°C) at various rotating speeds and working pressures.

Ag loaded PCL fibres were processed using Ag coated PCL pellets spun at different temperatures. These were obtained by immersing and soaking the PCL pellets in Ag nanoparticle solution using organic solvent triethylene glycol monomethyl ether at the ambient temperature (~23°C) for 5 hours. The melt spun Ag loaded PCL scaffolds were also coated with Ag nanoparticles using a gyratory vessel rotating at a speed of 36,000 rpm. 0.01% (v/v) Ag nanoparticle solution was made using organic solvent triethylene glycol monomethyl ether and distilled water. A homogenous solution was obtained after magnetically stirring for 1 hour at ambient conditions (temperature ~23°C and relative humidity ~45%). After coating, the Ag-PCL scaffolds were dried in a desiccator before their antibacterial properties were evaluated.

3.4.4 Poly(ethylene oxide), Silver and Copper Oxide Embedded

Poly(ethylene oxide) Nanofibres

Ag nanoparticle (2 wt.%) solution was added to PEO solutions (10 and 15 wt.%), while CuO nanoparticle (2 and 5 wt.%) solution was mixed into 15 wt.% PEO solution before spinning at a rotary speed of 36,000 rpm under three different working pressures (0, 0.1 and 0.2 MPa) and ambient temperature (22-24°C) using pressurised gyration to investigate the properties of the resulting nanofibres.

3.4.5 Chitosan-Poly(ethylene oxide) Blend, Silver and Copper Oxide

Embedded Chitosan-Poly(ethylene oxide) Blend Nanofibres

PEO (20 wt.%) solution was blended with chitosan (1 and 2 wt.%) and nanofibres were obtained by utilising the pressurised gyration process spun at same conditions as for other PEO solutions. Ag (0.5 wt.%) and CuO (1 wt.%) nanoparticles loaded onto PEO/chitosan fibres were mainly used in antibacterial activity studies.

3.5 Characterisation of Polymer Solutions

3.5.1 Physical Properties

Physical properties of solutions, such as surface tension and viscosity are crucial in pressurised gyration fibre forming (Mahalingam & Edirisinghe, 2013). The surface tension and viscosity of all the solutions, which govern the pressurised gyration process, were measured using a KRUSS tensiometer K9 (Wilhelmy's plate method) and a Brookfield viscometer, respectively, at ambient temperature.

The plate was hung from a hook and a sample was placed on the stage below. The surface tension of a sample was measured by completely immersing the plate into the solution and then gradually lifting it up. The reading for the surface tension of a sample was recorded at the point when the plate just detached from the surface of the liquid. Five measurements were taken to obtain the mean value.

For the viscosity of solutions, an appropriate spindle was put inside the solutions with a rotational speed, and the accuracy of measurement depend upon the torque required to

turn an object in a fluid. Five readings were measured consecutively and a mean value should be calculated for each sample.

3.5.2 Scanning Electronic Microscopy

The characteristics of polymer fibres were usually studied using field emission scanning electron microscopy (FE-SEM), energy dispersive x-ray spectroscopy (EDX) and focussed ion beam microscopy (Carl Zeiss –Gemini). The SEM can be used to study morphological features such as size and size distribution of the fibres. This can be backed up by EDX to study chemical features in the fibres. SEM assesses electron beam impact on the surface of a sample; electron beams with specific energy levels cannot directly pass through a sample, but are high enough to strike and excite the outer electrons of atoms on the sample surface (Kumar, 2009). SEM with EDX (SEM/EDX) is the best known and most widely-used surface analytical technique. High resolution images of surface topograph, with excellent depth of field, are produced using a highly-focused, scanning (primary) electron beam. The primary electrons enter the surface with an energy of 0.5 – 30 kV and generate many low energy secondary electrons (Joseph et al., 1992; John, 2003). Images were obtained from the secondary electrons when the nanofibre samples were coated with gold using a sputtering machine (sputter time ~150s) before loading into the microscope, which was worked at 3 kV. High and low magnification images were acquired at randomly selected positions (more than 20 different ones). The fibre diameter was obtained using Image J software, and around 150 measurements were made at random locations to plot the fibre diameter distribution.

3.5.3 Raman Spectra

The Raman spectroscopy as a characterisation tool is used to provide structural, purity, morphology and electronic information of the nanofibres. It is an excellent analytical performance tool with high resolution, and is fast and non-destructive. It can be used in various fields, physics, engineering, chemistry and biology. Many papers report the results of Raman spectra on inorganic materials every year (Duesberg et al., 2000; Ferrari et al., 2007). In this type of project, Raman spectra can be used to study the bonding characteristics of polymer and the Ag nanoparticles.

Raman spectroscopy was used for the Ag-loaded polymer fibres to identify the silver nanoparticles and polymer fibrous structures. Raman spectra of polymer and Ag-loaded polymer samples were obtained using a Renishaw Raman microscope excited with an incident wavelength radiation of 514.5 nm. The data acquisition covered the spectral range 2000-100 cm^{-1} with a spatial resolution of 4 cm^{-1} .

3.5.4 Inductively Coupled Plasma Mass Spectroscopy (ICP-MS)

As a powerful analytical technique, inductively coupled plasma-mass spectrometry (ICP-MS) was widely applied in geo-sciences in last few decades (Jenner et al., 1990). The ICP-MS can investigate problems in matrix, drift and interference areas. Recently, the ICP-MS is also used in ion-molecule chemistry for high performance elemental analysis.

The Ag ion released from Ag-loaded nanofibrous mats was tested using inductively coupled plasma mass spectroscopy (ICP-MS, Agilent, Japan) at ambient temperature.

Prepared samples were cut into an appropriate size and washed in de-ionised water (30 ml) for 24, 48 and 72 hours before immersing in 1% v/v nitric acid (HNO₃). For comparative and calibration purposes the de-ionised water and nitric acid was also screened using ICP-MS for ion content. Thus, the Ag ion concentration was quantified in the releasing medium and three measurements were made for each sample.

3.5.5 Differential Scanning Calorimetry

All differential scanning calorimetry (DSC) studies were conducted on a TA Instruments Q2000 unit (Newcastle, DE, USA) with a refrigerated cooling system attached and an accompanying dry nitrogen sample purge flow at 50 mL/min. Calibrations were performed using indium, *n*-octadecane, and tin; heat capacity constant calibration was performed using aluminium oxide TA sapphire discs at 2 °C/min with ± 0.212 °C modulation amplitude over a 60s period. All DSC experiments and calibrations were performed using a TA Instruments Tzero pan with an accompanying Tzero lid. Modulated Temperature DSC (MTDSC) experiments were conducted on all samples (i.e. PCL starting material and PCL PMG fibres), heating at 2°C/min with ± 0.212 °C modulation amplitude over a 60s period (over an appropriate temperature range). All experiments were conducted in triplicate. The data obtained was analyzed using the TA Instruments Universal Analysis 2000 software for Windows 2000/XP/Vista Version 4.7A.

3.5.6 UV/vis Spectroscopy

UV/vis spectroscopy (Perkin Elmer) was used to study the Ag ion release from PCL-Ag composite fibrous mats. For this purpose 100 mg of PCL-Ag mats spun at different temperatures were loaded into 10 ml de-ionised water and magnetically stirred at the ambient temperature. At a certain time interval 3ml solutions were taken and analysed in the wavelength range 300-700 nm. A PCL scaffold without Ag coating in de-ionised water was used as the control solution. Initially, a calibration curve was obtained for Ag ion concentrations and absorbance values. Various concentrations of Ag ion in de-ionised water was scanned in the wavelength range 300-700 nm and used to fit the calibration curve. This curve was used to measure the concentration (g/l) of Ag ion release in de-ionised water at a certain time interval.

3.5.7 Antibacterial Testing

In order to investigate the antibacterial activities of nylon and Ag-loaded nanofibres, standard antibacterial performance tests were conducted. The Gram-negative bacteria, *E. coli* (in-house strain number 3891) and *P. aeruginosa* (strain 25-09071215-05, a kind gift from Sanchutha Santhianamoorthy) were obtained from the Centre for Clinical Science and Technology, Division of Medicine, UCL. Bacterial broth suspensions were co-cultured under aerobic conditions with the samples for set periods of time, after which the number of viable colony-forming units (CFU) was determined and then the antibacterial rate for each sample calculated.

The assay was performed using bacteria cultured overnight from a single colony to stationary phase (approximately 10^9 CFU/ml) in Luria-Bertani (LB) broth or tryptic soy

broth (TSB) in a shaking aerobic incubator at 37°C. Next, a suspension of approximately 5×10^5 CFU/ml in LB or TSB was prepared for use as the experimental bacterial suspension. Working in a sterile laminar flow hood environment, the same weight of nanofibre samples (0.02 g) with a similar volume of nanofibres (0.02 ml) was placed using sterile tweezers into each well of a 24-well tissue culture plate (Corning) along with 0.5 ml of the experimental bacterial suspension of either *E. coli* or *P. aeruginosa*. Wells with media alone containing no bacteria were used as a negative control. The plates were cultured in an aerobic shaking incubator at 37°C for 2 hr and 24 hr. After co-culturing with the samples, the bacterial suspensions were diluted (1:2, 1:10, 1:100 and 1:1000) into sterile tubes, and 0.02 ml of each dilution was applied evenly onto quadrants of chromogenic agar plates (chromID CPS, Biomerieux) for enumeration using sterile L-spreaders. Chromogenic agar allows the confirmation of bacterial species by colony colour. The plates were incubated overnight at 37°C for 24 hr. Finally, the number of bacteria colonies (CFU) on each quadrant was counted to evaluate the effect of the original sample on the survival of the bacteria. In this test, culture medium without bacteria was used as the negative control.

The antibacterial rate of an antibacterial material can be determined by:

$$AR (\%) = [(N_1 - N_2) / N_1] \times 100$$

Where AR is the antibacterial ratio (%), N_1 is the bacterial count of the negative control, and N_2 is the bacterial count of the antibacterial nanofibres (Liao et al., 2010).

Chapter 4 - Fabrication of Polyurethane and Nylon Nanofibres Using Pressurised Gyration

4.1 Introduction

The pressurised gyration process to produce hybrid nanofibres combined both polymer and metallic nanoparticles for the very first time. In order to understand the key factors which affect the diameter and surface morphology of hybrid nanofibres, PU nanofibres were investigated first. The diameter of the nylon nanofibres produced varied with different polymer concentrations, different vessel rotating speed and different working pressure. It was shown that all of these conditions had a significant influence on the diameter and the morphology of nylon nanofibres. Moreover, the Ag ion release concentration into a stock solution of nitric acid after several repeated washing cycles in de-ionised water were investigated by ICP-MS, showed that the Ag ion concentration in the solution reduces after each washing cycle. Finally, the antibacterial activity of Ag-loaded nylon nanofibres exhibited a much higher antibacterial rate compared to nylon nanofibres for Gram-negative *E. coli* and *P. aeruginosa* microorganisms.

4.2 Analysis of the Polyurethane System

Figure 4.1 (a) and (b) show the plots of PU fibre diameter for the 36,000 rpm rotating speed at 0.1 MPa working pressure. It can be clearly seen that the fibre diameter reduced with decreasing weight percentage of the polymer or the weight percentage of the metal oxide. Similarly, the fibre diameter reduced from 150 nm to 120 nm when the weight percentage of PU was decreased from 10 wt.% to 5 wt.%. Likewise, when the concentration of copper oxide changed from 5 wt.% to 2 wt.% the fibre diameter reduction was from 211 nm to 123 nm. This is due to the higher weight percentage of the polymer and the higher viscosity of the polymer solution, which slowed the solvent evaporation for thicker fibres (Mahalingam & Edirisinghe, 2013).

In addition, the fibre diameter for 5 wt.% zinc oxide doped in 10 wt.% PU solution was 208 nm. However, during the spinning process, these polymer solutions formed fibres at the higher speed (36000 rpm) and 0.1 MPa working pressure, but decreasing the rotating speed reduced the centrifugal force and led to only polymer bead formation at lower speeds (i.e. 24000 and 10000 rpm).

Figure 4.1 (c) is a SEM image of one type of polymer nanofibre. The uneven fibre surface may be due to polymer particles or metallic particles that were not totally dissolved or due to polymer bead (bead on string) formation during the spinning process.

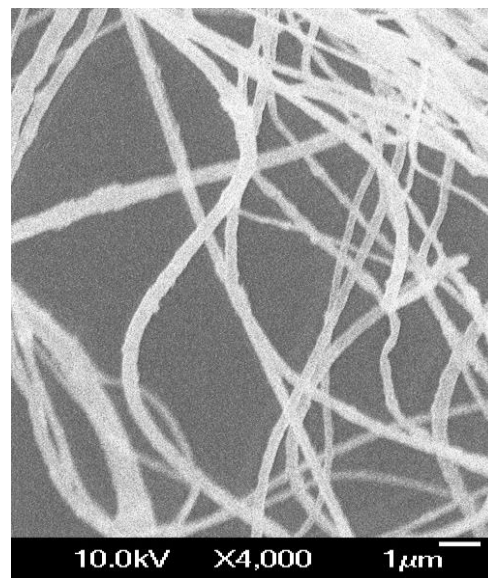
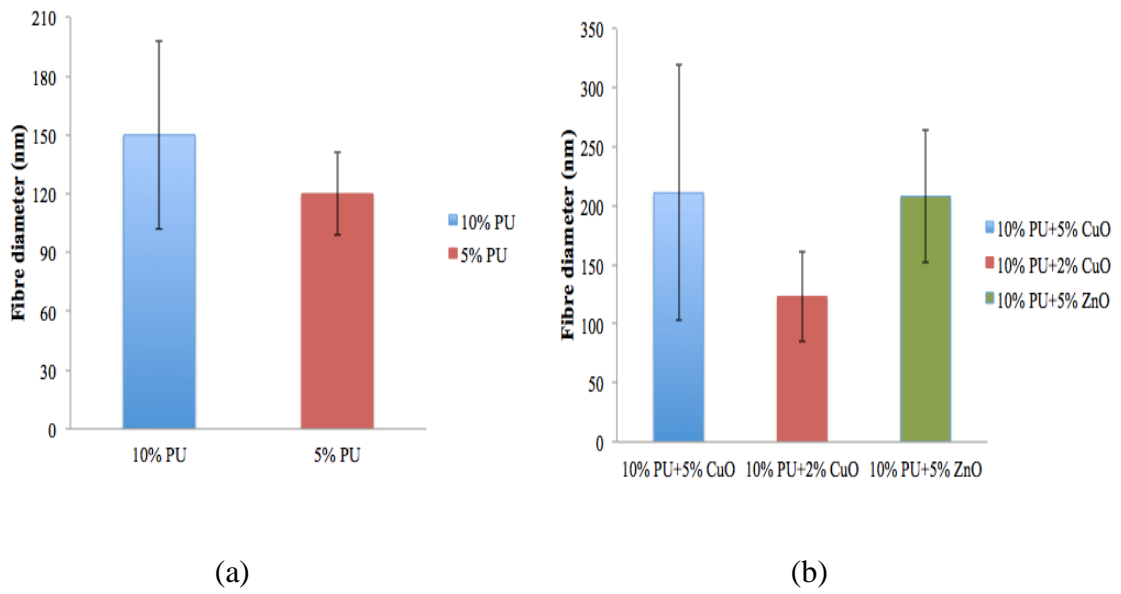
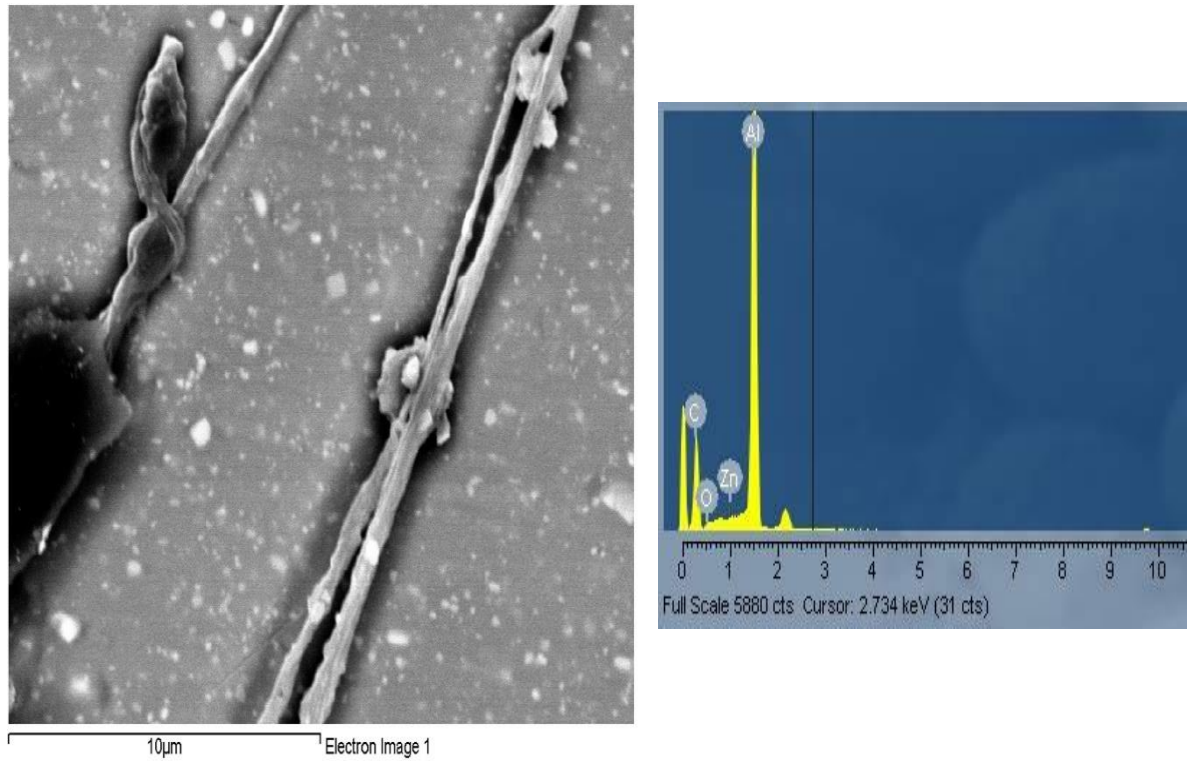


Figure 4.1: Analysis of polyurethane fibres fabricated by pressurised gyration

(a) Fibre diameter variation with a 36,000 rpm rotating speed and 5 and 10 wt.% PU at 0.1 MPa working pressure. (b) Fibre diameter variation at 36000 rpm rotating speed for 5 and 2 wt.% of CuO, and 5 wt.% ZnO added to 10 wt.% PU solution at 0.1 MPa working pressure. (c) SEM image of the fibres formed from 5 wt.% CuO added to 10 wt.% PU solution.

EDX analysis was also carried out during this investigation. However, the concentration of the zinc oxide was too low so that it was difficult to identify any metallic particles present on the nanofibres (Figure 4.2).



Element	Weight%	Atomic%	Compd%	Formula
C K	26.93	33.17	98.68	CO2
Zn L	1.06	0.24	1.32	ZnO
O	72.01	66.59		
Totals	100.00			

Figure 4.2: EDX analyses for PU and zinc oxide fibres

Due to the lack of polyurethane supply, and the better antibacterial ability of silver nanoparticles, it was decided to move away from this system and to develop the nylon and Ag-loaded nylon system and these results are discussed below.

4.3 Physical properties of nylon solutions

In pressurised gyration, a typical parametric plot of rotating speed and working pressure of processing solution and the mode of material discharge differs from one region to the other (Mahalingam et al., 2014). The physical properties of polymer solutions significantly influence the jet formation and subsequent structural formation during pressurised gyration.

Table 4.1: Measured values of surface tension and viscosity for nylon solutions

Nylon system solutions	Surface tension (mN/m)	Viscosity (mPa s)
5wt.% Nylon	38.33(±2.4)	53.54(±0.3)
10wt.% Nylon	42.72(±2.7)	236.92(±0.7)
15wt.% Nylon	52.09(±2.5)	461.12(±2.7)
20wt.% Nylon	73.45(±3.4)	2016.4(±14.6)
5wt.% Nylon + 1 wt.% Ag	38.18(±0.9)	29.82(±0.2)
10wt.% Nylon + 1 wt.% Ag	41.34(±1.2)	181.14(±2.1)
15wt.% Nylon + 1 wt.% Ag	49.69(±3.2)	245.6(±2.7)
20wt.% Nylon + 1 wt.% Ag	66.4(±5.2)	924.85(±5.0)

The surface tension and viscosity of nylon solutions increased with solute content (Table 4.1). For 20 wt.% nylon, the surface tension was ~73 mN/m which is nearly double the value of 5 wt.% nylon solution. The viscosity of 20 wt.% nylon solution was ~2016 mPa s which was an order of magnitude higher than that of the value at 10 wt.% nylon. Similarly, the surface tension and viscosity were increased with the solute

content in the Ag-loaded nylon solutions. For a given molecular weight, the increase of viscosity with the solute content was due to an increase of chain entanglement in the polymer solution where the polymer chains overlap each other to form a strong network. At the low concentration, low viscosity was observed due to insufficient chain entanglement as a result of lack of physical interlocking of chains (Shenoy et al., 2005).

4.4 Fibre diameter analysis

Figure 4.3 (a) and (b) show the plots of fibre diameter against the rotating speed for 10, 15 and 20 wt.% of nylon solutions with 1 wt.% Ag nanoparticles dispersed in the solutions under a fixed working pressure of 0.1 MPa. It was clearly demonstrated that the fibre diameter is reduced with an increase in rotating speed of the vessel. For 20 wt.% nylon solution the fibre diameter was reduced from 470 nm to 303 nm when the rotating speed changed from 24000 rpm to 36000 rpm. Similarly, a gradual reduction of fibre diameter is observed for 15 wt.% of nylon solution. The fibre diameter was reduced from 385 nm to 231 nm when the rotating speed increased from 24000 rpm to 36000 rpm. However, the fibre diameter was not significantly affected by increase of rotating speed for 10 wt.% of nylon solution. For 20 wt.% and 15 wt.% Ag-loaded nylon solutions, the variation of rotating speed had a remarkable influence on fibre diameter (Figure 4.3b). Here, the fibre diameter was reduced from 161 nm to 140 nm and 139 nm to 103 nm when the rotating speed increased from 10000 rpm to 36000 rpm for 20 wt.% and 15 wt.%, respectively. Again, for the 10 wt.% Ag-loaded nylon solution, the fibre diameter produced was not significantly changed with rotating speed and the obtained value was ~90 nm. This is likely to be due to low viscosity of polymer solution and rapid evaporation of solvent during the spinning process. Moreover, there are only

polymer beads were generated with the 5 wt.% nylon solution and Ag-loaded nylon solution at 0.1 MPa working pressure.

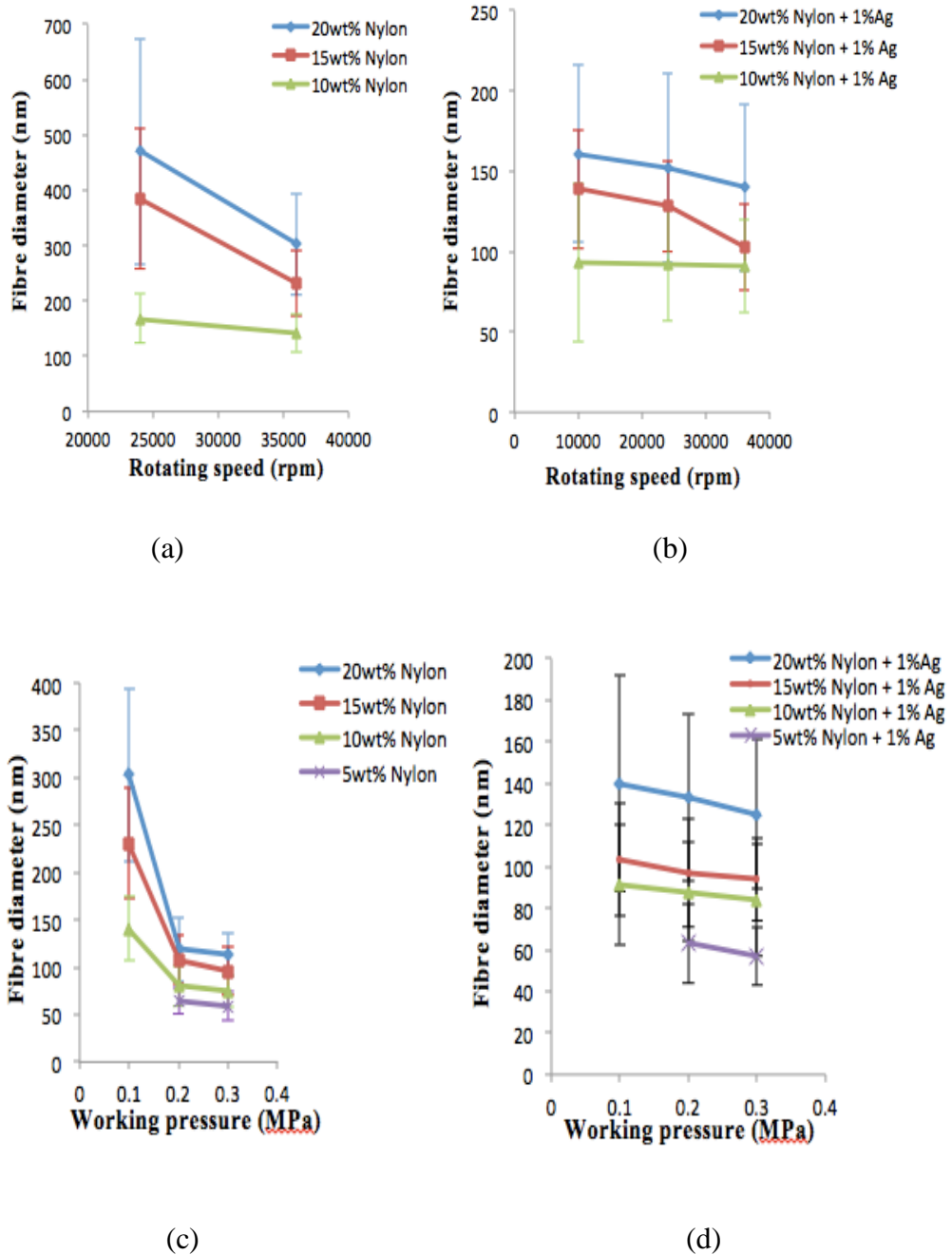


Figure 4.3: Fibre diameter variation for 5, 10, 15 and 20 wt.% of nylon and nylon with Ag nanoparticle incorporation (a), (b) varying rotating speed at a constant working pressure of 0.1MPa. (c), (d) varying working pressure at a fixed rotating speed of 36000 rpm.

Figure 4.3 (c) and (d) show the graphs of fibre diameter variation with working pressure for pressurised gyration at a fixed rotating speed of 36000 rpm for nylon and Ag-loaded nylon polymer solutions, respectively. A fibre diameter in the range of 59 nm to 303 nm was observed for the nylon samples, and the fibre diameter was in the range of 57 nm to 140 nm for Ag-loaded nylon samples in the fibre fabrication. It is clearly seen that increase of the working of pressure dramatically reduced the fibre diameter. For 20 wt.% nylon solution the fibre diameter was reduced from 303 nm to 113 nm on the increasing the working pressure from 0.1 MPa to 0.3 MPa at a rotating speed of 36000 rpm. Similarly, the fibre diameter was reduced from 231 nm to 96 nm and 141 nm to 75 nm for 15 wt.% and 10 wt.% nylon solutions, respectively. The 5 wt.% nylon solution formed fibres at higher working pressures (0.2 MPa and 0.3 MPa) compared to lower working pressure. It is an interesting observation and associated with how the pressure difference at the orifice couples with centrifugal force to initiate the fibre formation. Similarly, the Ag-loaded nylon solutions also showed a reduction of fibre diameter with working pressure.

The change in fibre diameter is influenced by the combined effects of concentration of polymer, the vessel rotating speed and the working pressure and these are summarised in Table 4.2. Firstly, there is a definite possibility that higher the polymer concentration, the larger fibre diameter generated, because a higher weight percentage of the polymer impacts higher viscosity and a lower solvent evaporation rate to the polymer solution. Secondly, the lack of centrifugal force and shear force at a low rotation speed can lead to a higher time constant of forces on the polymer solution, subsequently this results in a longer viscous response of the polymer solution to form thicker fibres. Thus, increasing the rotation speed will reduce the polymer fibre diameter. Meanwhile, at low polymer concentrations, in order to form fibres a minimum rotating speed is required to

ensure the critical value of viscous response is reached (Mahalingam & Edirisinghe, 2013). Hence, there are only beads formed at low rotating speed in the low concentration polymer solutions, but this situation can be changed by increasing the working pressure.

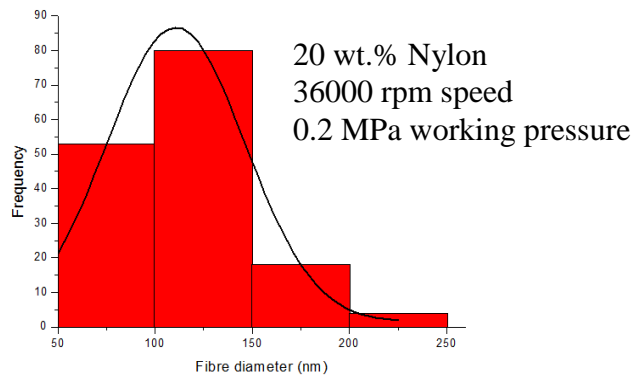
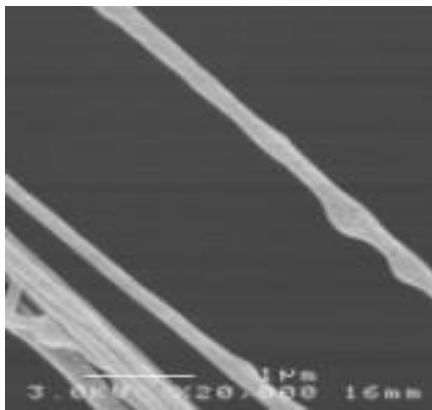
Table 4.2: Fibre diameter variation for different conditions of pressurised gyration

Nylon + Ag nanoparticles Loading	Fiber Diameter (nm) at Rotating Speed (rpm), Working Pressure (MPa) combinations				
	10000, 0.1	24000, 0.1	36000, 0.1	36000, 0.2	36000, 0.3
5 wt.% + 0 wt.%	–	–	–	65 (±14)	59 (±15)
10 wt.% + 0 wt.%	–	168 (±44)	141 (±34)	80 (±21)	75 (±17)
15 wt.% + 0 wt.%	–	385 (±127)	231 (±59)	108 (±26)	96 (±25)
20 wt.% + 0 wt.%	–	470 (±204)	303 (±92)	119 (±34)	113 (±23)
5 wt.% + 1 wt.%	–	–	–	63 (±19)	57 (±14)
10 wt.% + 1 wt.%	93 (±49)	92 (±35)	91 (±29)	88 (±24)	84 (±27)
15 wt.% + 1 wt.%	139 (±37)	128 (±28)	103 (±27)	97 (±26)	94 (±20)
20 wt.% + 1 wt.%	161 (±55)	152 (±59)	140 (±52)	133 (±40)	125 (±36)

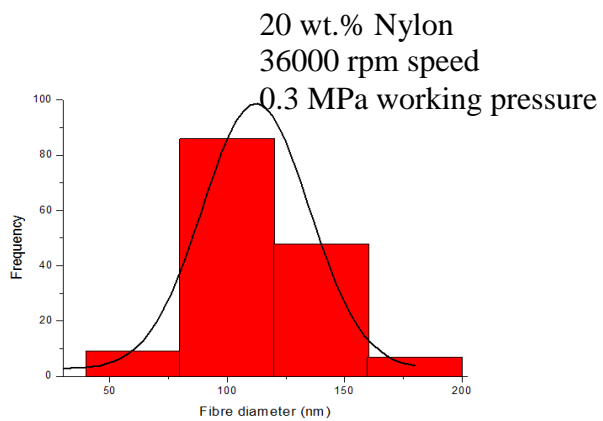
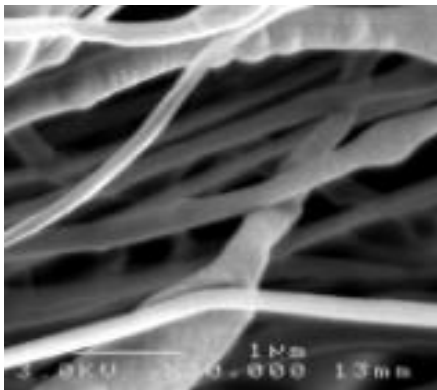
Figure 4.4 displays the SEM images for the 20 wt %, 15 wt.%, 10 wt.% and 5 wt.% of nylon fibres obtained under different working pressure at 3600 rpm speed and the corresponding fibre diameter distribution. The fibres have straight, smooth and cylindrical morphology and they are bead-free in all instances. Previous electrospinning work has shown that higher viscosities favour bead free thicker fibres but increased surface tension encourages the formation of beaded fibres (Fong, Chun & Reneker,

Chapter 4 – Polyurethane and Nylon Nanofibres

1999). The increase of nylon solution concentration increased the viscosity of the polymer solution rapidly and was the main parameter controlling morphology of the formed fibres. It is also noteworthy that in dilute polymer solutions the polymer molecules have coil-like conformation and can be visualised as separated spheres. However, in the concentrated regime they form macromolecular entanglement which are crowded and touch with each other (Huang et al., 2006). Thus, increase of the viscosity promotes the occurrence of bead-free smooth fibre morphologies.

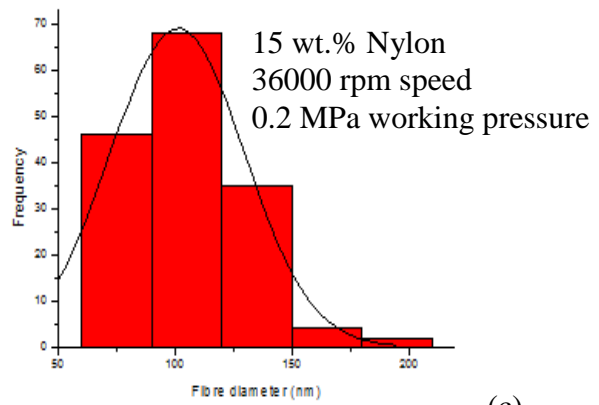
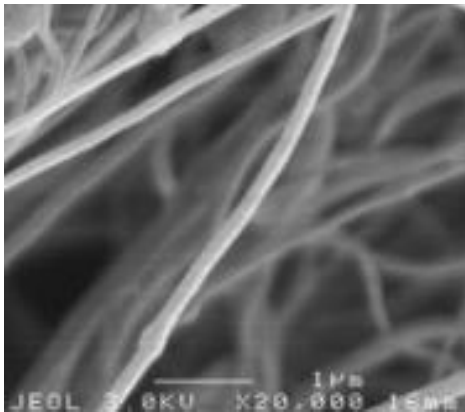


(a)

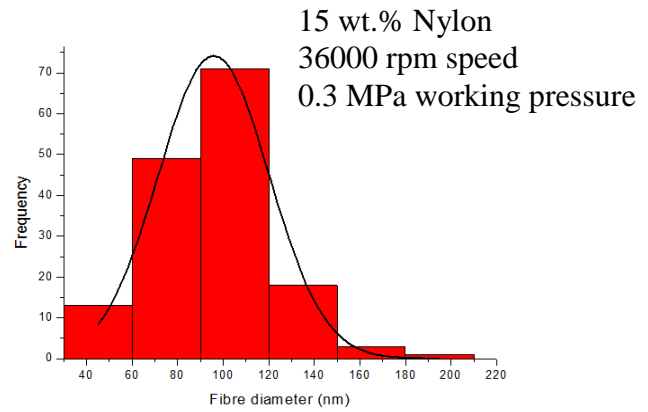
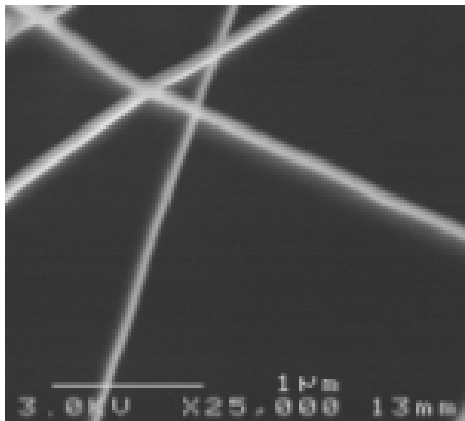


(b)

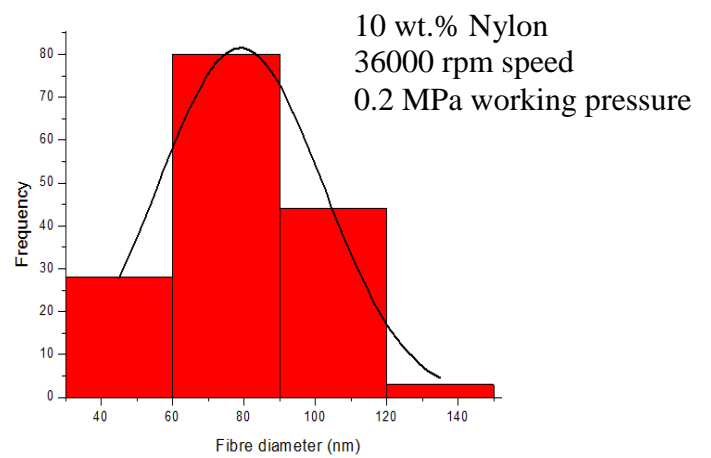
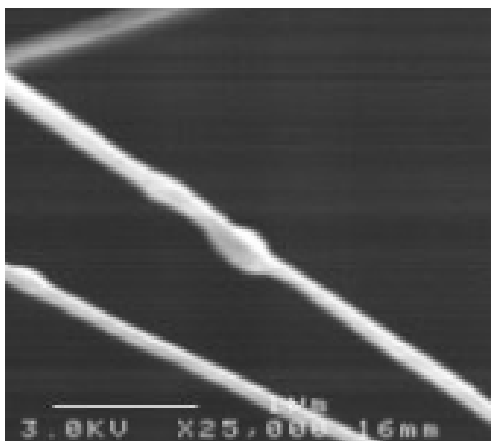
Chapter 4 – Polyurethane and Nylon Nanofibres



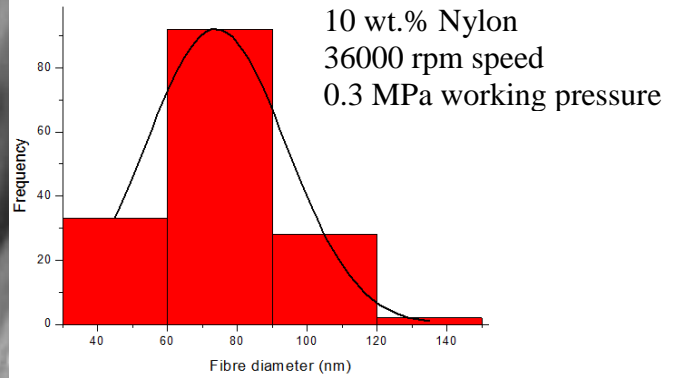
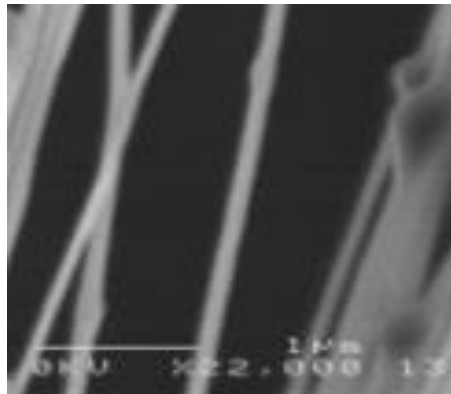
(c)



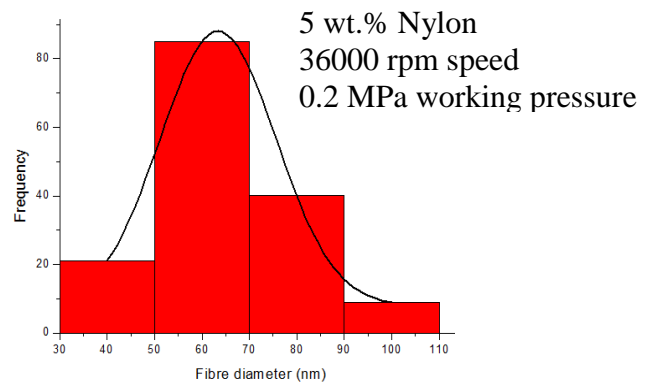
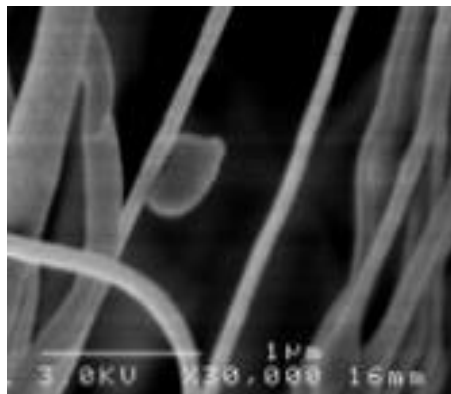
(d)



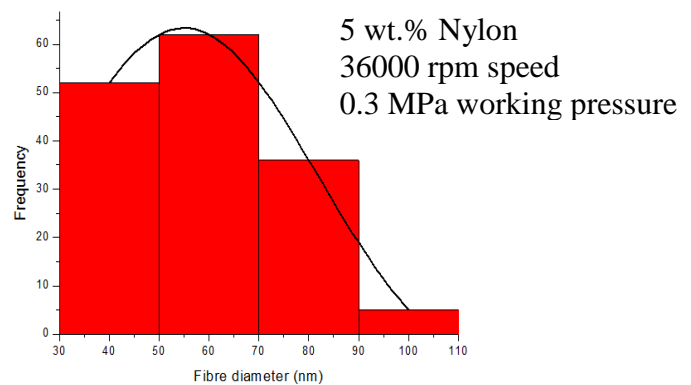
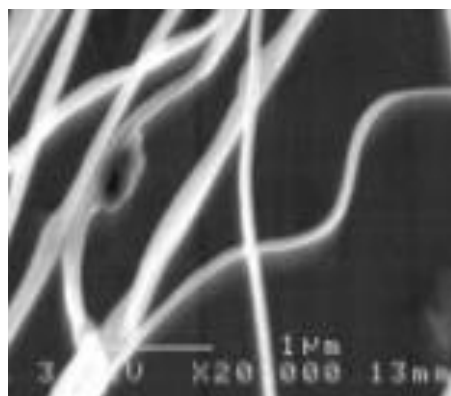
(e)



(f)



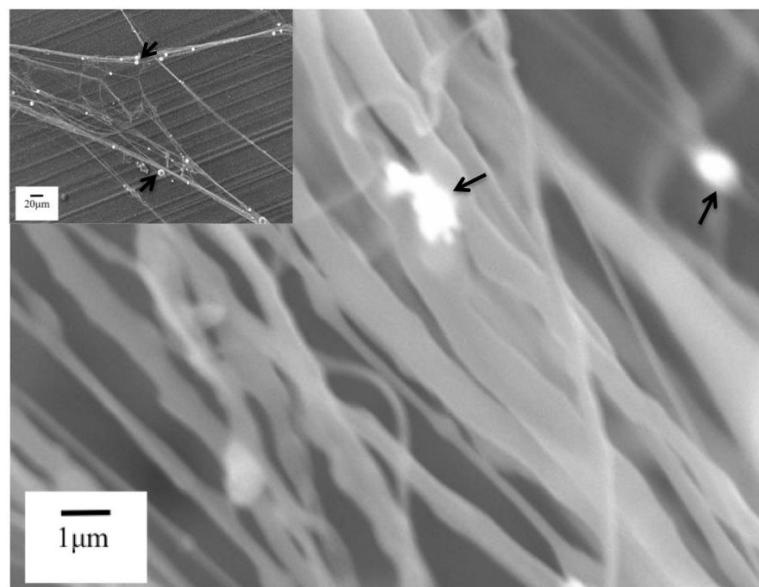
(g)



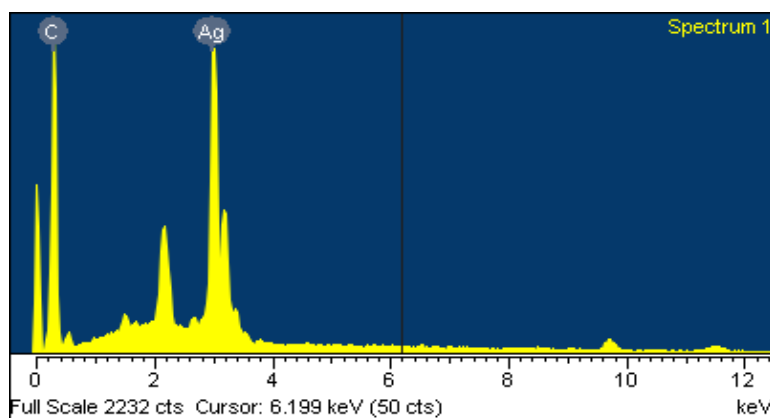
(h)

Figure 4.4: (a)-(h) SEM images of nanofibres generated with 20, 15, 10 and 5 wt.% nylon solutions under different working pressure and maximum rotating speed (36000 rpm) and corresponding fibre diameter distributions.

Figure 4.5 shows the focussed ion beam SEM image of the Ag-loaded nylon nanofibres. The contrast change of the image shows that Ag nanoparticles are incorporated in nanofibres. EDX analysis was also performed to study the distribution of silver nanoparticles. It also shows the percentage of composition in Ag-loaded nanofibres and indicates that there are Ag nanoparticles in the fibre. Thus, pressurised gyration was successful in generating nanoparticle containing nanofibers.



(a)



(b)

Figure 4.5: (a) FE-SEM (FIB-SEM inset) micrograph showing that the Ag nanoparticles (see arrows) were distributed on nanofibers made using the 20 wt.% nylon – 1 wt.% Ag suspension, and (b) the corresponding EDX analysis.

4.5 Raman spectra

Raman spectroscopy is a powerful and very sensitive technique for the study of interfacial properties of the hybrid nanofibres (Blaszczyk-Lezak et al., 2013; Wang et al., 2006). It can provide a variety of information about crystalline perfection to type of bonding between molecules. It also helps to identify ordered/disordered materials' structures. Figure 4.6 (a) shows the Raman spectra of 20 wt.% nylon nanofibres. The Raman bands observed at 1600 cm^{-1} , 1436 cm^{-1} and 1371 cm^{-1} corresponds to Amide I (C=O), CH₂ bending and CH₂ wagging, respectively. CH₂ twisting is shown at 1313 cm^{-1} . The peak at 1241 cm^{-1} is N-H wagging. The C-C-O stretch is identified at 938 cm^{-1} (Cho, 2007).

Raman spectra for Ag-loaded nylon nanofibres are shown in Figure 4.6 (b) and (c). Figure 4.6 (b) represents the lower Ag concentration (i.e. 1 wt.%), and Figure 4.6 (c) denotes the higher Ag concentrations (i.e. 4 wt.%). The Raman band for C-H and N-H bonding is suppressed when the concentration of Ag increased in nylon nanofibres. However, the Amide I band (1600 cm^{-1}) is clearly seen in both spectra. In the case of the Ag-loaded nanofibres Raman band of Amide I was shifted to higher wave number ($\sim 13\text{ cm}^{-1}$) compared to the nylon nanofibres indicating that the Ag nanoparticles are bonded to nylon. The charge transfer between the nylon and the Ag nanoparticles are inevitable where nylon is partially positive and Ag is partially negative. This charge transfer effect indicates that the nylon and Ag are acting as donor and acceptor in the hybrid nanofibre system. It is also consistent with the results obtained for Au-loaded polyaniline nanofibres (Tseng et al., 2007).

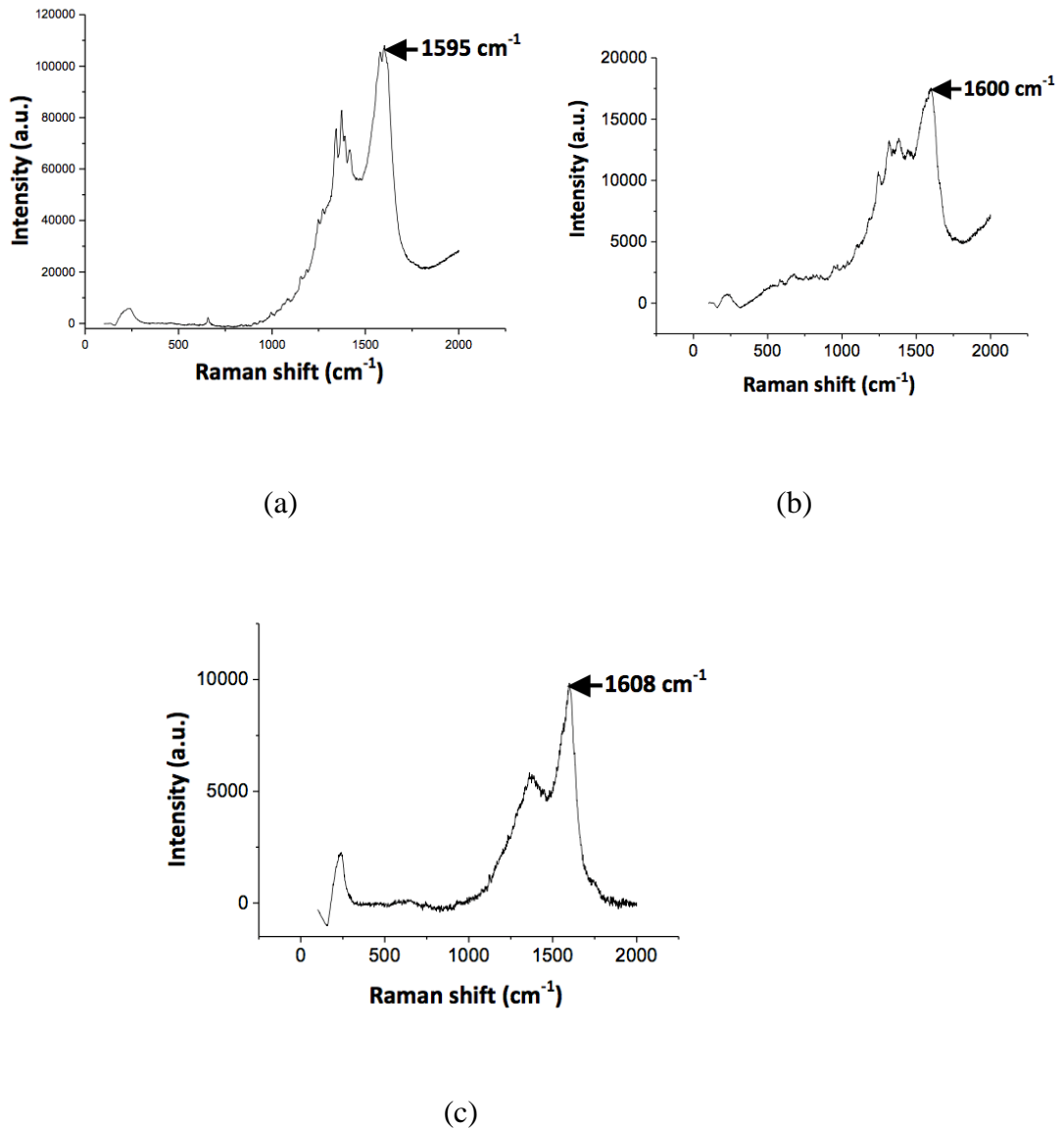


Figure 4.6: Raman spectra (baseline corrected) for nanofibres (a) nylon (20 wt.%) (b) lower concentration 1 wt.% of Ag-20 wt.% nylon (c) higher concentration 4 wt.% of Ag-20 wt.% nylon. Arbitrary units are indicated by a.u.

4.6 Silver ion release

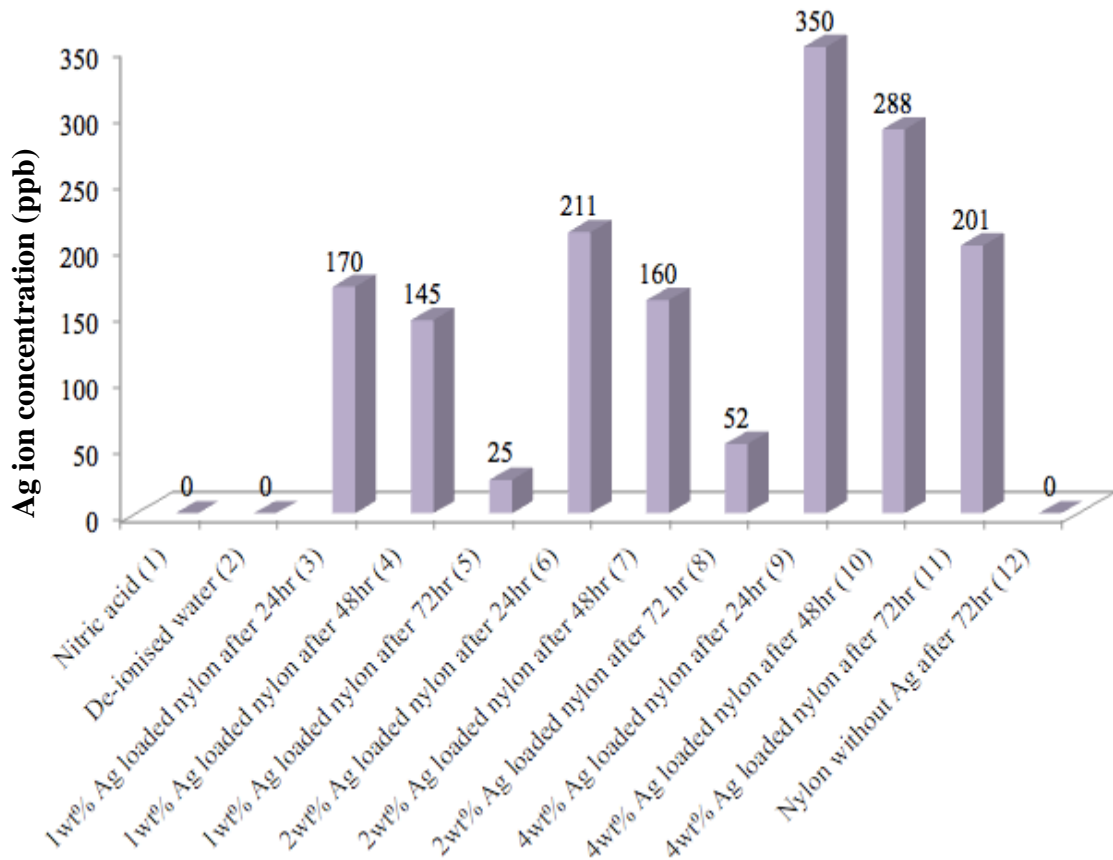


Figure 4.7: Silver ion concentration in various nylon nanofibre mats after 24, 48 and 72 hr of washing. Sample numbers are shown in brackets.

Figure 4.7 shows the Ag ion release concentration in a stock solution of nitric acid after 24, 48 and 72 hr washes of the nylon fibre produced in de-ionised water studied by ICP-MS. Samples 1 and 2 show there is no Ag ion to begin with and the de-ionised water, respectively. Samples 3, 4 and 5 represent the 1 wt.% Ag-loaded nylon nanofibres after undergoing the 24, 48 and 72 hr washing cycle. As expected, Ag ion concentration in the solution reduces after each washing cycle. The rate of Ag ion release after the first washing cycle is less compared to the second. This is also true for samples 6, 7 and 8 which are for 2 wt.% Ag-loaded nylon. Although samples 9, 10 and 11 (which are for 4

wt.% Ag-loaded nylon nanofibres) show a reduction in Ag ion concentration, the rate of ion release for consecutive washing cycles does not show a significant variation. These results are consistent with the Ag ion release from polyamide 66 composite where faster release is observed in the initial period and subsequently the release abruptly slowed down (Wu, Li et al., 2010). It is also clearly seen that the Ag ion concentration in the solution is higher after each cycle of wash for 4 wt.% Ag-loaded samples compared to the others. Sample 12 is for nylon nanofibres without any silver nanoparticles where no Ag ion is detected after a 72 hr wash cycle. Effective anti-bacterial properties require a concentration level as low as 0.1 ppb (parts per billion) and therefore the release of Ag ion from the hybrid system is sufficient even after a 72 hour of wash cycle (Shi et al., 2011).

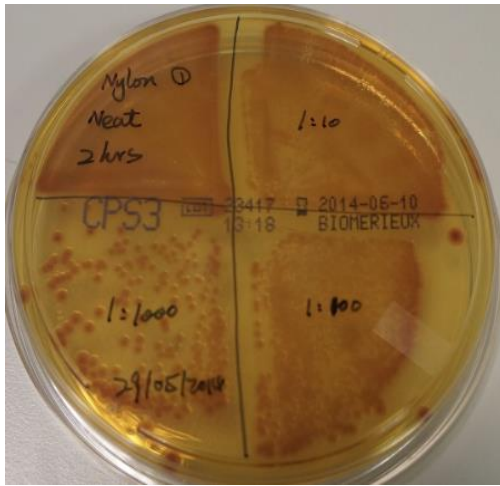
The Ag ion release to an aqueous medium consists of three distinct steps. Initially, water molecules diffuse in to the hybrid sample, then they will react with the Ag nanoparticles that eventually results in the formation and release of the Ag ions to an aqueous environment. The crystallinity and polarity of the matrix material influence the Ag ion release to an aqueous medium. These properties determine the level of diffusion barrier to water molecules and Ag ion release during the mass transfer. The release characteristics of Ag ion in polypropylene was found to be influenced by crystallinity and water absorption potential of the polypropylene matrix (Radheshkumar et al., 2006). Soaking time, concentration of silver powder, and silver specific surface area were identified as controlling factors in Ag ion release in polyamide (R. Kumar et al., 2005). A polyamide matrix has shown greater release potential than a polypropylene matrix due to its inherent hygroscopicity (Radheshkumar et al., 2006; Kumar et al., 2005). The Ag ion release from the matrix is also influenced by the dissolution and swelling behaviour of the matrix polymer (Abdelgawad et al., 2014).

The rate of Ag ion release can include two mechanisms. Initially, Ag ions are released from the nanoparticles embedded in the surface of the nylon matrix. Secondly, when the washing or soaking time increases, the oxidation of interior Ag nanoparticles happens and subsequently Ag ion release can take place. The former is instantaneous and the latter occurs with prolonged time where water molecules have time to diffuse across many crystalline layers (Kumar et al., 2005). The onset of plasticisation and equilibrium sorption would impart a degree of mobility to the macromolecular chains and changes in the matrix region, and in this way Ag nanoparticles embedded within the matrix can get oxidised and release Ag ions over a prolonged time. In addition, polar groups in the nylon chains will be separated and induce water dipole interaction. This will provide a more flexible structure for Ag ion release (Kumar et al., 2005). It is also noteworthy that the thickness of the polymer matrix barrier decreases the Ag ion release and the barrier height and the hydrophobicity of the polymer matrix influences water uptake and the diffusivity of the molecules to the medium (Alissawi et al., 2012). Moreover, mobility and the solubility of the water molecules in the polymer has to be taken into account during Ag ion release. Thus, for samples with a thicker barrier the water uptake is not sufficient to cause a high Ag ion release rate compared to samples with a thinner barrier height (Damm et al., 2008). This shows that as the diameter of nanofibers change in the chosen tested samples the Ag ion release rate also tends to change. This can promote increase in the Ag ion release rate due to the barrier becoming thinner allowing easier penetration of (OH) molecules in exchange with Ag ions.

4.7 Antibacterial activity

Antibacterial properties of the nanofibre samples were evaluated on Gram-negative *E. coli* and *P. aeruginosa* microorganisms. Due to a strong bactericidal ability of formic acid, all of the nanofibre samples for the antibacterial test were washed with distilled water (pH 6.5) for 96 hr to remove any residual formic acid. Post-washing, the pH values of nylon nanofibres were around 6 and the pH values of the Ag-loaded nylon nanofibres were almost 5.

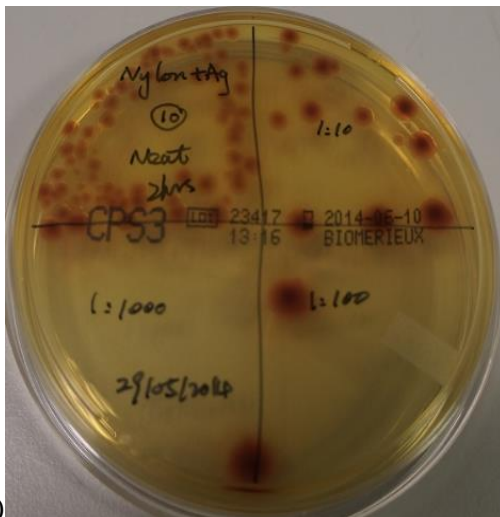
In these tests, 10 samples were tested for each bacterium, 5 samples of nylon nanofibres and 5 samples of Ag-loaded nylon nanofibres. Five 20 wt.% nylon nanofibres, five 1 wt.% Ag-loaded 20 wt.% nylon nanofibres and two-control group were investigated for *E. coli* and *P. aeruginosa*, respectively. As shown in Figure 4.8, the *E. coli* colonies appeared burgundy on the chromogenic culture plate and the *P. aeruginosa* colonies were a glossy cream in color. It is clearly seen that the Ag-loaded nylon nanofibres host a smaller number of bacterial colonies compared to nylon nanofibres. The increase in contact time of the nanofibre samples with the bacterial solution also reduced the number of bacterial colonies. Figure 4.9 shows the plots of anti-bacterial rate for *E. coli* and *P. aeruginosa* after 2 hr and 24 hr. As the contact time increased, the percentage (%) reduction increased and reached an asymptotic value for nylon nanofibres and Ag-loaded nylon nanofibres. The percentage reduction was higher for Ag-loaded nylon nanofibres than for the nylon nanofibres. There was no significant difference observed in percentage reduction after 2 hr for Ag-loaded nylon nanofibres. However, nylon nanofibres showed reduced antibacterial activity after 2 hr for both *E. coli* and *P. aeruginosa* microorganisms.



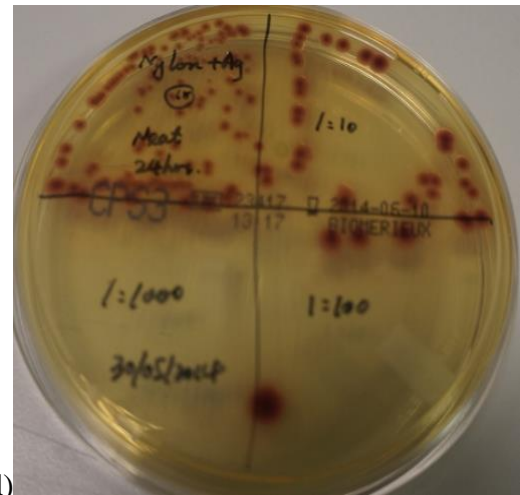
(a)



(b)



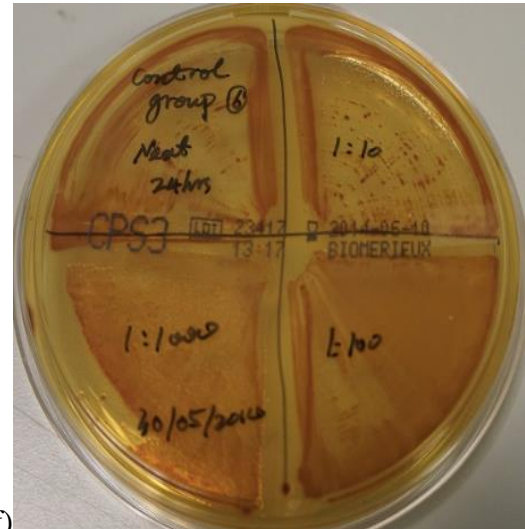
(c)



(d)



(e)



(f)

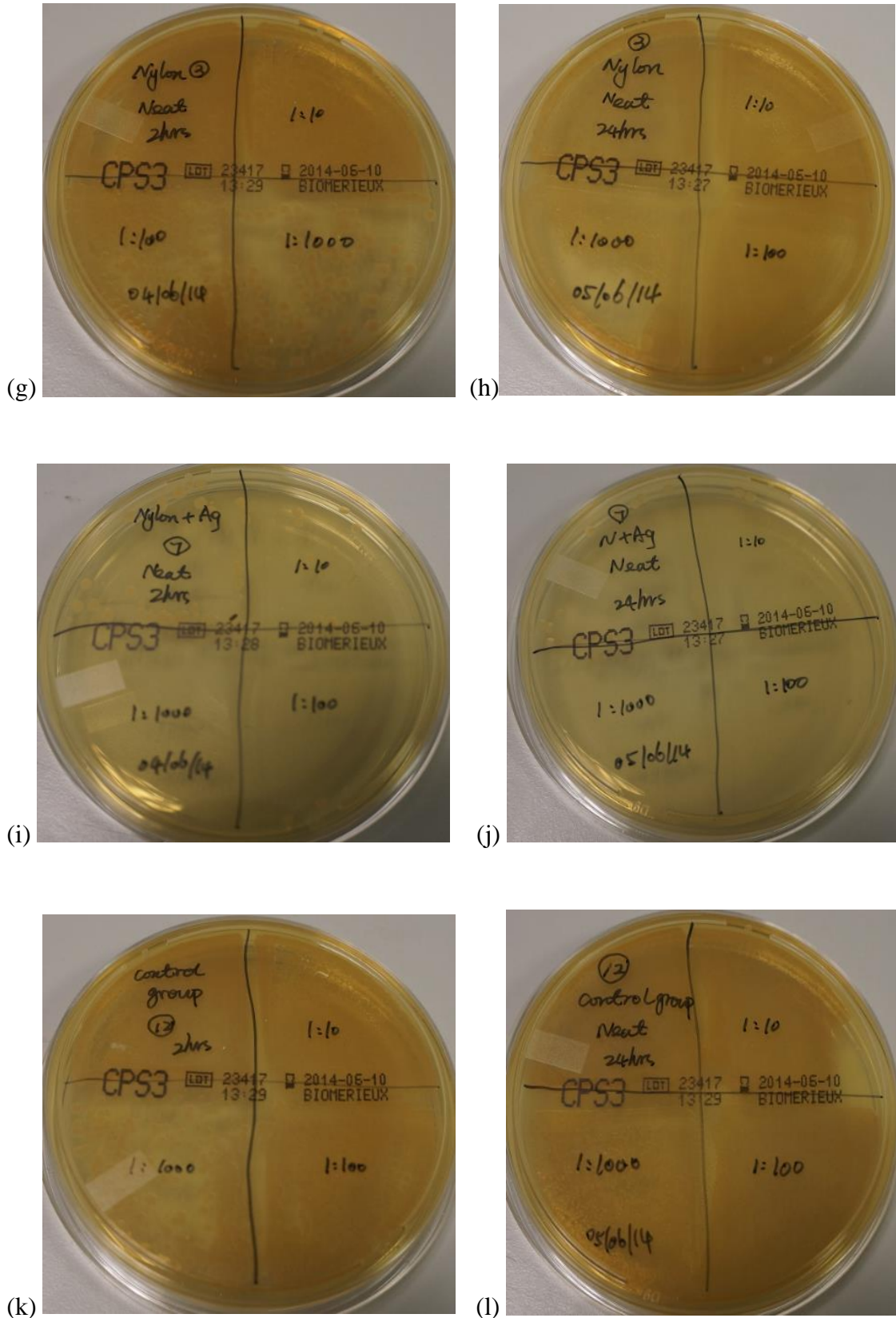
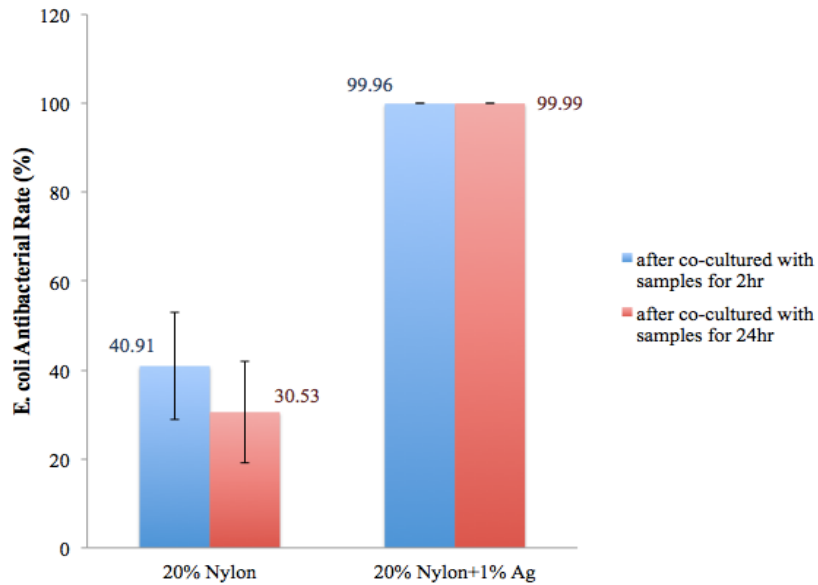
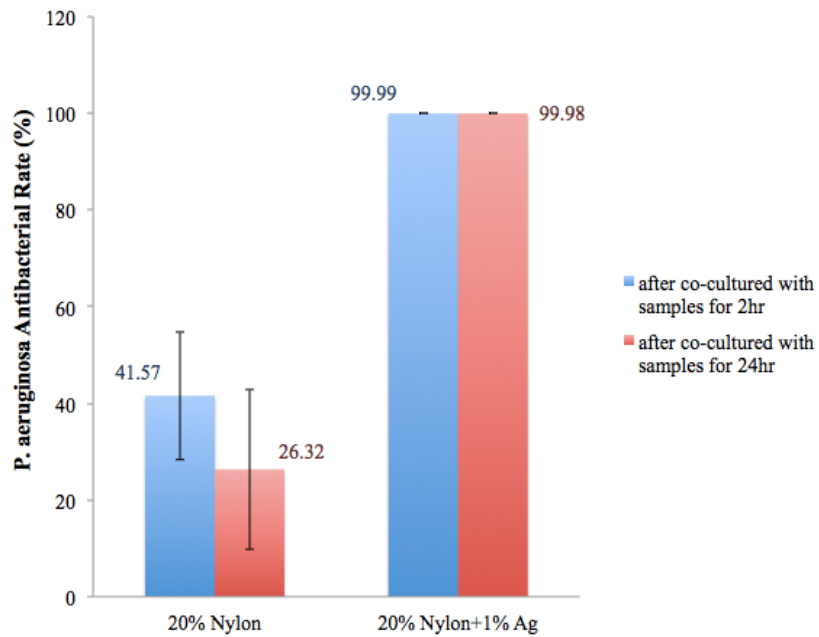


Figure 4.8: Bacterial colonies (a), (b) *E. coli* co-cultured with 20 wt.% nylon nanofibre for 2 hr and for 24 hr; (c), (d) *E. coli* co-cultured with Ag-loaded 20 wt.%

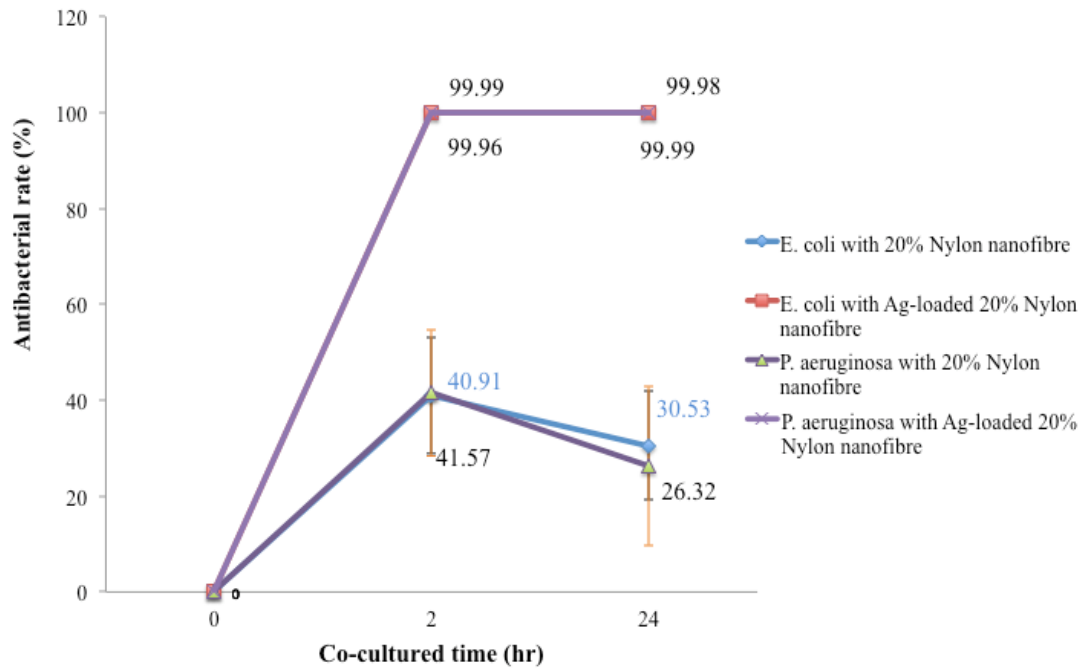
nylon nanofibre for 2 hr and for 24 hr; (e), (f) *E. coli* control group for 2 hr and for 24 hr; (g), (h) *P. aeruginosa* co-cultured with 20 wt.% nylon nanofibre for 2 hr and for 24 hr; (i), (j) *P. aeruginosa* co-cultured with Ag-loaded 20 wt.% nylon nanofibre for 2 hr and for 24 hr; (k), (l) *P. aeruginosa* control group for 2 hr and for 24 hr.



(a)



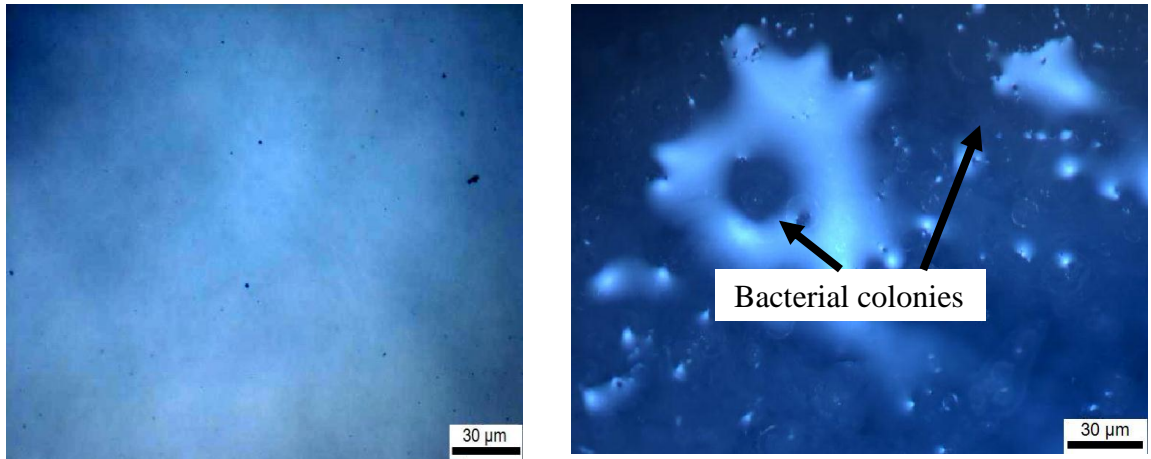
(b)



(c)

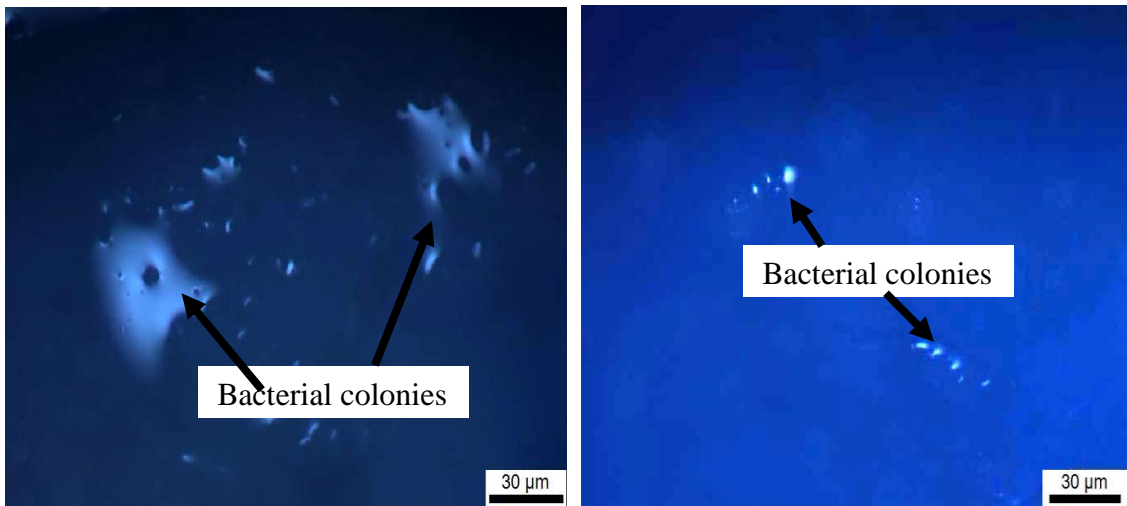
Figure 4.9: Antibacterial rates of (a) *E. coli* at two time points; (b) *P. aeruginosa* at two time points; (c) Graph of antibacterial rate versus co-cultured time for nylon nanofibres and Ag-loaded nylon nanofibres on *E. coli* and *P. aeruginosa*.

The morphological characteristics of the bacterial cells cultured onto the nanofibres were also investigated. For this purpose, bacterial cells were co-cultured with nanofibres as in the above assay and incubated at 37 °C for 24 hours. Following incubation, nanofibres were washed three times with phosphate buffered saline (PBS) to remove unbound and loosely adhered bacteria. Subsequently, they were stained with methylene blue in PBS solution that were diluted to 1:2 ratio for 10 min and observed using an optical microscope (Olympus).



(a)

(b)



(c)

(d)

Figure 4.10: Optical micrographs showing *E. coli* bacterial cells cultured in media
(a) Glass slide control; (b) Nylon nanofibres after 2 hr; (c) Nylon nanofibres after
24 hr; (d) Ag-loaded Nylon nanofibres after 2 hr.

Figure 4.10 shows the bacterial cell proliferation and spreading after each of the time points for nylon nanofibres and Ag-loaded nylon nanofibres. The nylon nanofibres contained a denser cell population than the glass slide and the Ag-loaded nylon nanofiber.

The mechanisms underlying the antibacterial activity of silver are not fully understood. Even though there are many reports proposing different mechanisms, there is no consensus. In the presence of Gram-negative bacteria, Ag nanoparticles attach to the cell walls and disturb cell wall permeability and cell respiration (Abdelgawad et al., 2014; An et al., 2009). Other studies have shown that interaction between the Ag ions and the constituents of the bacterial membrane causes structural changes and damage in the cell membranes accompanied by intracellular metabolic activity, thus causing cell death (Jung et al., 2008). The concentration of Ag nanoparticles and the formation of "pits" have also been proposed as a reason for the antibacterial activity, where the accumulation of Ag nanoparticles in the membrane caused permeability and the cell death (Sondi et al., 2004; Zhou et al., 2013). Cell death was shown not to be caused directly by Ag nanoparticles but instead by Ag ion release from the Ag nanoparticles (Xiu et al., 2012). However, the fraction of metal that is bioavailable (that is, the actual amount which have entered into the cells) is the most important parameter, compared with percent dissolution of Ag nanoparticles that determines the efficiency of cell death (Ivask et al., 2014). The formation of free radicals influences cell lysis when the Ag nanoparticles are in contact with the bacteria. The free radicals have the ability to destroy the cell membrane and make porous surfaces which lead to cell death (Kim et al., 2007).

In addition, Ag ions released from the silver nanoparticles can react with the thiol groups of vital enzymes in the bacteria and inactivate them (Matsumura et al., 2003). Such studies have also shown that the soft acidic form of Ag ions (metal ions with the highest

affinity for soft bases are soft acids) may react with soft bases in the cells such as sulfur and phosphorous which can cause cell death. DNA, for example, contain sulfur and phosphorous; when they react with Ag they become damaged ultimately leading to cell death (Morones et al., 2005). Thus, although the exact mechanism responsible for antibacterial activity is to be resolved, and may be multifactorial, it is very clear that Ag-loaded nanofibres resulted in high efficacy of antibacterial activity than the pure nylon nanofibres and the control groups. Our results showed that Ag has contributed to cell death in the *E. coli* and *P. aeruginosa* microorganisms. As shown in the Ag ion release studies (ICP-MS) initially Ag nanoparticles in the matrix of the nylon have a great effect on the anti-bacterial activity and as the time lapses the nanoparticles embedded in the nylon will cause cell death.

4.8 Summary

Polyurethane and Copper/Zinc oxidized embedded Polyurethane nanofibers, Nylon and Ag-loaded nylon nanofibers were fabricated using a pressurised gyration process which has not been used before to fabricate antibacterial fiber mats. The process makes use of simultaneous centrifugal force and fluid flow to form the fibers. The fiber diameter generated was in the range of 50-500 nm. Key parameters such as vessel rotating speed, working pressure and polymer concentration had a significant effect on nanofiber diameter and morphology. The fiber diameter increased when increasing weight percentage of polymer, reduced with increasing vessel rotating speed and the process working pressure. Effective and proper incorporation of Ag nanoparticles into the nylon nanofibers was confirmed by advanced microscopy. The Raman spectra elucidated the bonding characteristics of nylon and the Ag nanoparticles. Ag ion release after repeated washing of the nanofibrous mats was detected by inductively coupled plasma mass

spectroscopy which showed the Ag ion existence and concentration in the initial nanofibrous mats which influences the Ag ion release profile. A strong antibacterial-activity of Ag-loaded nylon was clearly demonstrated with bacterial killing rates reach ~100% for gram-negative *E. coli* and *P. aeruginosa* microorganisms.

Chapter 5 - Making Poly(ϵ -caprolactone) fibres by Pressurised Melt Gyration

5.1 Introduction

Pressurised melt gyration does not require any solvent that could eliminate the toxicity of solvent. Due to the low melting point of PCL, it was the best material to investigate the pressurised melt gyration process technique. Gyration vessel speed, working pressure and melt temperature were varied and these parameters influenced the fibre diameter and the temperature enabled changing the surface morphology of the fibres. Two types of non-woven PCL fibre constructs were prepared, PCL fibres and Ag coated PCL fibres. The bonding characteristics, crystallinity of PCL and Ag ion release were studied. Ag doped PCL was studied for antibacterial activity using Gram-negative *Escherichia coli* and *Pseudomonas aeruginosa* microorganisms. The melt temperature used to make these constructs significantly influenced antibacterial activity.

5.2 Physical Properties of Poly(ϵ -caprolactone) pellets

The thermal properties of the PCL scaffolds are summarized in Table 5.1. Generally, the crystallization temperature decreased with increasing melt temperature used for gyration. The crystallinity of the PCL scaffold (X%) was calculated using the equation $X\% =$

$\Delta H_m/\Delta H_m^0$, where ΔH_m is the melting enthalpy taken from DSC curve and ΔH_m^0 is the melting enthalpy of a reference PCL with 100% crystallinity. ΔH_m^0 was taken as 135.6 J/g (Ong & Price, 1978). A moderate crystallinity was observed for scaffolds spun at 95°C. Scaffolds spun at 125°C show higher crystallinity and thereafter the crystallinity reduces with melt (gyration) temperature. This is due to variation in nucleation sites and the limited PCL molecular chain movement with the melt temperature (Liang et al, 2013).

Table 5.1: Thermal properties of scaffolds prepared by PMG. ΔH_m , ΔH_c , T_m , T_c and X represent melting enthalpy, crystallization enthalpy, melting temperature, crystallization temperature and crystallinity, respectively.

Sample	ΔH_m (J/g)	ΔH_c (J/g)	T_m (°C)	T_c (°C)	X(%)
PCL pellet	-35	36	59	31	26
PCL-95°C	-28	49	58	37	21
PCL-125°C	-70	68	58	36	51
PCL-155°C	-50	57	59	36	37
PCL-200°C	-26	40	58	38	19

5.3 Fibre diameter analysis

Table 5.2 shows fibre diameter variation with melt temperature. It is clearly seen that the fibre diameter reduces with increasing temperature (Figure 5.1). For PCL molten polymer, increasing the temperature from 95°C to 200°C reduced the fibre diameter from 38 μ m to 28 μ m at a rotating speed 24000 rpm (Table 5.2 a). At a rotating speed

36000 rpm, increasing the temperature from 95°C to 200°C reduced the fibre diameter further, from 31 μ m to 18 μ m (Table 5.2 a). Therefore, the fibre diameter was affected by two factors, namely the rotating speed of the vessel and melt temperature. Table 5.2 b show the variation of fibre diameter with melt temperature and working pressure. The fibre diameter reduced from 24 μ m to 19 μ m when increasing the temperature from 105°C to 200°C at a rotating speed 36000 rpm and a working pressure 0.01 MPa. At a rotating speed 36000 rpm and a working pressure 0.02 MPa, the fibre diameter reduced further, from 22 μ m to 14 μ m when increasing the temperature from 105°C to 200°C. This indicates that the working pressure had a significant influence on variation of the fibre diameter.

Sample	Fibre diameter at 24000 rpm (μm)	Fibre diameter at 36000 rpm (μm)
PCL 95°C	38 (\pm 12)	31 (\pm 7)
PCL 125°C	35 (\pm 15)	26 (\pm 13)
PCL 155°C	31 (\pm 11)	22 (\pm 12)
PCL 200°C	28 (\pm 10)	18 (\pm 12)

(a)

Sample	Fibre diameter at 36000 rpm and	Fibre diameter at 36000 rpm and
	0.01 MPa (μm)	0.02 MPa (μm)
PCL 105°C	24 (\pm 12)	22 (\pm 13)
PCL 150°C	21 (\pm 11)	18 (\pm 8)
PCL 200°C	19 (\pm 7)	14 (\pm 8)

(b)

Table 5.2: PCL fibre diameter variations at various melt temperatures, rotating speeds and working pressures (a) 24000, 36000 rpm (b) 0.01, 0.02 MPa.

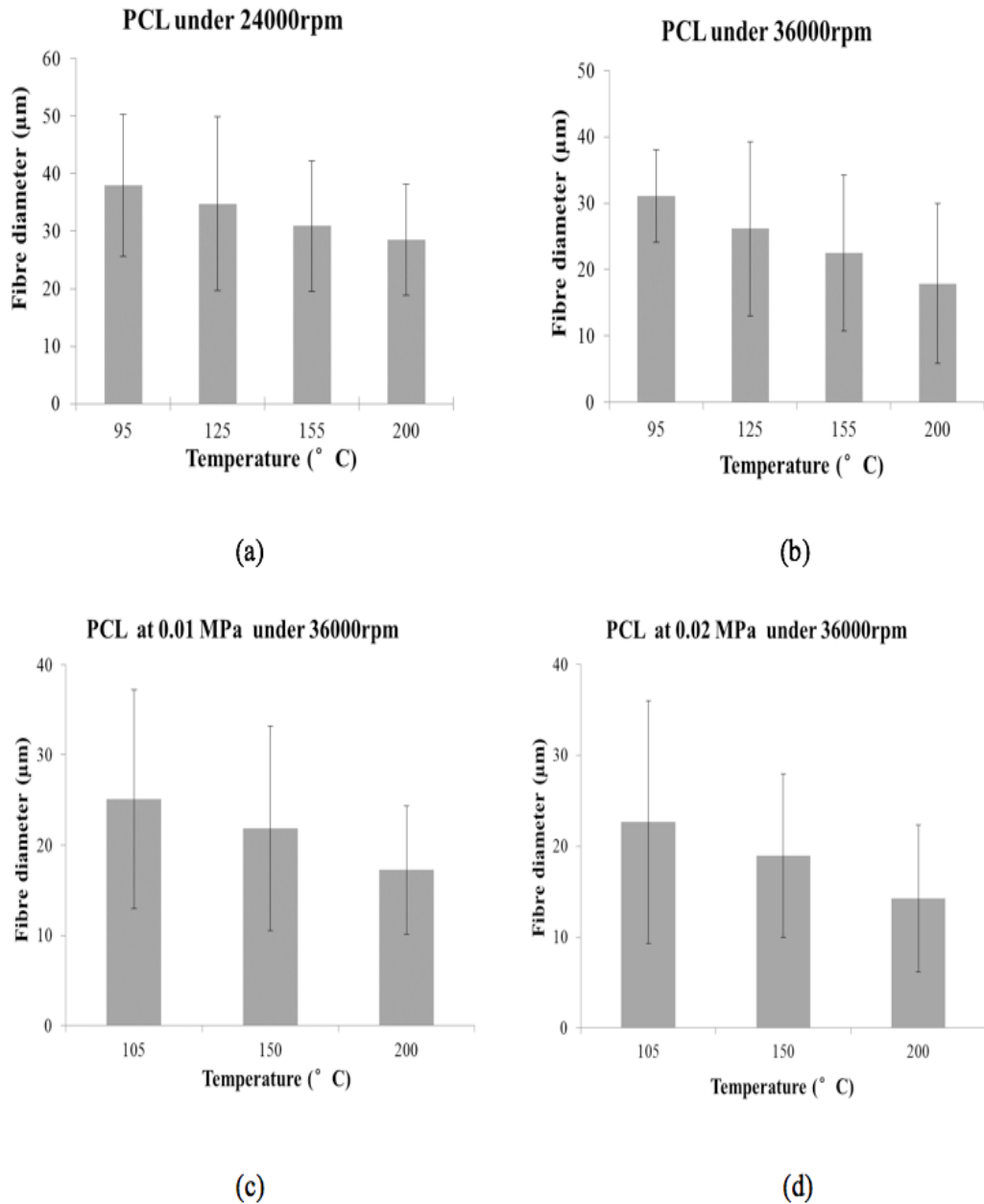
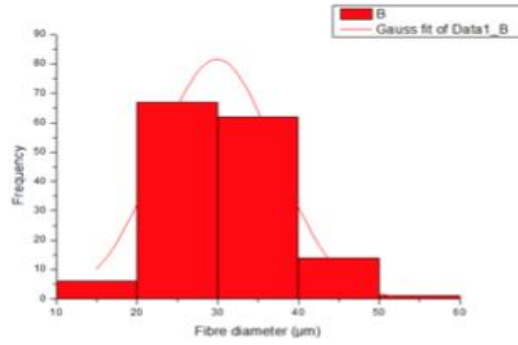
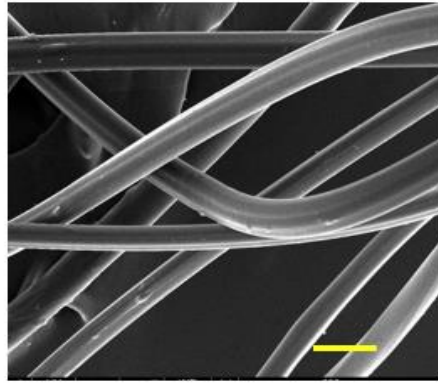


Figure 5.1: Fibre diameter variation of PCL fibres processed at various temperatures under different rotating speeds and working pressure (a) 24000 rpm (b) 36000 rpm (c) 0.01 MPa (d) 0.02 MPa.

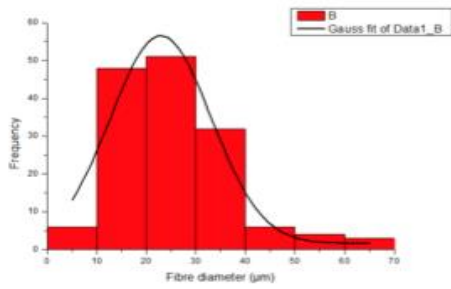
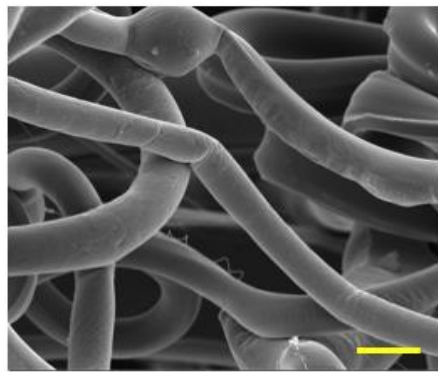
The effect of the melt temperature on fibre diameter is very significant as it can influence the fibre formation and solidification by different ways. Increasing the temperature allows the molten liquid jet to remain in a liquid state for longer time, thus causing the additional stretching of fibre jets. The fibre jets cool very rapidly when ejected from the orifices. Additionally, the polymer melt viscosity reduces when increasing the temperature. It has been shown that an order of magnitude reduction in shear viscosity occurs when increasing the temperature by 40°C (Vera-Sorroche et al, 2014). Therefore, thinner fibres were obtained at a higher melt temperature due to additional stretching time as well as the lower melt viscosity. It has been reported that the competition between the centrifugal force and dynamic fluid flow at the orifice against the surface tension of the polymeric solution is responsible for fibre formation in pressurised gyration (Mahalingam & Edirisingh, 2013). This is also true in PMG where the centrifugal force accelerates the molten liquid stream and stretching of the jets. The acceleration of liquid stream and stretching is enhanced by blowing where liquid exerts more force to overcome the surface tension force and thus results in thinner fibres at higher rotating speed and working pressure.

The surface morphology of PCL fibrous scaffolds spun at different temperatures under 3600 rpm speed and the corresponding fibre diameter distribution are shown in Figure 5.2. Each consists of high and low magnification images. The surface of fibrous scaffolds formed at 95°C and 105°C appeared to be very smooth. The surface of the fibrous scaffolds spun at 125°C were very rough and some particles were observed on the surface, which were probably caused by incomplete melting of polymer particles caused by non-uniform melting of the pellets during fibre forming. The fibrous scaffolds formed at higher temperatures (155°C and 200°C) shows extrusion lines on the surface. These also contained fibril lines as well as small hollow regions ("pits"). The observation

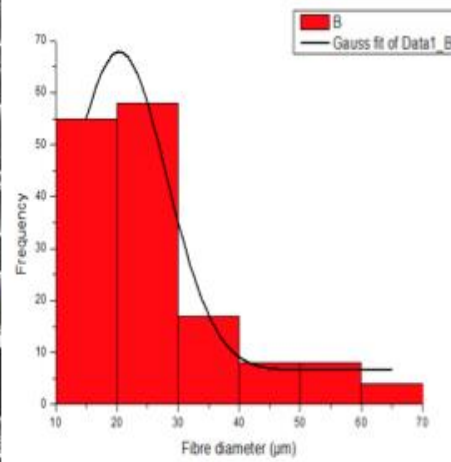
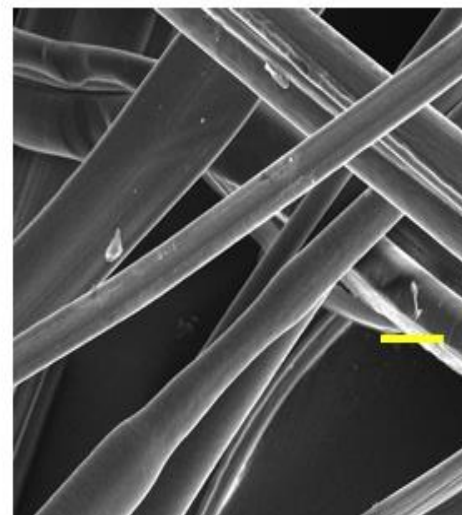
suggests that the melting temperature of the PCL plays a vital part in creating the surface morphology of the spun fibrous scaffolds.



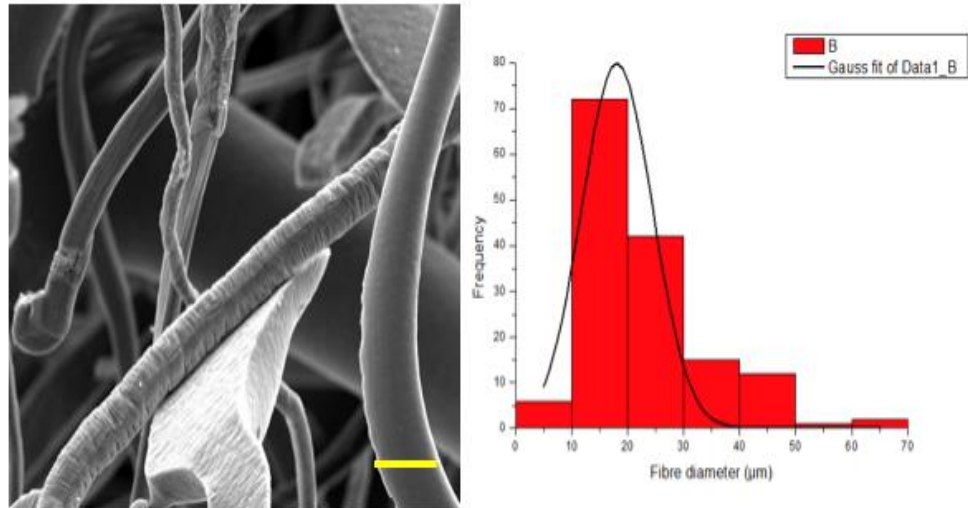
(a)



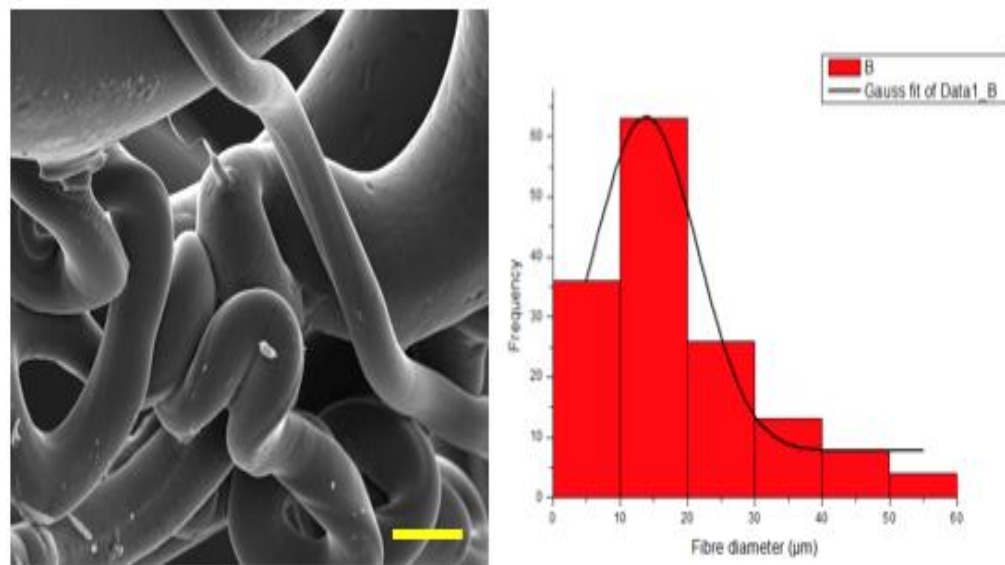
(b)



(c)



(d)



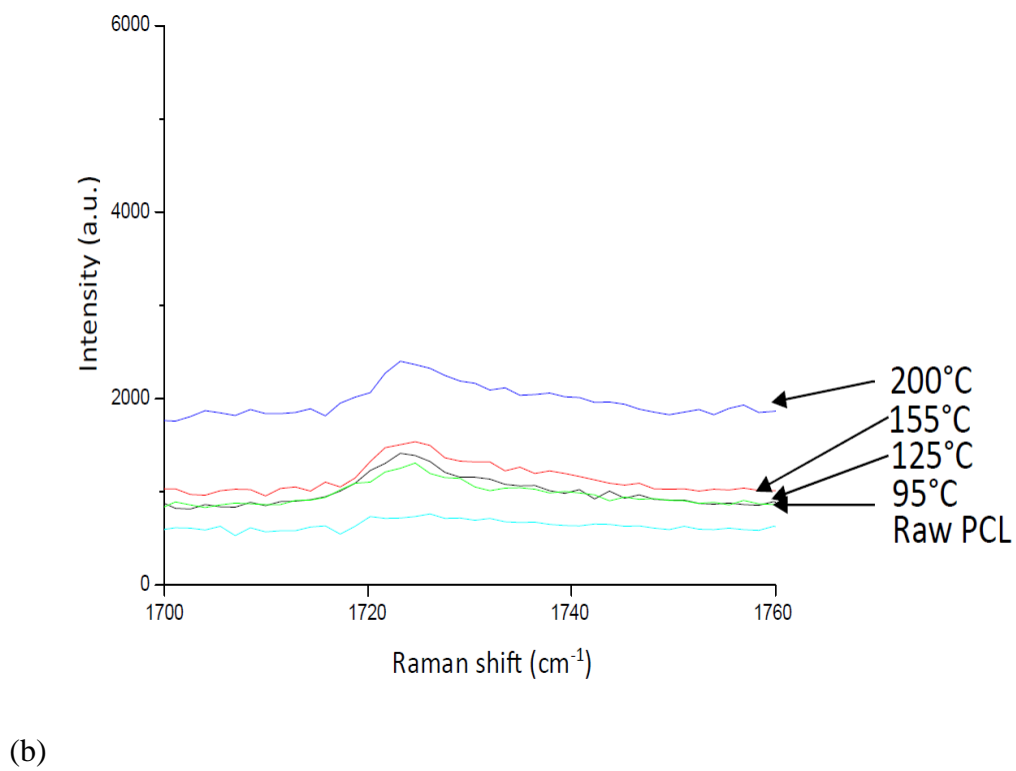
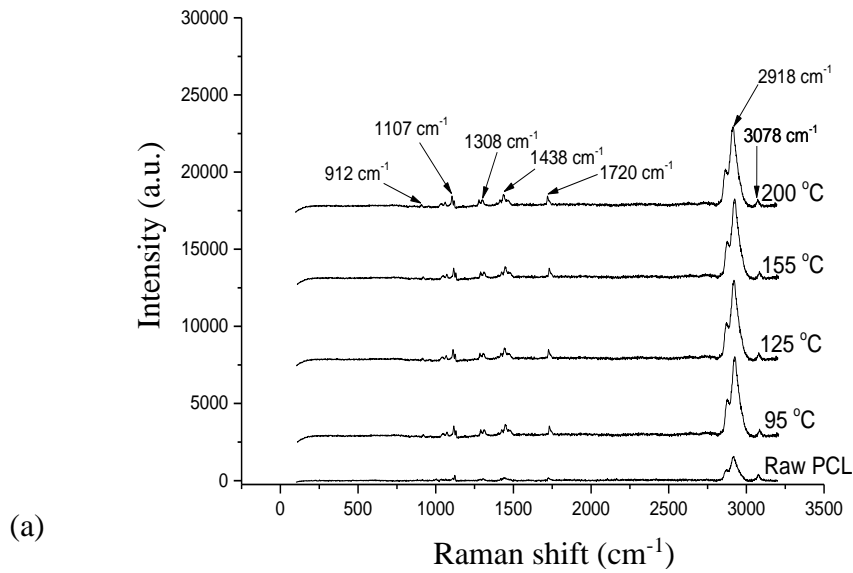
(e)

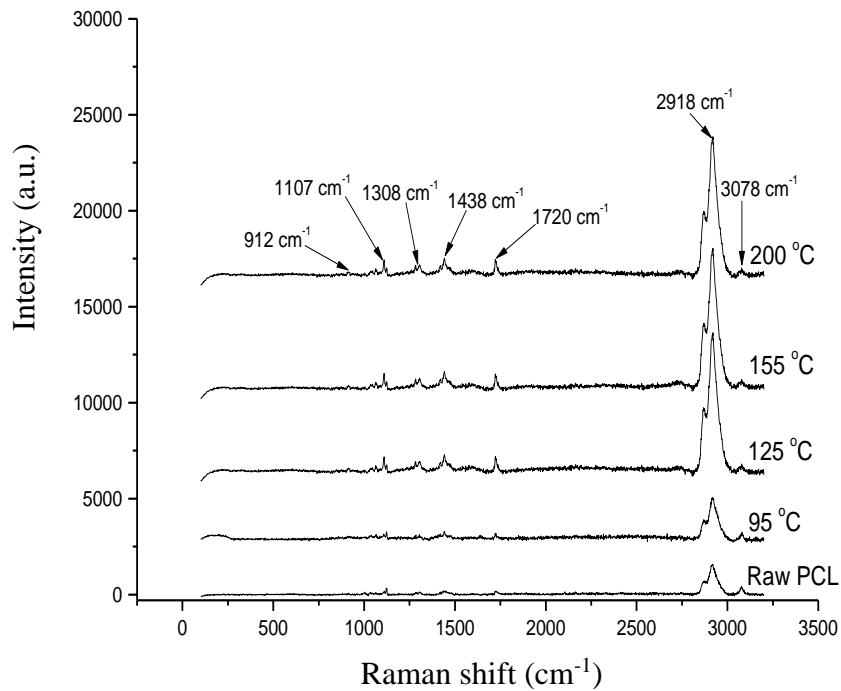
Figure 5.2: Scanning electron micrographs of PCL fibres obtained at various temperatures at 36000 rpm (a) 95°C (b) 105°C, 0.01 MPa working pressure (c) 125°C (d) 155°C (e) 200°C, 0.01 MPa working pressure. Scale bars in the in-set images are 20 μm .

5.4 Raman spectra

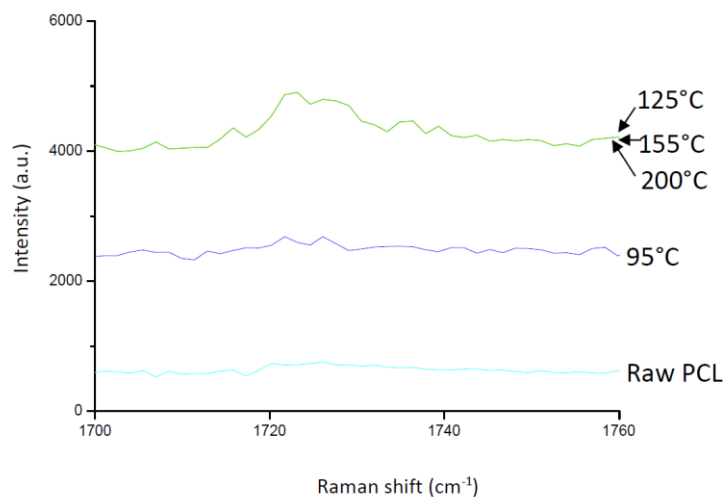
Figure 5.3 (a) shows Raman of PCL fibrous scaffolds obtained at various temperatures at a fixed rotating speed 36000 rpm and 0.01 MPa working pressure. Sharp and intense peaks were observed for PCL fibrous scaffolds compared to raw PCL pellets. The intensity and the sharpness of the peaks increased with temperature and is attributed to increase in crystallinity in the PCL scaffolds generated. The peaks at 1438 cm^{-1} , 1308 cm^{-1} , 1107 cm^{-1} , and 912 cm^{-1} correspond to (δCH_2), (ωCH_2) bonding, skeletal stretching and $\nu\text{C-COO}$ bonding, respectively, and belongs to crystalline phases. The peak obtained between $1720\text{-}1739\text{ cm}^{-1}$ is assigned to C=O stretching vibration (Gupta et al, 2012). The microanalysis of the Raman band in this region is shown in Figure 5.3 (b). The PCL pellets did not reveal any peaks. However, scaffolds made at temperatures from 95°C to 200°C show a peak at $\sim 1723\text{ cm}^{-1}$ and belongs to crystalline phase (Kister et al, 2000). Increase of intensity and narrowing of the peak with increase in temperature indicates increase in crystallinity in the PCL scaffolds prepared. Figure 5.3 (c) shows Raman spectra of Ag-coated PCL scaffolds. The main peaks identified were similar to PCL scaffolds and therefore there is not any significant difference in their molecular structure, compared to PCL scaffolds. However, the microanalysis in the wavelength range $1700\text{-}1760\text{ cm}^{-1}$ showed difference in their crystallinity (Figure 5.3 (d)). The appearance of peaks at ~ 1730 and $\sim 1736\text{ cm}^{-1}$ at higher temperatures indicate the formation of amorphous structures in the scaffolds (Kister et al, 2000). This is very likely because incorporation of nanoparticles hinders the movement of molecular chains and decreases the crystallinity. It is also seen that the peak at $\sim 1723\text{ cm}^{-1}$ shifted to higher wavenumbers in the Ag-coated PCL scaffolds. This is attributed to the compressive stress present in the polymer matrix in the composite structure. It is well known that

Raman peaks are associated with the lattice vibration and hence are affected by the chemical structure and atomic bonding of the material. Therefore, the stress present in the structure can affect Raman peaks (Lahiri et al, 2010).





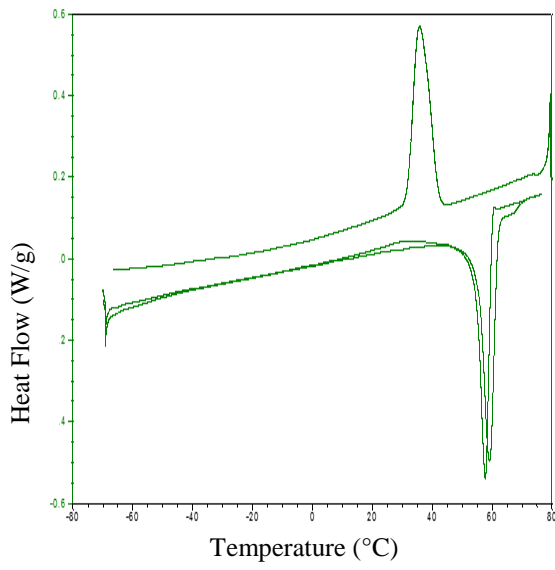
(c)



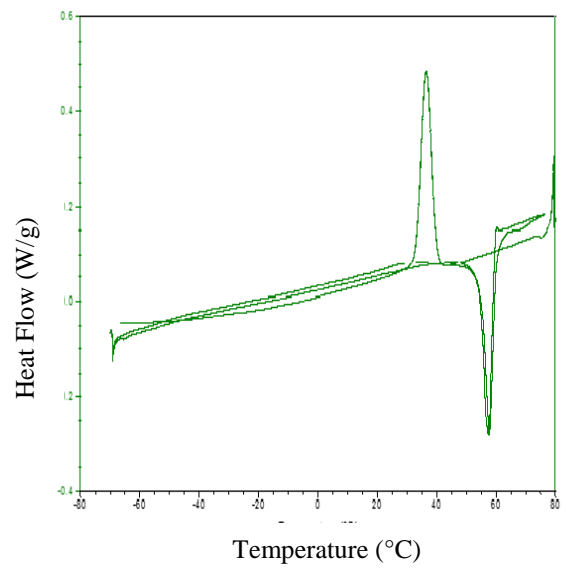
(d)

Figure 5.3: (a) Raman spectra of PCL fibres made at various temperatures at 36000 rpm and 0.01 MPa working pressure and raw PCL pellets. (b) Microanalysis of Raman band of (a) in the range 1700-1760 cm^{-1} . (c) Raman spectra of Ag-coated PCL fibres and raw PCL pellets. (d) Microanalysis of Raman band of (c) in the range 1700-1760 cm^{-1} .

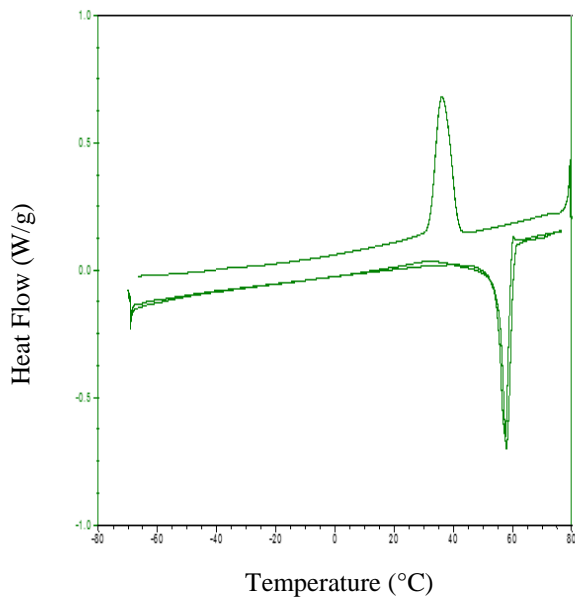
5.5 Differential scanning calorimetry



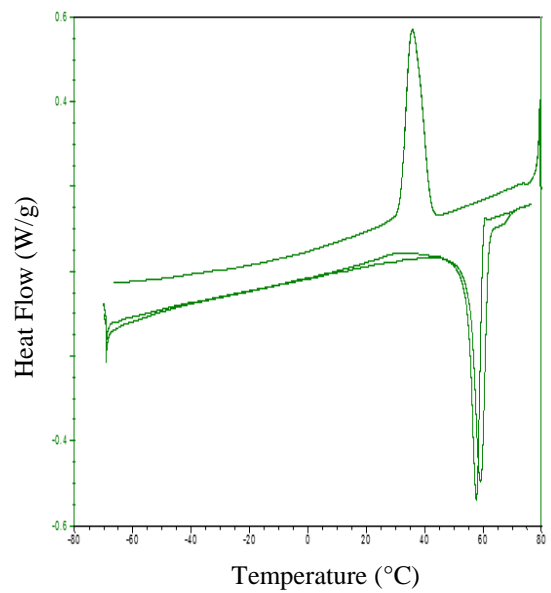
(a)



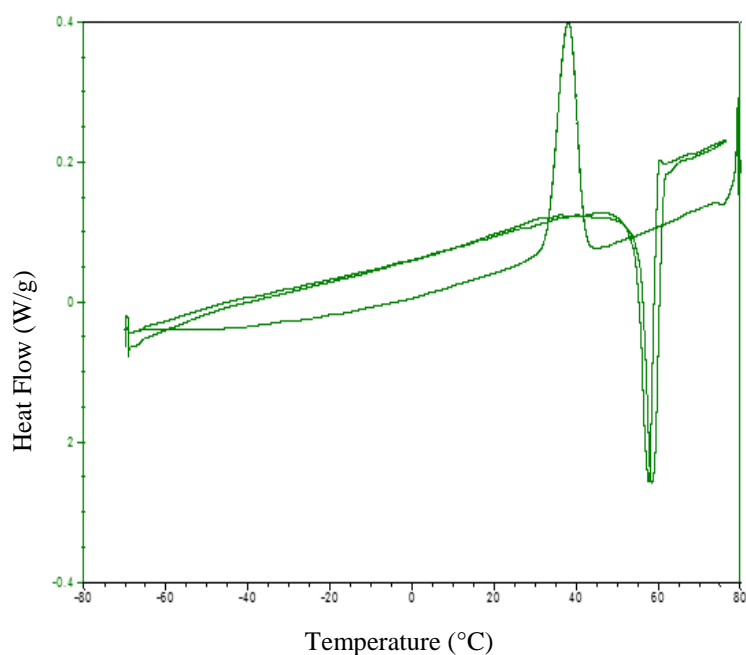
(b)



(c)



(d)



(e)

Figure 5.4: MTDSC results (heat-cool-heat cycle) of (a) PCL pellets, fibres spun at different temperatures (b) 95°C (c) 125°C (d) 155°C (e) 200°C.

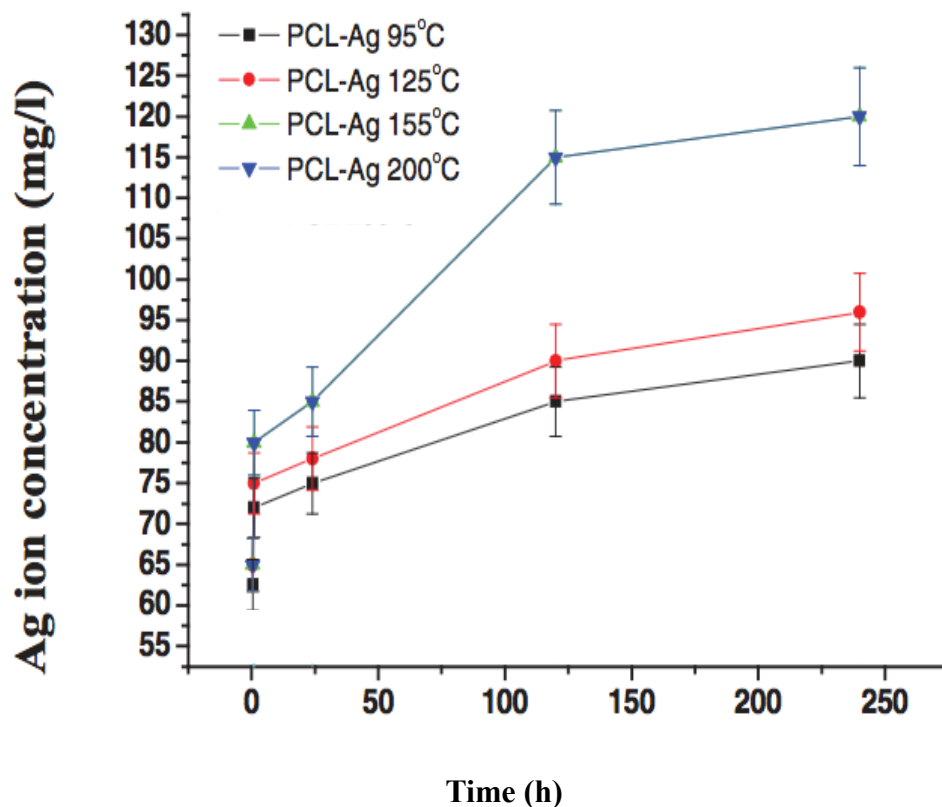
The modulated DSC results (heat-cool-heat cycle) of the PCL pellets and the fibrous scaffolds spun at different temperatures are shown in Figure 5.4. From the first heating scans of the products, the melting point of spun scaffolds was less than that of raw PCL pellets. The melting point of PCL pellets is 59°C and that for the spun scaffolds lies between 57.5°C-59°C and were closer to the values reported in the literature (Jana et al, 2014). There is no apparent correlation between the melting point of scaffolds and the gyration temperatures.

5.6 UV/vis spectroscopy

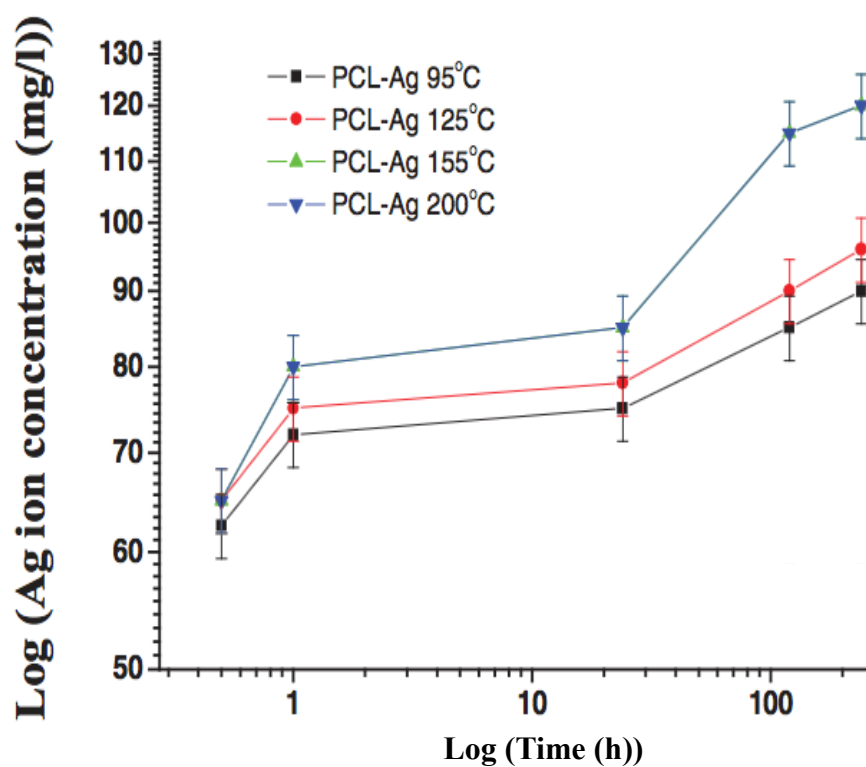
Silver ion (Ag^+) release profiles of different PCL-Ag fibrous scaffolds spun at different temperatures are shown in Figures 5.5 (a) and 5.5 (b). The PCL scaffold spun at 200°C without Ag ions is also shown for comparison. The release of Ag ions from fibrous scaffolds followed an exponential increase with time, dependent on melt temperature and Ag ion content. As expected the PCL fibrous scaffolds spun at 200°C showed no release after 0.5 hour to 240 hours. The PCL scaffolds spun at 95°C with Ag showed low amounts of Ag ion release after 1 hour. However, there was significant amount of Ag ion release observed after 120 hours and 240 hours. This was also true for PCL-Ag scaffolds spun at 125°C. Although a significant amount of Ag ion release occurred in PCL-Ag scaffolds spun at higher temperatures (155°C and 200°C) throughout the release time studied, i.e. from 0.5 hour to 240 hours, the amount of Ag ion release was almost same for both temperatures. The amount of Ag ion release from PCL scaffolds spun at higher temperatures (155°C and 200°C) started to level off and reached a plateau after 120 hours in contrast to PCL scaffolds spun at lower temperatures (125°C and 95°C).

Power law exponent, n , the slope of linear fitting between $\log(\text{Ag}^+)$ and $\log(t)$ and fitting coefficient R^2 deduced from graph in Figure 5.5 (b) are shown in Table 5.3 and points out that n varied for the different samples which is indicative of different transport mechanisms. For all the samples the power law exponent lies between ~ 0.095 - 0.208 with R^2 fitting coefficient $>81\%$. This indicates that there is no statistical correlation between the power law exponents and the experimental measurements. Thus, these release phenomena do not closely follow $t^{1/2}$ time dependence of physical diffusion-controlled drug transport in polymer thin films based on the Higuchi model or pure

Fick's second law of diffusion in a thin polymer film (Paul, 2011). The power law of Ag ion release from fibrous scaffolds spun at higher temperatures (155°C and 200°C) yields a value of 0.208 which is <0.5 with a lower R^2 fitting coefficient of 0.829. The anomalous transport of Ag ion release from the PCL fibrous scaffolds may be attributed to predominant and rapid dissolution of a large quantity of free Ag nanoparticles absorbed on the surface of fibres at the early stage of release. In addition, water permeation and crystallinity of the PCL scaffolds which constitute the diffusion barriers to water molecules and Ag ions during the propagation of release can also determine the Ag ion release rate which might contribute to the anomalous transport mechanism (Radheshkumar & Munstedt, 2006).



(a)



(b)

Figure 5.5: (a) Silver ion (Ag^+) release from scaffolds in de-ionised water at the ambient temperature (23°C) for various PCL fibrous scaffolds (b) Log (Ag ion concentration) vs Log (time) graphs.

Table 5.3: Release quantity of Ag^+ ions from various PCL-Ag mats

Sample	0.5 hour Release quantity (mg/l)	24 hours Release quantity (mg/l)	Slope of fitting (n)	Fitting coefficient (R^2)
PCL-200°C	55 (± 6)	56 (± 5)	0.005	0.824
PCL-Ag 95°C	63 (± 6)	90 (± 8)	0.095	0.814
PCL-Ag 125°C	65 (± 7)	96 (± 10)	0.110	0.839

PCL-Ag 155°C	65 (± 6)	120 (± 11)	0.208	0.829
PCL-Ag 200°C	65 (± 7)	120 (± 10)	0.208	0.829

5.7 Antibacterial studies

Antibacterial properties of the melt spun PCL scaffolds were evaluated on Gram-negative *E. coli* and *P. aeruginosa* microorganisms. In these tests, 8 samples spun at 36000rpm rotating speed were tested for each bacterium including 4 samples of PCL scaffolds produced at different temperatures (95°C, 125°C, 155°C and 200°C) and 4 samples of Ag-coated PCL scaffolds made at the same temperatures.

For PCL scaffolds, four PCL-Ag coated scaffolds and two control groups were investigated with *E. coli* and *P. aeruginosa*, respectively. Figure 5.6 shows the plots of antibacterial rate for *E. coli* and *P. aeruginosa* microorganisms after 2 hours. It is clearly seen that the antibacterial rate for PCL-Ag coated scaffolds is higher than the PCL scaffolds for both microorganisms. The antibacterial rate of PCL scaffolds shows significant variation according to the spinning temperature used. The scaffolds spun at 200°C shows ~40% activity which is much higher than the other scaffolds spun at lower temperatures (95°C, 125°C, 155°C) for *E. coli*. Surprisingly, scaffolds spun at 95°C shows highest activity ~70% for *P. aeruginosa*. For this microorganism the antibacterial rate is lower for scaffolds spun at higher temperatures (125°C, 155°C, 200°C).

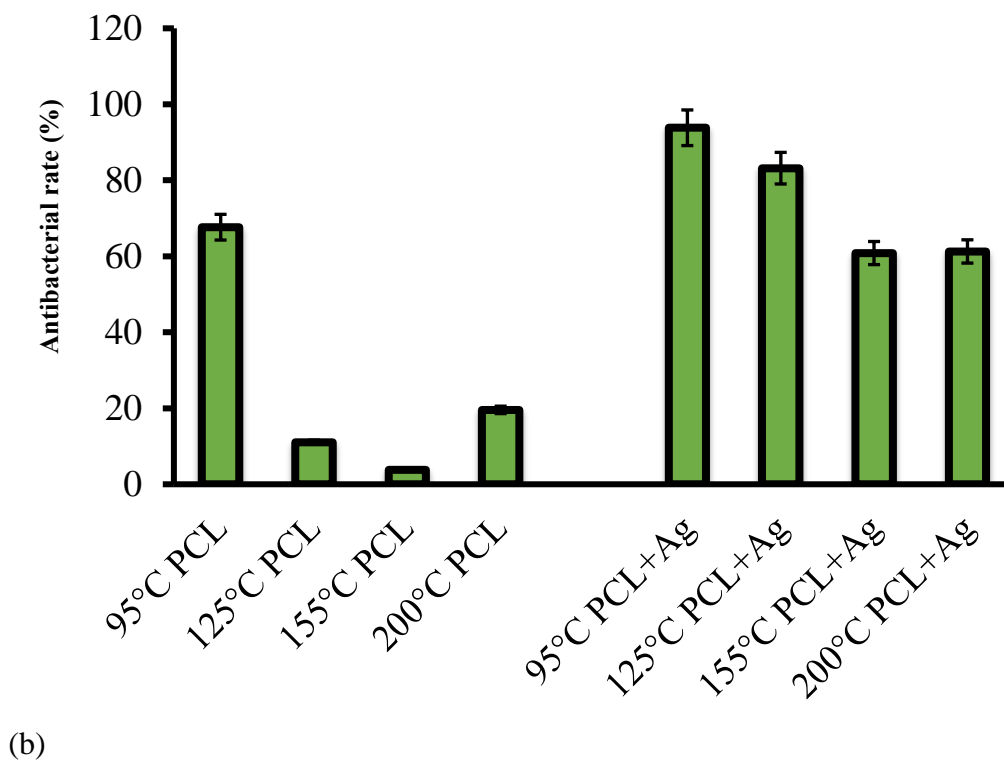
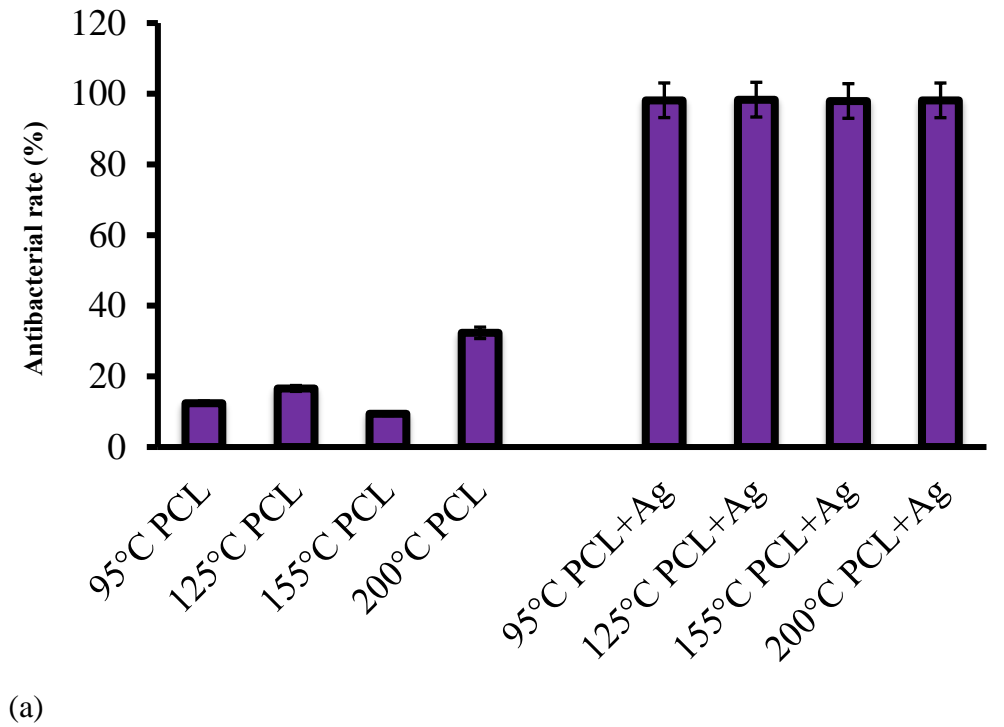


Figure 5.6: Antibacterial rates against (a) *E. coli* after 2 hours (b) *P. aeruginosa* after 2 hours for different types of fibre mats prepared in this work.

However, all PCL-Ag coated scaffolds showed enhanced antibacterial activity after 2 hr for *E. coli*. Although, the antibacterial activity of PCL-Ag coated scaffolds showed variation with spun temperatures for *P. aeruginosa*, the antibacterial activity was gradually reduced with increase in spinning temperature. The pure PCL fibres spun at 95°C showed non-ideal result of antibacterial activity for *P. aeruginosa* which the pure polymer fibre might not cause high bacterial death rate. The reason for this could be due to inhomogeneities in the processing and collection of fibres.

It is also worth noting that there was not any antibacterial activity observed after 24 hours for both microorganisms. It has been reported that Ag nanoparticle and Ag ions are responsible for bacterial cell death in Ag-coated polymer fibres. Moreover, the wettability of polymer fibres increases the antibacterial activity (Jung et al, 2007). Since PCL is hydrophobic polymer the antibacterial activity suffers from a longer period of exposure to bacterial cells.

5.8 Summary

A pressurised melt gyration process has been used for the first time to generate poly(ϵ -caprolactone) (PCL) fibres. Gyration speed, working pressure and melt temperature were varied and these parameters influenced the fibre diameter and the latter enabled changing the surface morphology of the fibres. Two types of non-woven PCL fibre constructs were prepared. Firstly, Ag-doped PCL was studied for antibacterial activity using Gram-negative *Escherichia coli* and *Pseudomonas aeruginosa* microorganisms. The melt temperature used to make these constructs significantly influenced antibacterial activity.

Chapter 6 - Making Pure poly(ethylene oxide)

Chitosan-Poly(ethylene oxide) Nanofibres by Pressurised Gyration

6.1 Introduction

In this chapter, two types of PEO nanofibres are investigated: different weight percentages of pure PEO nanofibres, and Ag nanoparticles and CuO nanoparticles loaded PEO nanofibres obtained using the pressurised gyration device. The solutions spun varied due to different polymer concentration, and different working pressures but at a fixed rotating speed of 36,000 rpm. The SEM images and the fibre diameter results show that concentration and working pressure exerted a significant influence the nanofibres formed.

PEO is soluble in both water and organic solvents, therefore this type of nanofibres cannot be used to assess the antibacterial activities of Ag nanoparticles and CuO nanoparticles. Consequently, chitosan solutions were added to the PEO solutions to form chitosan/PEO blend nanofibres. EDX analysis demonstrated the successful incorporation of CuO nanoparticles and Ag nanoparticles into the PEO/chitosan nanofibres. This enabled a comparison of antibacterial activities against the Gram-

negative *E. coli* and *P. aeruginosa* microorganisms. Different concentrations of bacterial suspensions were used to investigate the efficiency of the antimicrobial agents.

6.2 Formation of Poly(ethylene oxide) Nanofibres

6.2.1 Physical Properties of Poly(ethylene oxide) Solutions

In the pressurised gyration process the physical properties of polymer solutions significantly influences the formation of fibres. The surface tension and viscosity of the PEO solutions and nanoparticle loaded PEO solutions are presented in Table 6.1.

Table 6.1: Measured values of surface tension and viscosity for PEO solutions and nanoparticle loaded PEO solutions

PEO system solutions	Surface tension (mN/m)	Viscosity (mPa s)
10wt.% PEO	51.55 (± 1.9)	284.1 (± 1.2)
15wt.% PEO	53.05 (± 1.5)	1803 (± 2.6)
10wt.% PEO + 2wt.% Ag	52.35 (± 1.8)	291.08 (± 1.5)
15wt.% PEO + 2wt.% Ag	53.66 (± 3.4)	1743.5 (± 11.4)
15wt.% PEO + 2wt.% CuO	71.03 (± 0.8)	2363.5 (± 48.1)
15wt.% PEO + 5wt.% CuO	74.53 (± 1.5)	2465 (± 17.1)

The surface tension and viscosity of the PEO solution increased with solute content. For the 15 wt.% PEO solution the surface tension was ~ 53.05 mN/m, which is nearly double the value for the 10 wt.% PEO solution. The viscosity of the 15 wt.% PEO solution was

~1803 mPa, which was an order of magnitude higher than that for the 10 wt.% PEO solution. Similarly, the surface tension and viscosity were increased with the solute content in the Ag-loaded PEO solutions. Compared to the values of surface tension and viscosity for 2 wt.% CuO loaded 15 wt.% PEO solution and 5 wt.% CuO loaded 15 wt.% PEO solution, the higher weight percentage of CuO nanoparticles also resulted in higher surface tension and viscosity. For a given molecular weight, the increase in viscosity with the solute content was due to an increase in chain entanglement in the polymer solution, where the polymer chains overlap each other to form a strong network. At a low concentration, low viscosity was observed due to insufficient chain entanglement as a result of the lack of physical interlocking of the chains (Shenoy et al., 2005).

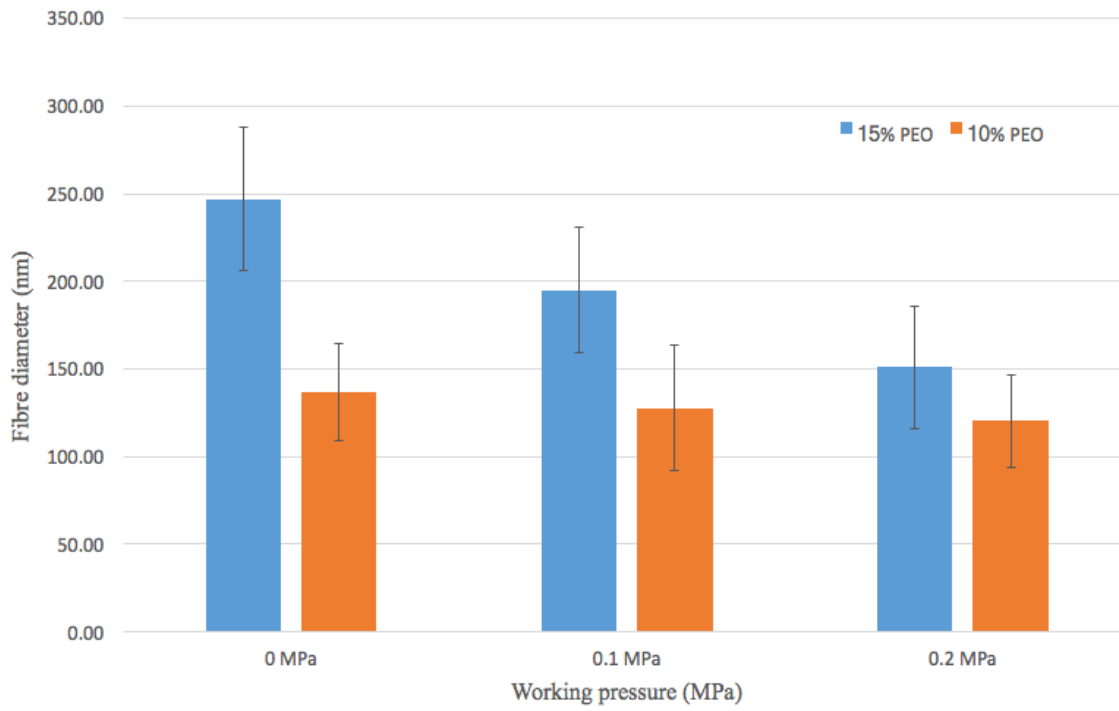
6.2.2 Fibre Diameter Analysis

Table 6.1 and Figure 6.1 (a), (b) and (c) show the nanofibre diameter variation with working pressure for pressurised gyration at a fixed rotating speed of 36,000 rpm for different weight percentages of pure PEO, Ag (2 and 5 wt.%) loaded PEO and CuO (2 and 5 wt.%) loaded PEO polymer solutions. The fibre diameters obtained were in the range 130 nm to 263 nm. Compared to the fibre diameters for different weight percentages of PEO or nanoparticles, thicker fibres were produced at higher polymer or nanoparticle concentrations. The mean diameter of 15 wt.% PEO fibres was 246.97nm, and 136.98 nm for 10 wt.% PEO solution. The fibre diameter of 2 wt.% Ag loaded 10 wt.% PEO solution was smaller than that for 2 wt.% Ag loaded 15 wt.% PEO, and also smaller than for 5 wt.% Ag loaded 15 wt.% PEO solution. Not only did solution concentration effect the fibre diameter, but also the working pressure. Table 6.2 and Figure 6.1 show that there an increase in the working pressure reduces the fibre diameter.

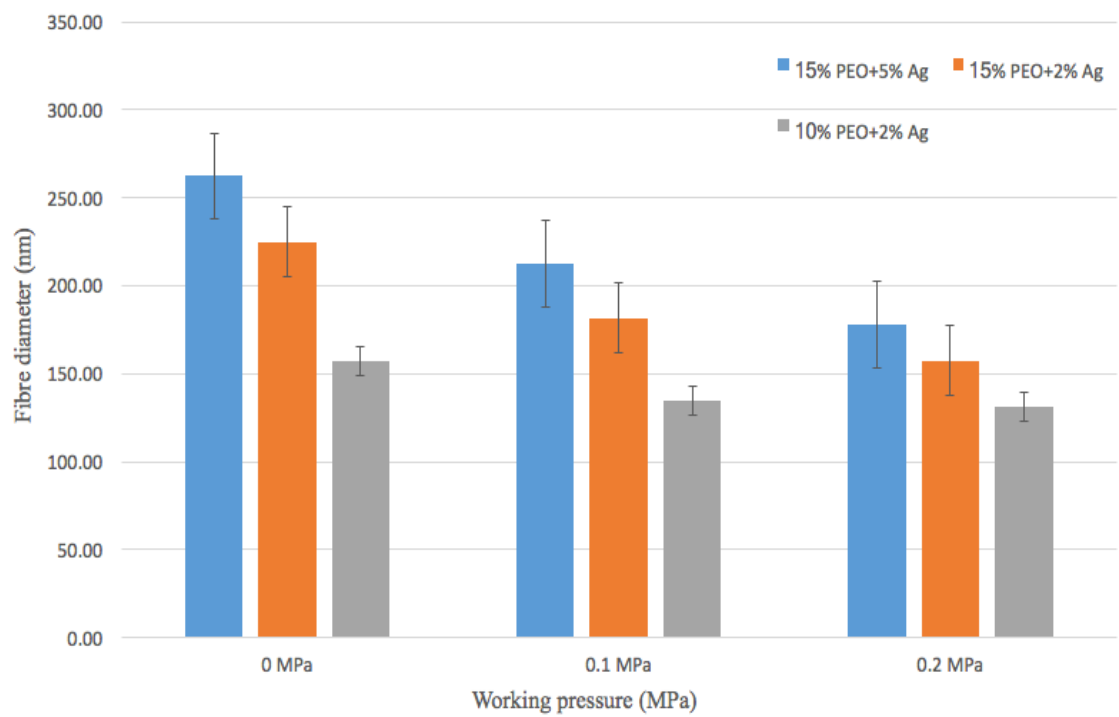
For the 15 wt.% PEO solution the fibre diameter was reduced from 247 nm to 151 nm when the working pressure was raised from 0 MPa to 0.2 MPa at a rotating speed of 36,000 rpm. The fibre diameter at no working pressure was also found to be larger than that at higher working pressures for fibres fabricated from the other solutions.

Table 6.2: Fibre diameter variation for different conditions of pressurised gyration.

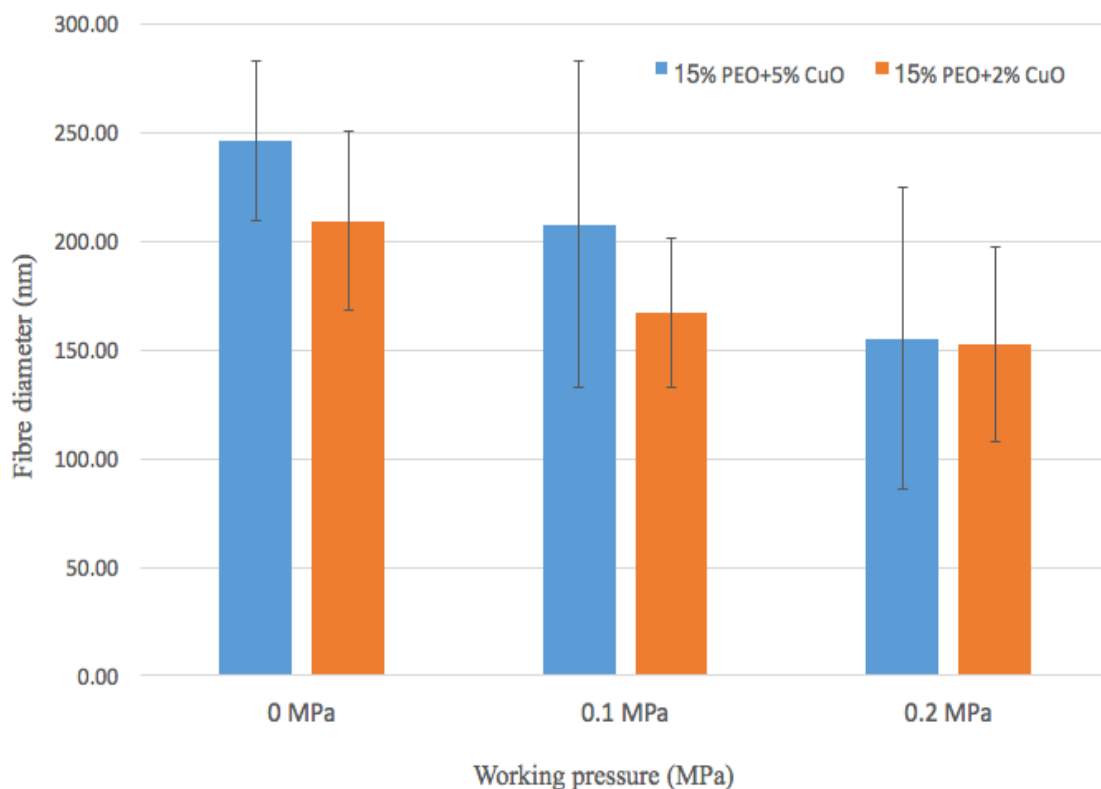
PEO + nanoparticle loading	Fibre Diameter (nm) at rotating speed (rpm); working pressure (MPa) combinations		
	36000; 0	36000; 0.1	36000; 0.2
15wt.% PEO	247 (\pm 41)	195 (\pm 36)	151 (\pm 35)
10wt.% PEO	137 (\pm 28)	128 (\pm 36)	120 (\pm 26)
15wt.% PEO + 5 wt.% Ag	262 (\pm 71)	212 (\pm 59)	178 (\pm 84)
15wt.% PEO + 2 wt.% Ag	225 (\pm 66)	181(\pm 34)	157 (\pm 43)
10wt.% PEO + 2 wt.% Ag	157 (\pm 9)	134 (\pm 50)	131 (\pm 40)
15wt.% PEO + 5 wt.% CuO	246 (\pm 37)	208 (\pm 75)	155 (\pm 69)
15wt.% PEO + 2 wt.% CuO	209 (\pm 41)	167 (\pm 34)	153 (\pm 45)



(a)



(b)

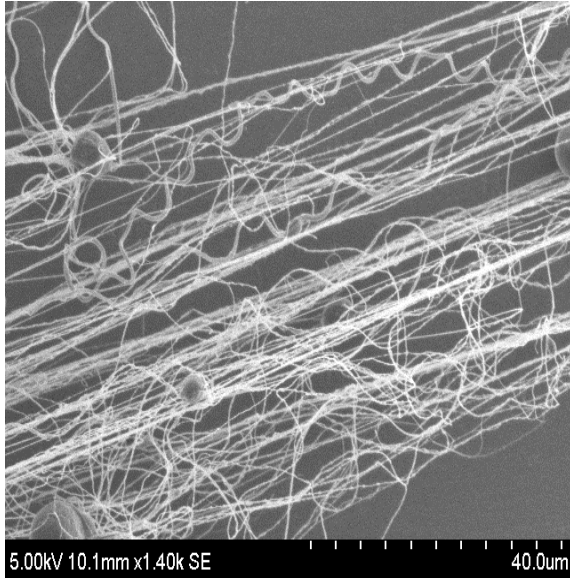


(c)

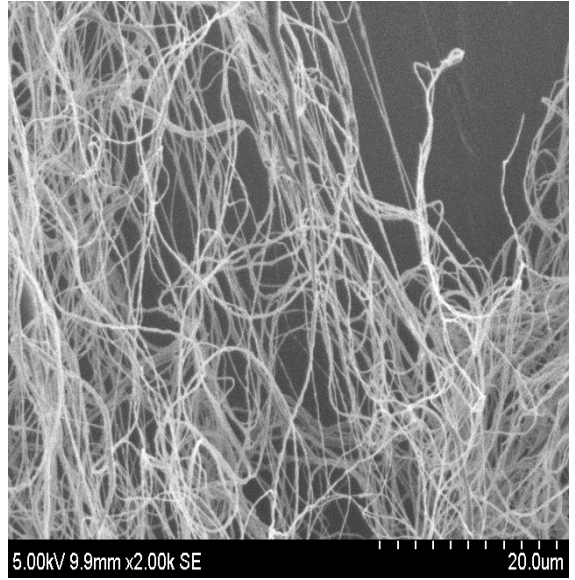
Figure 6.1: Fibre diameter under varying concentrations and working pressures at a fixed rotating speed of 36000 rpm (a) Pure PEO solutions; (b) Ag nanoparticle loaded PEO solutions; (c) CuO nanoparticle loaded PEO solutions.

6.2.3 Fibre Diameter Analysis

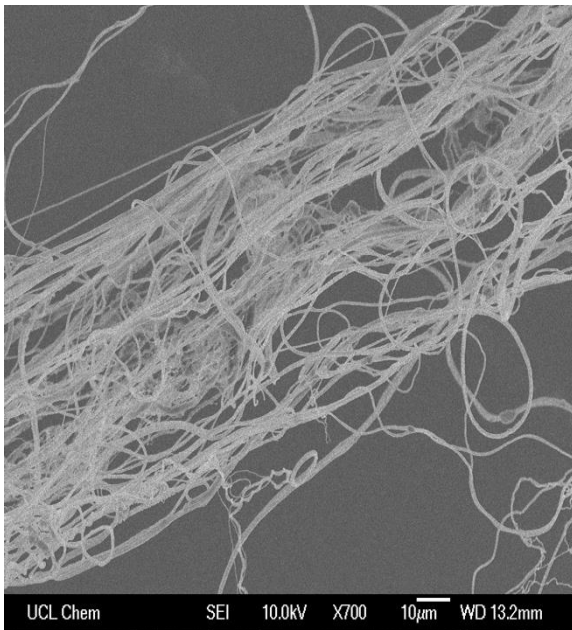
In order to investigate the fibre diameter and surface morphology, SEM was used to obtain high resolution images. Figure 6.2 shows the SEM images for PEO, Ag loaded PEO, and CuO loaded PEO nanofibres. Ag loaded PEO fibres were revealed to have more beads present on their surface, while PEO fibres and CuO loaded PEO fibres were smoother than the Ag loaded PEO fibres.



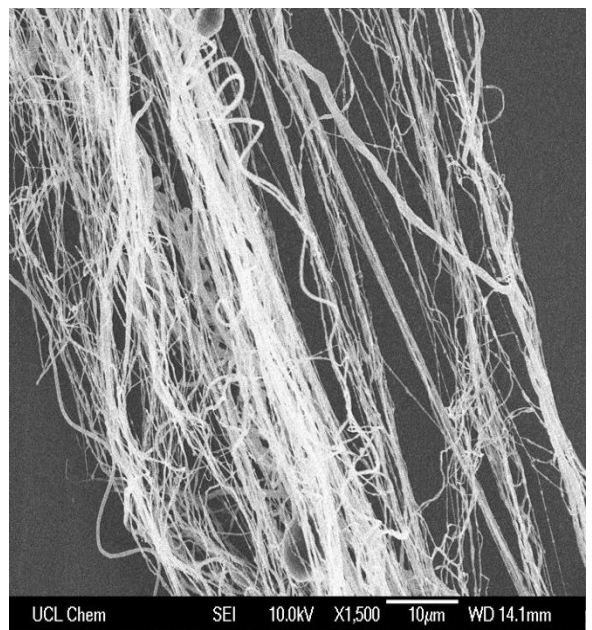
(a)



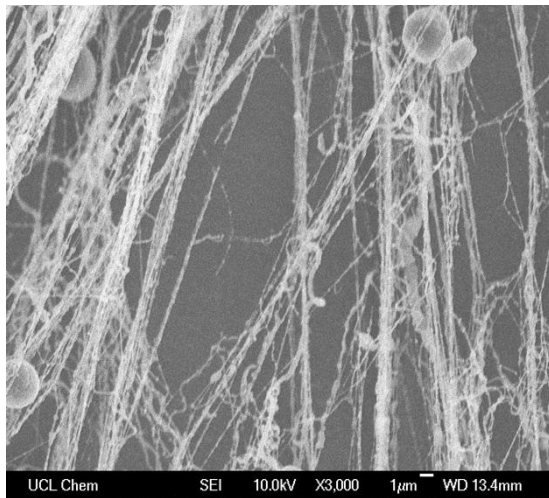
(b)



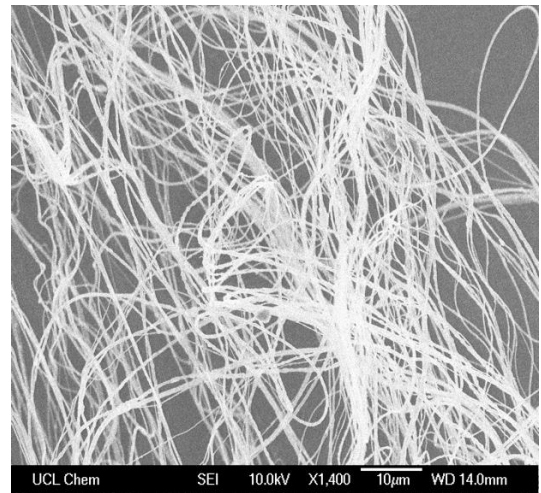
(c)



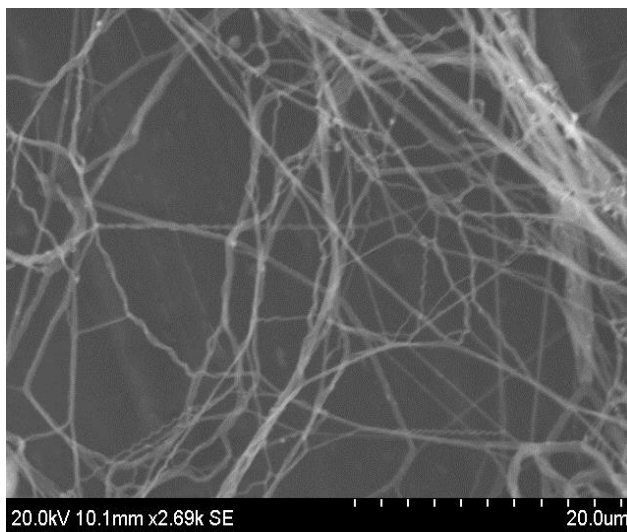
(d)



(e)



(f)



(g)

Figure 6.2: SEM images of PEO and Ag and CuO loaded PEO fibres (a) 15 wt.% PEO (b) 10 wt.% PEO (c) 5 wt.% Ag loaded 15 wt.% PEO (d) 2 wt.% Ag loaded 15 wt.% PEO (e) 2 wt.% Ag loaded 10 wt.% PEO (f) 5 wt.% CuO loaded 15 wt.% PEO (g) 2 wt.% CuO loaded 15 wt.% PEO.

6.3 Formation of Chitosan-Poly(ethylene oxide) Blend Nanofibres

6.3.1 Physical Properties of Chitosan-Poly(ethylene oxide) Blend

Solutions

The experimentally measured values of surface tension and viscosity are given in (Table 6.3). The surface tension of the nanoparticle (CuO and Ag) loaded polymer solution is higher than the pure polymer solutions. The viscosity is increased with the loading concentration of polymer solution and nanoparticles.

Table 6.3: Measured values of surface tension and viscosity

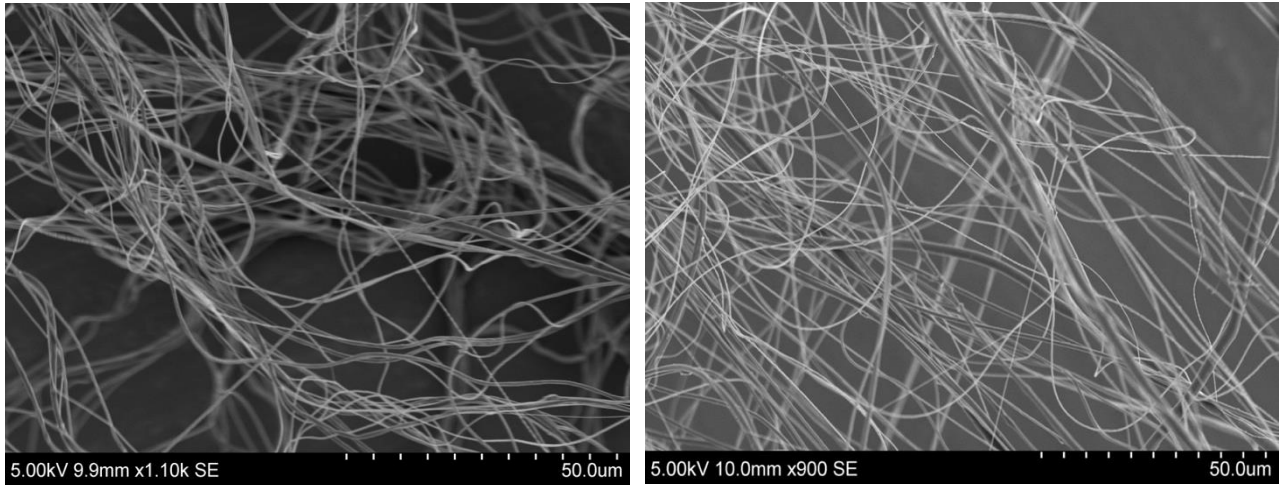
PEO/chitosan solutions	Surface tension (mN/m)	Viscosity (mPa s)
20wt.% PEO	59.2 (± 2.5)	3000 (± 110)
1wt.% Chitosan	64.9 (± 1.8)	125 (± 1.2)
2wt.% Chitosan	76.3 (± 3.5)	570.5 (± 6.6)
20wt.% PEO + 1wt.% Chitosan	73.4 (± 1.4)	2800 (± 100.8)
20wt.% PEO + 2wt.% Chitosan	76.7 (± 1.5)	3198 (± 114.1)
20wt.% PEO + 1wt.% Chitosan + 0.5wt.% Ag	69.6 (± 1)	1512 (± 52.4)
20wt.% PEO + 1wt.% Chitosan + 1wt.% Ag	70.1 (± 1.7)	924.9 (± 43.5)

20wt.% PEO + 1wt.% Chitosan + 0.5% CuO	83.2± 2.4	1850 ± 75.6
20wt.% PEO + 1wt.% Chitosan + 1% CuO	88.9± 3.5	1520 ± 80.5

6.3.2 Fibre diameter analysis

Pressurised gyration of pure chitosan was not possible at all the processing parameters. This is mainly attributed to the low solubility of chitosan in common organic solvents thus resulting in a too low concentration of chitosan for the gyration process. For an effective gyration process a higher concentration of polymer solution and a higher degree of chain entanglement is required. To overcome this problem PEO was added to the chitosan solution as a binder and a blending agent. The addition of PEO increased the chain entanglement which becomes sufficient enough for effective pressurised gyration. The polymer solution's physical properties such as surface tension and viscosity govern the gyration process. The influence of these physical properties has been explained previously (Mahalingam & Edirisinghe, 2013; Mahalingam, Ren & Edirisinghe, 2014).

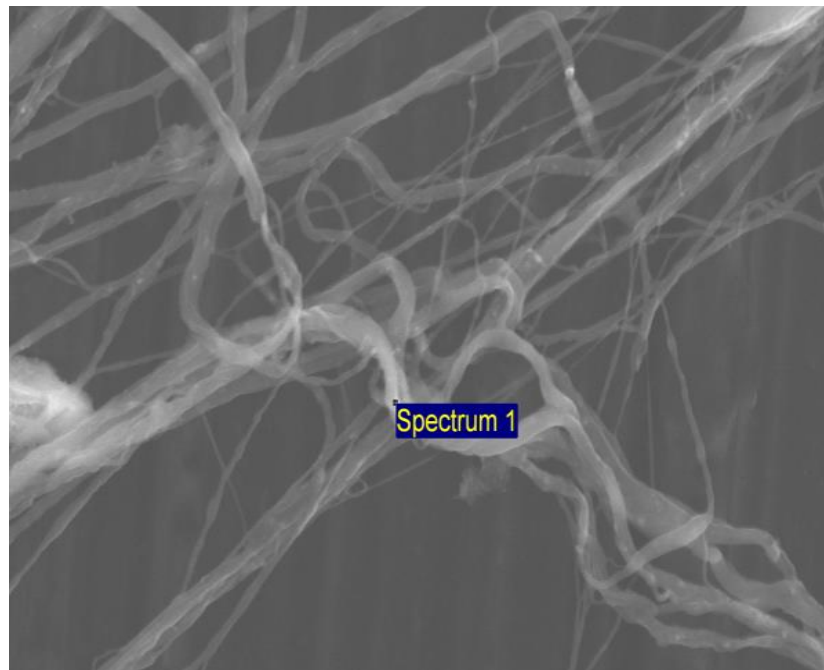
Figure 6.3 shows the electron micrographs of the PEO/chitosan fibres obtained at 36000 rpm and 0.2 MPa working pressure. Geometrically uniform and bead-less fibres could be obtained with a weight ratio of 4:1 PEO/chitosan solutions.



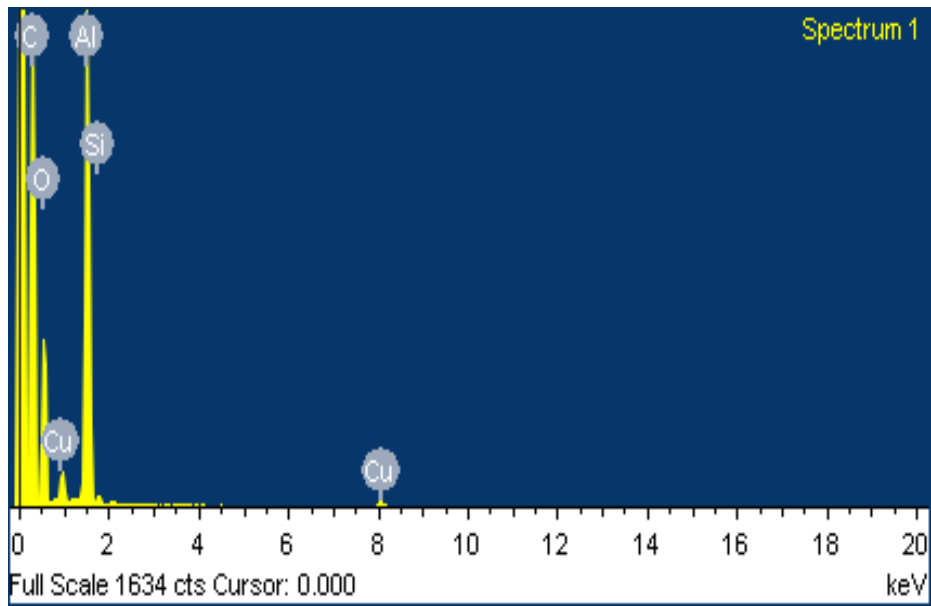
(a)

(b)

Figure 6.3: SEM images of the 20wt.% PEO/chitosan fibres obtained at 36000 rpm and 0.2 MPa working pressure (a) 1wt.% chitosan; (b) 2wt.% chitosan.

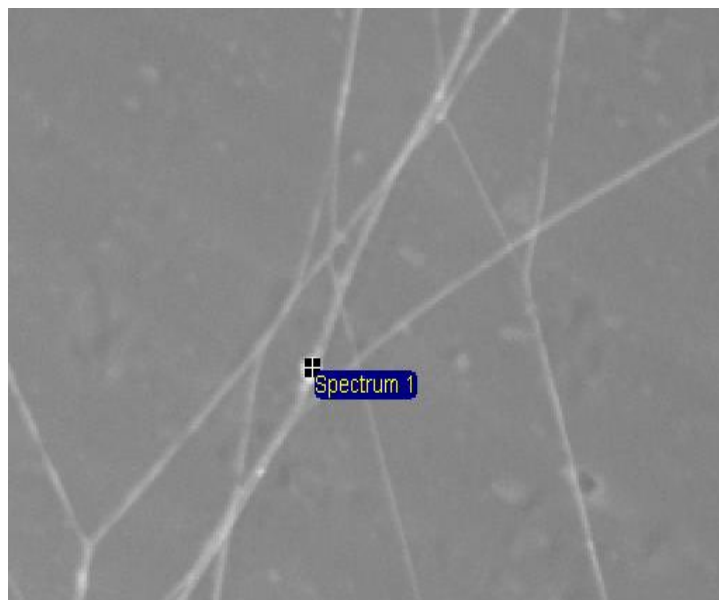


(a)

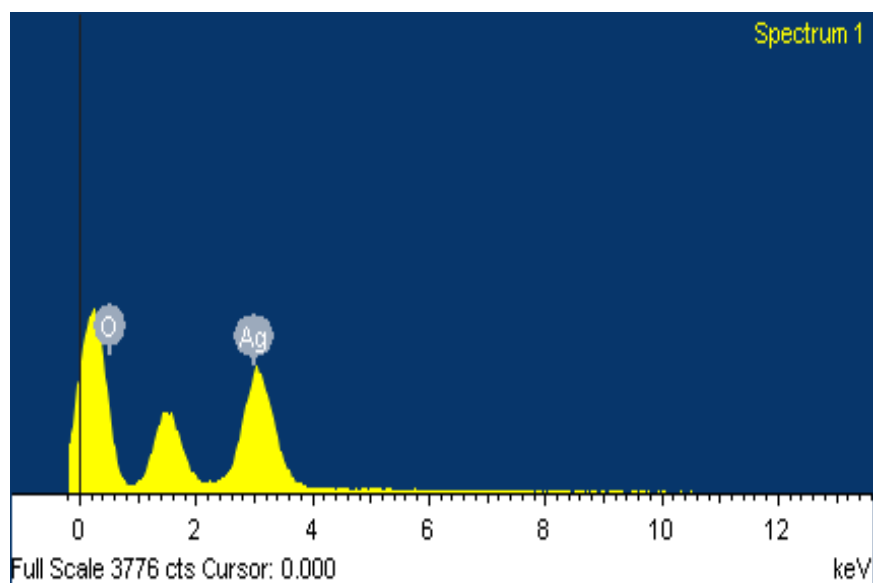


(b)

Figure 6.4: (a) SEM micrograph showing that the CuO nanoparticles were distributed on nanofibers made using the 20 wt.% PEO with 1 wt.% Chitosan – 1 wt.% CuO nanoparticle, and (b) the corresponding EDX analysis



(a)



(b)

Figure 6.5: (a) SEM micrograph showing that the Ag nanoparticles were distributed on nanofibers made using the 20 wt.% PEO with 1 wt.% Chitosan – 1 wt.% Ag nanoparticle, and (b) the corresponding EDX analysis.

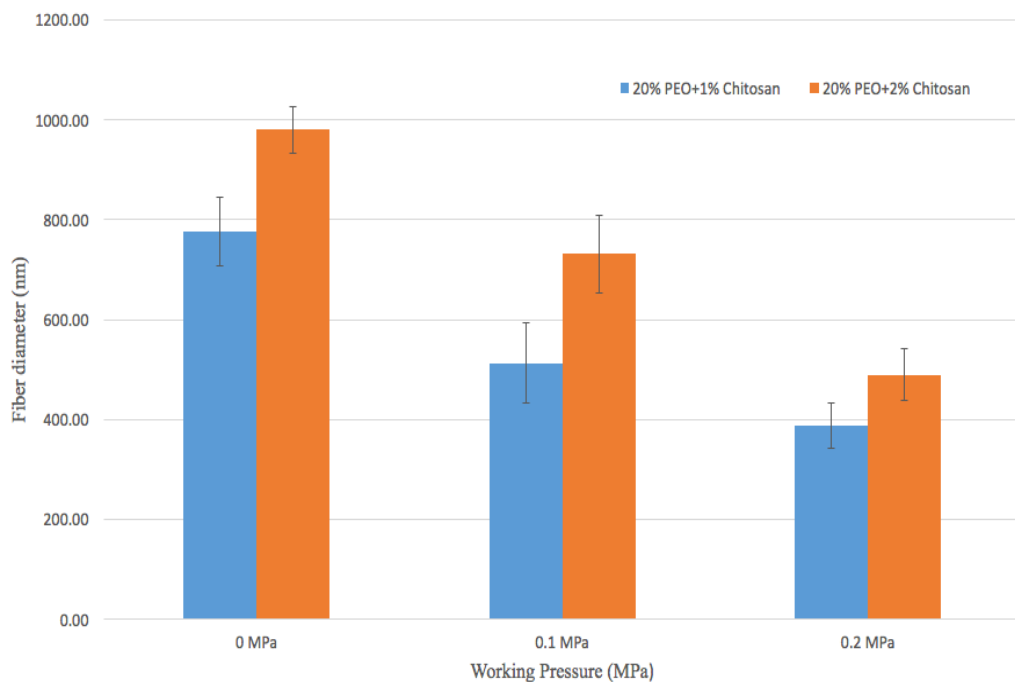
The SEM - EDX analysis (Figure 6.4) on the fibres confirmed the embedding of CuO nanoparticles on the surface of the fibres. The elemental analysis gave copper to oxygen ratio percentage 60:40 which corroborates the results of EDX analysis on the CuO nanoparticles. Figure 6.5 also clearly show the Ag nanoparticles incorporated in fibres. Thus, pressurized gyration was also successful in generating nanoparticle containing PEO/Chitosan nanofibers.

Figure 6.6 (a) and (b) show the nanofiber diameter variation with working pressure for pressurised gyration at a fixed rotating speed of 36000 rpm for PEO/Chitosan, CuO loaded and Ag-loaded PEO/Chitosan polymer solutions, respectively. A fiber diameter in the range of 388 nm to 980 nm was achieved for the PEO/Chitosan samples, and this

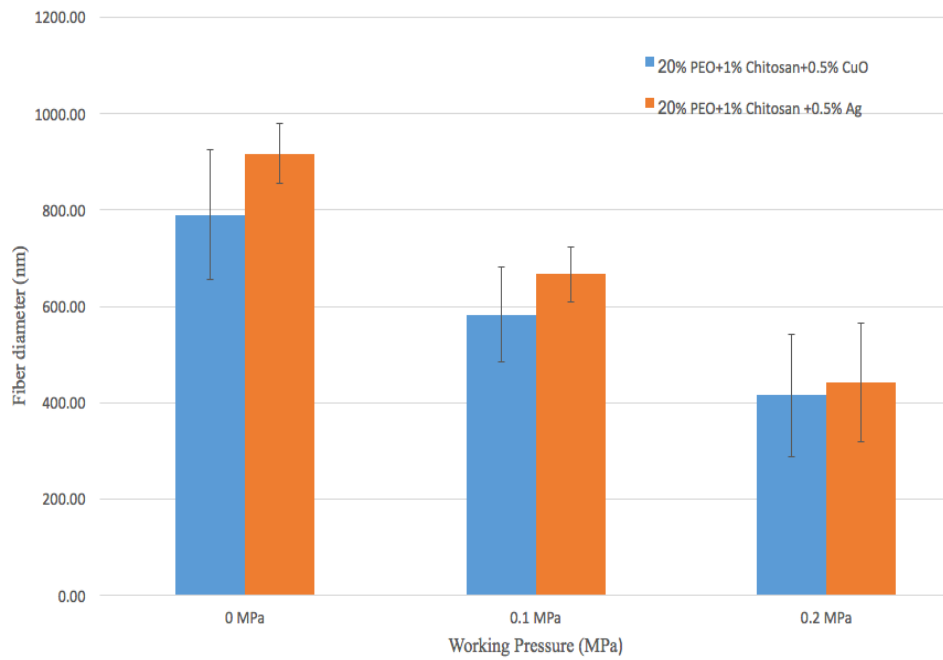
was 415 nm to 790 nm for CuO-loaded PEO/Chitosan, 442 nm to 917 nm for Ag-loaded PEO/Chitosan. It is clear that increase of the working pressure reduced the fiber diameter. For 20wt.%PEO/1wt.%chitosan solution the fiber diameter was reduced from 776 nm to 388 nm on increasing the working pressure from 0 MPa to 0.2 MPa at a rotating speed of 36000 rpm. Similarly, the fiber diameter was reduced from 980 nm to 490 nm 20wt.%PEO/2wt.%chitosan solutions.

The results also confirmed that the viscosity of solution has a significant influence on the fibre diameter, the solution has high viscosity, the fibre will be thicker. Ag-loaded PEO/Chitosan fibre has larger fibre diameter (eg. 917 nm at 0 bar working pressure) correspond to its high viscosity than the CuO-loaded PEO/Chitosan fibre diameter (790 nm at 0 bar working pressure) at the same spinning condition.

The change in fiber diameter is influenced by the combined effects of concentration of polymer, and the working pressure and these are summarised in Table 6.4.



(a)



(b)

Figure 6.6: Fiber diameter for 20 wt.% PEO with Chitosan under varying working pressure at a fixed rotating speed of 36000 rpm (a) 1 wt.% and 2 wt.% of Chitosan. (b) 0.5 wt.% CuO nanoparticles and 0.5 wt.% Ag nanoparticles.

Table 6.4: Fibre diameter variation for different conditions of pressurised gyration

PEO + Chitosan + nanoparticles loading	Fiber Diameter (nm) at Rotating Speed (rpm); working Pressure (MPa) combinations		
	36000; 0	36000; 0.1	36000; 0.2
20 wt.% +1 wt.%+0 wt.%	776 (±69)	513 (±80)	388 (±45)
20 wt.% +2 wt.%+0 wt.%	980 (±48)	731 (±77)	489 (±52)

20 wt.% +1 wt.%+0.5 wt.% CuO	790 (\pm 135)	583 (\pm 98)	415 (\pm 128)
20 wt.% +1 wt.%+0.5 wt.% Ag	917 (\pm 62)	667 (\pm 57)	442 (\pm 123)

6.4 Antibacterial Activity

The pure PEO nanofibres dissolved in the bacteria suspensions immediately as PEO is water soluble. Consequently, PEO with chitosan fibres were used to slow the dissolution rate of the nanofibres.

The antibacterial properties of the nanofibre samples were evaluated using Gram-negative *E. coli* and *P. aeruginosa*. The assay was performed using bacteria cultured overnight from a single colony to stationary phase (approximately 10^9 CFU/ml) in TSB in a shaking aerobic incubator at 37°C. Two different concentrations of bacteria suspensions, $\sim 0.5 \times 10^6$ CFU/ml and $\sim 1 \times 10^6$ CFU/ml in TSB, were prepared in a sterile laminar flow hood environment. Six fibre samples all of the same weight (0.05 g) were prepared from : 20 wt.% PEO/1 wt.% chitosan nanofibres, 20 wt.% PEO/2 wt.% chitosan nanofibres; 20 wt.% PEO/1 wt.% chitosan with 0.5 wt.% CuO nanofibres; 20 wt.% PEO/1 wt.% chitosan with 1 wt.% CuO nanofibres; 20 wt.% PEO/1 wt.% chitosan with 0.5 wt.% Ag nanofibres; and 20 wt.% PEO/ 1 wt.% chitosan with 1 wt.% Ag nanofibres. The samples and two controls were placed in a small tube together with 0.5 ml of the *E. coli* or *P. aeruginosa* bacterial suspensions. The tubes were cultured in an aerobic shaking incubator at 37°C for set periods of time.

6.4.1 Antibacterial activity of gram-negative *E.coli* cells

Antibacterial activity of blended fibres with different concentration of chitosan and the different concentration of CuO and Ag were evaluated using *E-Coli* gram-negative cells for 30, 60, 120 and 180 minutes in control atmosphere. Figure 6.7 shows the viability of *E-Coli* cells for different samples and at varying time intervals. There were two marked trends observed for these samples. Firstly, the viability of the cells was decreased when increasing the time from 30 to 180 minutes for 20wt.%PEO/1wt.%chitosan and 20wt.%PEO/2wt.%chitosan. The antibacterial rate decreased from 18.5%, 15.7%, 10.5% and 9.1% for 20wt.%PEO/1wt.%chitosan after incubating 30, 60, 120 and 180 minutes, respectively. The antibacterial rate decreased from 32%, 27.8%, 10.5% and 12.7% for 20wt.%PEO/2wt.%chitosan after incubating 30, 60, 120 and 180 minutes, respectively. Blended fibres with higher concentration of chitosan show stronger antibacterial activity than blended fibres with lower concentration of chitosan.

Secondly, the viability of *E. Coli* cells was increased with increase of incubating time for 20wt.%PEO/1wt.%chitosan/0.5wt.%CuO and 20wt.%PEO/1wt.%chitosan/1wt.%CuO. The antibacterial rate increased from 34%, 82%, 96.6% and 99.9% for 20wt.%PEO/1wt.%chitosan/0.5wt.%CuO after incubating 30, 60, 120 and 180 minutes, respectively. Meanwhile, the antibacterial rate increased from 46.3%, 85.3%, 99.9% and 99.9% for 20wt.%PEO/1wt.%chitosan/1wt.%CuO after incubating 30, 60, 120 and 180 minutes, respectively. There is a significant increase in antibacterial activity of 20wt.%PEO/1wt.%chitosan/0.5wt.%CuO and 20wt.%PEO/1wt.%chitosan/1wt.%CuO which are consisting of CuO nanoparticles. Addition of CuO nanoparticles to the PEO/chitosan blended fibres increased the

antibacterial rate by an order of magnitude after 180 minutes of incubating time. Increasing the concentration of CuO nanoparticles from 0.5 to 1wt.% to the existing blended fibres also increased the antibacterial activity. The increase of antibacterial activity is more pronounced for 30 minutes of incubation time when increasing the concentration of CuO nanoparticles from 0.5 to 1 wt.% in 20wt.%PEO/1wt.%chitosan blended fibres.

Moreover, the samples contain Ag nanoparticles shows the increased antibacterial activity compared to samples PEO/chitosan. There is a significant increase in antibacterial activity is observed with addition of Ag nanoparticles to PEO/chitosan blends. The antibacterial rate increased from 44.4%, 88.5%, 97.7% and 99.9% for 20wt.%PEO/1wt.%chitosan/0.5wt.%Ag after incubating 30, 60, 120 and 180 minutes, respectively. On contrary, the antibacterial rate increased from 76.9%, 98.6%, 99.9% and 99.9% for 20wt.%PEO/1wt.%chitosan/1wt.%Ag after incubating 30, 60, 120 and 180 minutes, respectively. There is a marked increase in antibacterial activity when increasing the Ag nanoparticle concentration from 0.5 to 1 wt.% in 20wt.%PEO/1wt.%chitosan blended fibres after incubating 30 and 60 minutes. However, increasing the incubating time to 120 and 180 minutes resulted in less pronounced increase in antibacterial activity.

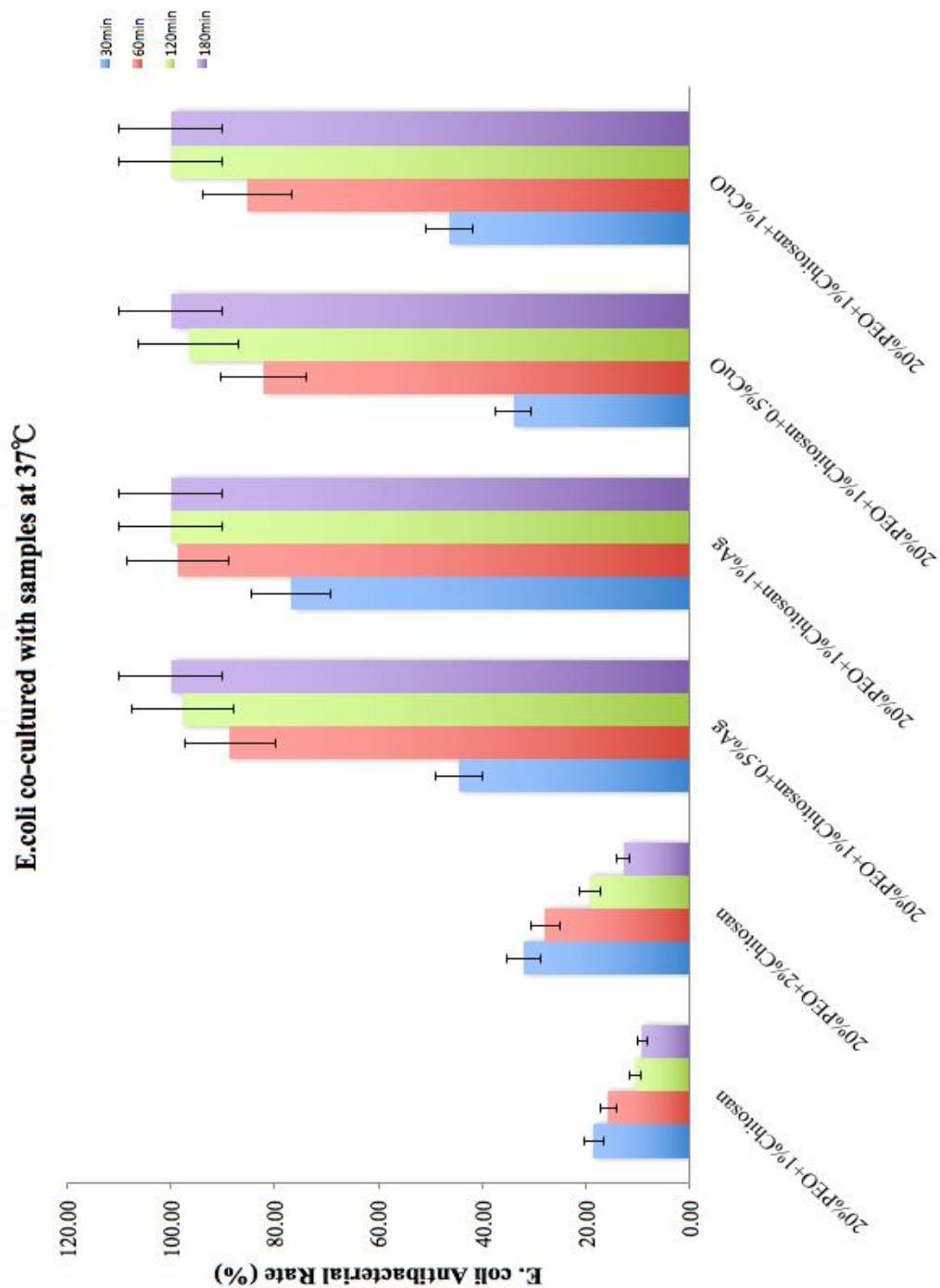


Figure 6.7: Antibacterial rate for 20wt.%PEO/1wt.%chitosan, 20wt.%PEO/2wt.%chitosan, 20wt.%PEO/1wt.%chitosan/0.5wt.%CuO, 20wt.%PEO/1wt.%chitosan/1wt.%CuO, 20wt.%PEO/1wt.%chitosan/0.5wt.%Ag and 20wt.%PEO/1wt.%chitosan/1wt.%Ag nanofibre mats after 30, 60, 120 and 180 minutes incubation with *E-coli* suspension ($\sim 0.5 \times 10^6$ CFU/ml).

6.4.2 Antibacterial activity of gram-negative *P. aeruginosa* cells

Antibacterial performance of PEO/chitosan blended fibres was also evaluated using *P. aeruginosa* gram-negative cells for 30, 60, 120 and 180 minutes in control atmosphere. Figure 6.8 shows the viability of *P. aeruginosa* cells for different samples and at varying time intervals. PEO/chitosan blended fibres without any metal nanoparticles show a weaker antibacterial activity compared with PEO/chitosan blended fibres with CuO, Ag nanoparticles. The antibacterial rate decreased from 15.3%, 10.5%, 8.3% and 7.7% for 20wt.%PEO/1wt.%chitosan after incubating 30, 60, 120 and 180 minutes, respectively. The antibacterial rate decreased from 17.62%, 13.01%, 10.5% and 9.9% for 20wt.%PEO/2wt.%chitosan after incubating 30, 60, 120 and 180 minutes, respectively. Blended fibres with higher concentration of chitosan show stronger antibacterial activity than blended fibres with lower concentration of chitosan. The results also consistent with our previous observation that PEO/chitosan blended fibre's antibacterial activity decreases with incubation time. Antibacterial performance of PEO/chitosan blended CuO nanoparticles and Ag nanoparticles fibres was increased with increase of incubating time. The antibacterial rate increased from 20.4%, 40.9%, 59.03% and 85.9% for 20wt.%PEO/1wt.%chitosan/0.5wt.%CuO after incubating 30, 60, 120 and 180 minutes, respectively. On the other hand, the antibacterial rate increased from 28.2%, 51.2%, 83.9% and 99.9% for 20wt.%PEO/1wt.%chitosan/1wt.%CuO after incubating 30, 60, 120 and 180 minutes, respectively. 20wt.%PEO/1wt.%chitosan/0.5wt.%CuO shows slightly weaker antibacterial activity than 20wt.%PEO/1wt.%chitosan/1wt.%CuO. It should also noted that the shaking speed for all the tests was kept constant. Although some of the particles may precipitate during the testing for 3 hours, under shaking condition nanoparticles were well suspended in the

solution and interacting with *P. aeruginosa* cells.

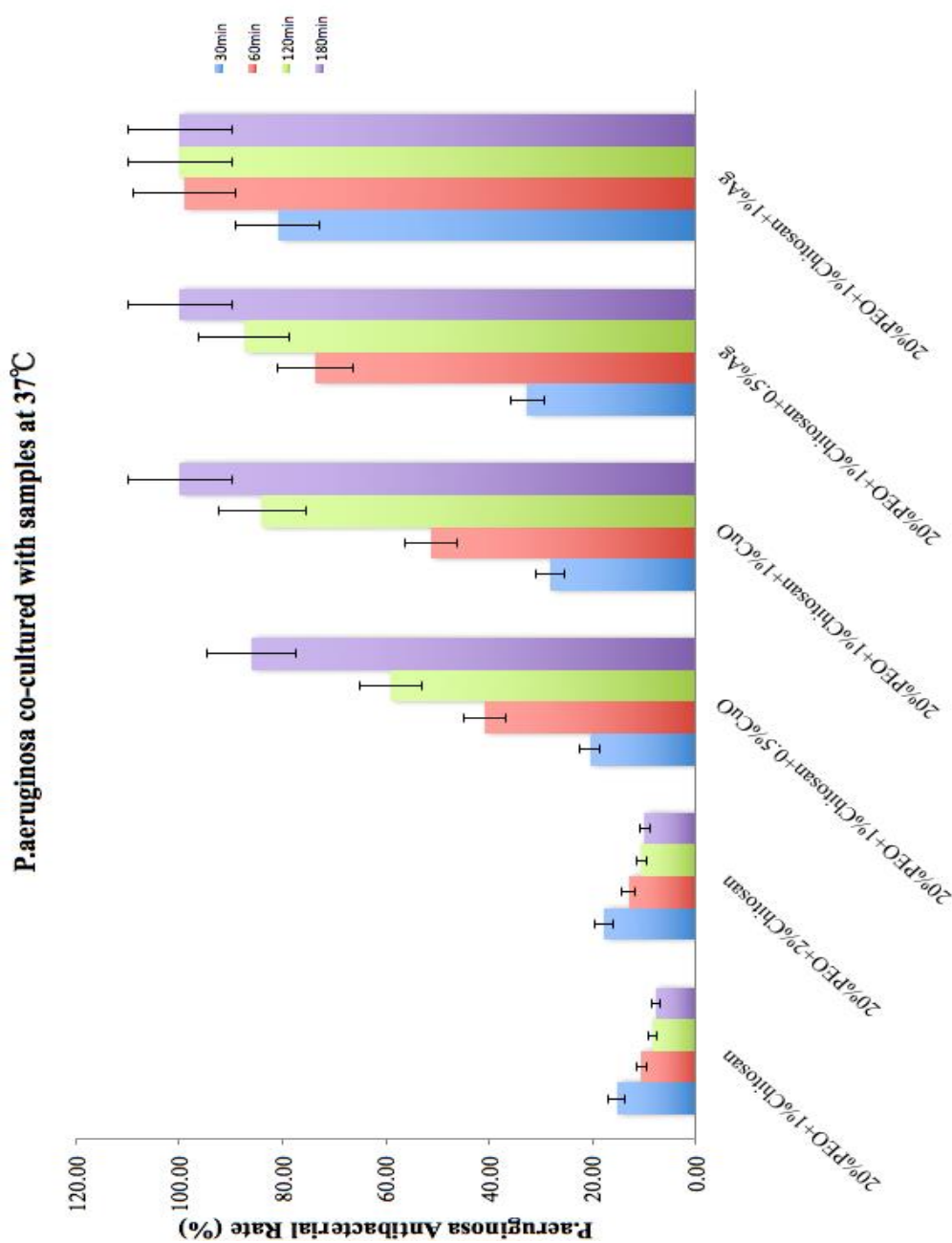
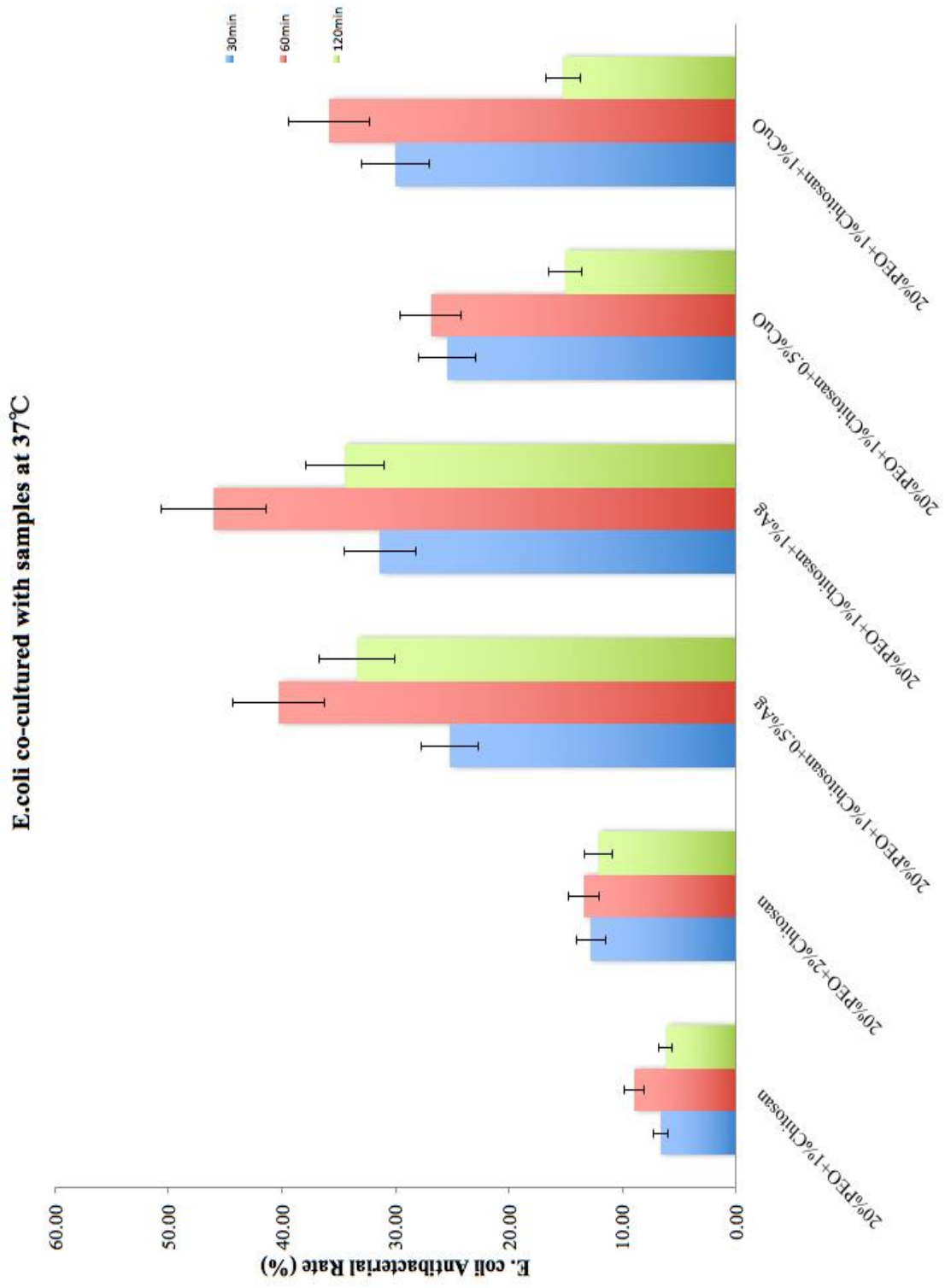


Figure 6.8: Antibacterial rate for 20wt.%PEO/1wt.%chitosan, 20wt.%PEO/2wt.%chitosan, 20wt.%PEO/1wt.%chitosan/0.5wt.%CuO, 20wt.%PEO/1wt.%chitosan/1wt.%CuO, 20wt.%PEO/1wt.%chitosan/0.5wt.%Ag and 20wt.%PEO/1wt.%chitosan/1wt.%Ag nanofibre mats after 30, 60, 120 and 180 minutes incubating with *P. aeruginosa* suspension ($\sim 0.5 \times 10^6$ CFU/ml).

In addition, as shown in Figure 6.8, the loss of *P. aeruginosa* viability progressively goes up with incubation time. The loss of *P. aeruginosa* viability increases to 32.6%, 73.6%, 84.4% and 99.9% for 20wt.%PEO/1wt.%chitosan/0.5wt.%Ag after incubating 30, 60, 120 and 180 minutes, respectively. On contrary, the antibacterial rate increased from 80.9%, 98.9%, 99.9% and 99.9% for 20wt.%PEO/1wt.%chitosan/1wt.%Ag after incubating 30, 60, 120 and 180 minutes, respectively. There is a 2.5 fold increase in antibacterial activity when increasing the Ag nanoparticle concentration from 0.5 to 1 wt.% in 20wt.%PEO/1wt.%chitosan blended fibres after incubating 30 minutes. Samples treated after 1 hour also shows increase in antibacterial performance, although the increase in less than previous case. However, increasing the incubating time to 120 and 180 minutes resulted in a complete inactivation of *P. aeruginosa* cells for 20wt.%PEO/1wt.%chitosan/1wt.%Ag blended fibres.

The comparative antibacterial performance of *E. Coli* and *P. aeruginosa* cells in PEO/chitosan, PEO/chitosan/CuO and PEO/chitosan/Ag nanoparticles as follows. There is an increase in antibacterial activity observed for PEO/chitosan blended fibres treated with *E. Coli* suspension than *P. aeruginosa*. Increasing the chitosan concentration in the blended fibres increased the antibacterial activity for both suspensions. PEO/chitosan/CuO blended fibres incubated with *E. Coli* cells show a stronger antibacterial performance than PEO/chitosan/CuO blended fibres incubated *P. aeruginosa* with cells. Increasing the CuO nanoparticle concentration in the blended fibres increased the antibacterial activity for both suspensions. A similar observation is found for PEO/chitosan/Ag blended fibres where a stronger antibacterial performance is observed for *E. Coli* suspensions than *P. aeruginosa* suspensions. Although the concentration of the suspensions, incubation time and shaking speed is kept constant for all the tests, this indicates that the nature of microorganisms influences the antibacterial

performance.



(a)

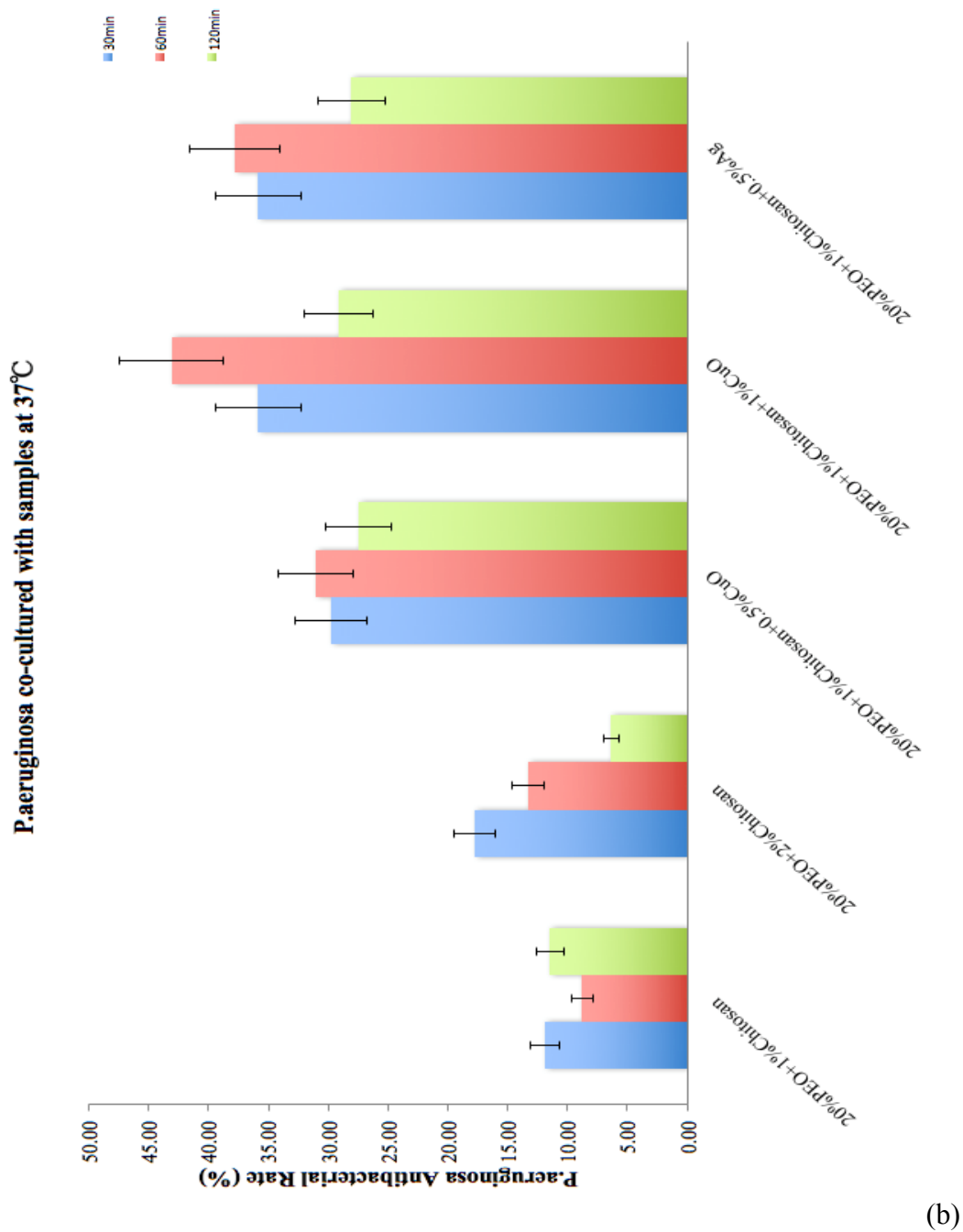


Figure 6.9: Antibacterial rate for 20wt.%PEO/1wt.%chitosan, 20wt.%PEO/2wt.%chitosan, 20wt.%PEO/1wt.%chitosan/0.5wt.%Ag, 20wt.%PEO/1wt.%chitosan/1wt.%Ag, 20wt.%PEO/1wt.%chitosan/0.5wt.%CuO, and 20wt.%PEO/1wt.%chitosan/1wt.%CuO, nanofibre mats after 30, 60, and 120 minutes incubation with (a) *E. coli* ($\sim 1 \times 10^6$ CFU/ml); (b) *P. aeruginosa* ($\sim 1 \times 10^6$ CFU/ml).

As the contact time increased the percentage (%) of bacterial colonies reduced and plateaued for CuO-loaded and Ag-loaded PEO/Chitosan nanofibers. The percentage reduction was higher for Ag-loaded PEO/Chitosan nanofibers than for the CuO-loaded PEO/Chitosan nanofibers. This results also confirmed the antimicrobial activity of Ag nanoparticle and CuO nanoparticle in a descending order (Vargas-Reus *et al.* 2012). However, PEO/Chitosan nanofibers showed reduced antibacterial activity after 30 min for *E. coli* microorganisms.

The antibacterial rates became lower when increased the concentration of bacterial suspension for both *E. coli* and *P. aeruginosa* microorganism. The antibacterial activities of silver nanoparticles still higher than copper oxide nanoparticles at same weight percentage. According to Figure 6.7, 6.8 and 6.9, the efficacies of copper oxide or silver nanoparticles embedded PEO/Chitosan blended nanoparticles against *E. coli* were higher than that against *P. aeruginosa* microorganism. All of the values for antibacterial rate are listed as below Table 6.5.

Table 6.5: Antibacterial rates

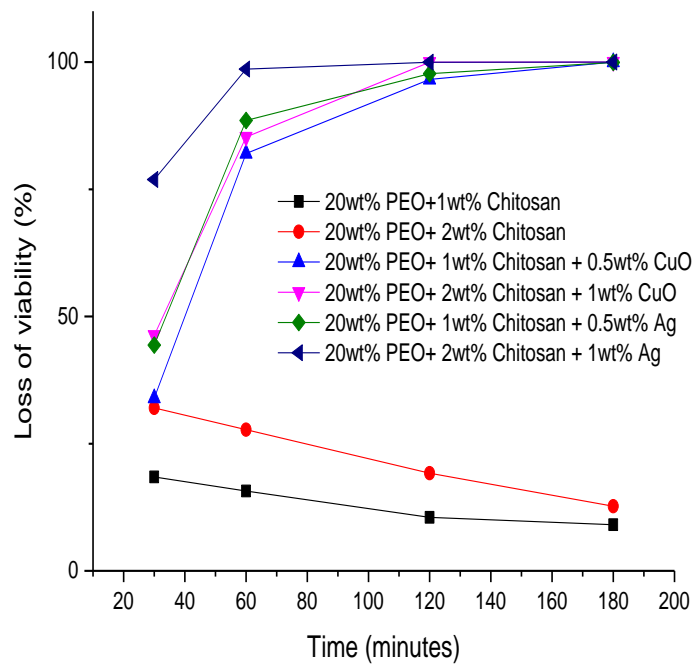
	Antibacterial rate against with Bacteria suspension				
		<i>E. coli</i> (0.5×10 ⁶ CFU/ml)	<i>E. coli</i> (1×10 ⁶ CFU/ml)	<i>P.</i> <i>aeruginosa</i> (0.5×10 ⁶ CFU/ml)	<i>P.</i> <i>aeruginosa</i> (1×10 ⁶ CFU/ml)
1 wt.% Chitosan	30 min	18.5 (±6)	6.6 (±2.1)	15.3 (±3)	11.9 (±4)
	60 min	15.7 (±5.2)	9 (±3)	10.5 (±3.5)	8.8 (±3)
	120 min	10.5 (±3)	6.2 (±2)	8.3 (±5.1)	11.5 (±3.8)

	180 min	9.1 (± 3)	–	7.7 (± 2.5)	–
2 wt.% Chitosan	30 min	32 (± 12)	12.8 (± 4.2)	17.6 (± 5.8)	17.8 (± 2.1)
	60 min	28 (± 9.2)	13.4 (± 4)	13 (± 2.8)	13.3 (± 4.5)
	120 min	19.2 (± 6.3)	12.1 (± 3.9)	10.5 (± 4.3)	6.4 (± 5.9)
	180 min	12.7 (± 4.1)	–	9.9 (± 3.3)	–
1 wt.% Chitosan + 0.5wt.% CuO	30 min	34 (± 11)	25.4 (± 8.3)	20.4 (± 6.8)	29.8 (± 10)
	60 min	82 (± 7.1)	26.9 (± 8.9)	40.9 (± 13.5)	31.1 (± 10.2)
	120 min	96.6 (± 0.2)	15 (± 5)	59 (± 19.5)	27.5 (± 9)
	180 min	99.9 (± 0.1)	–	85.9 (± 8.4)	–
1 wt.% Chitosan + 1wt.% CuO	30 min	46.3 (± 15.3)	30 (± 10)	28.2 (± 9.3)	35.9 (± 11.9)
	60 min	85.3 (± 1.8)	35.9 (± 11.8)	51.2 (± 16.8)	43.1 (± 14.2)
	120 min	99.9 (± 0.1)	15.2 (± 5)	83.9 (± 7.7)	29.1 (± 9.6)
	180 min	99.9 (± 0.1)	–	99.9 (± 0.1)	–
1 wt.% Chitosan + 0.5wt.% Ag	30 min	44.4 (± 14.7)	25.2 (± 8)	32.6 (± 10.8)	35.9 (± 9.8)
	60 min	88.5 (± 3)	40.3 (± 13.3)	73.6 (± 14.3)	37.9 (± 12.5)
	120 min	97.7 (± 0.7)	33.4 (± 11)	84.4 (± 8.8)	28.1 (± 9.3)
	180 min	99.9 (± 0.1)	–	99.9 (± 0.1)	–
1 wt.% Chitosan + 1wt.% Ag	30 min	76.9 (± 5.4)	31.34(± 10.4)	80.9 (± 1)	–
	60 min	98.6 (± 0.6)	46 (± 15)	98.9 (± 0.5)	–
	120 min	99.9 (± 0.1)	34.4 (± 11.4)	99.9 (± 0.1)	–
	180 min	99.9 (± 0.1)	–	99.9 (± 0.1)	–

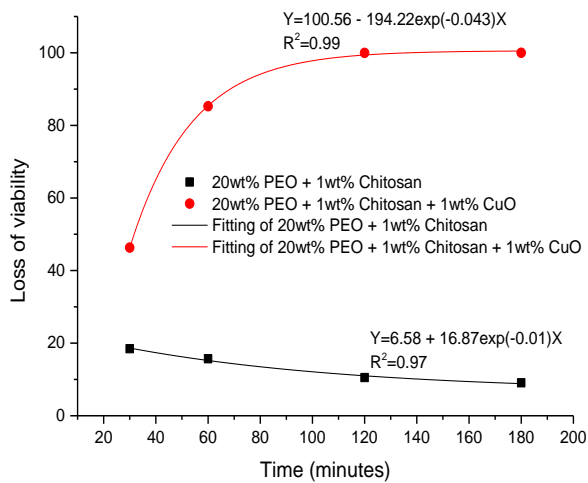
6.4.3 Time-Dependent Antibacterial Activity Against *E. coli*

The time-dependent antibacterial activity of all the samples was examined up to 180 minutes, and the loss of viability after different incubation periods is shown in Figure 6.10 (a). Generally, increasing the incubation time increased the antibacterial activity. However, increasing the incubation time decreased the antibacterial activity for samples which did not contain nanoparticles. Therefore, the loss of viability for PEO/chitosan blended fibres reduced after set periods of time. Moreover, Ag nanoparticles showed better antibacterial activity than their CuO counterparts in the same PEO/chitosan blended fibres. The loss of viability for 20wt.%PEO/1wt.%chitosan and 20wt.%PEO/1wt.%chitosan/1wt.%CuO blended fibres is shown in Figure 6.10 (b). For blended fibres with CuO nanoparticles the loss of *E. coli* cell viability increased sharply from 46.3% after 30 minutes incubation to 85.3% after 1 hour incubation, but only increased slightly to 99.7% after 2 hours incubation and 99.9% after 3 hours incubation. The change after 1 hour of incubation was due to the fact that the loss of cell viability had approached complete inactivation (99.99%). In contrast, the antibacterial activity of 20wt.%PEO/1wt.%chitosan blended fibres decreased sharply, from 18.5% after 30 minutes incubation to 15.7% , 10.5%, and 9.1% after 1, 2, and 3 hours of incubation, respectively. Figure 6.10 (c) illustrates the inactivation rate of *E. coli* cells. The antibacterial activity for 20wt.%PEO/1wt.%chitosan/1wt.%CuO blended fibres showed a higher rate in the first hour which sharply decreased in the second hour and by the third hour of incubation the inactivation rate is nearly constant, indicating it had approached complete inactivation (99.99%). In contrast, the rate of inactivation was slightly increased for the control sample, 20wt.%PEO/1wt.%chitosan blended fibres in the time period 1 to 3 hours.

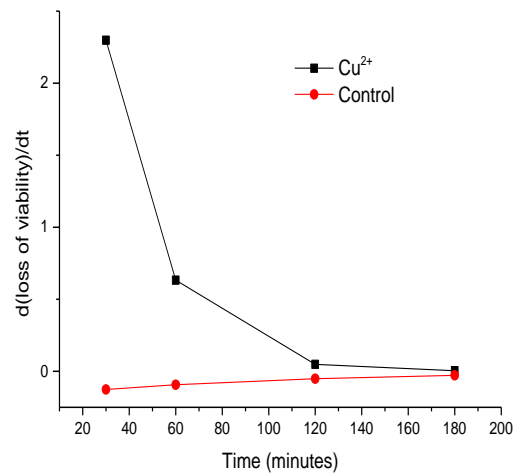
The loss of viability for 20wt.%PEO/1wt.%chitosan and 20wt.%PEO/1wt.%chitosan/1wt.%Ag blended fibres is shown in Figure 6.10 (d). For blended fibres with Ag nanoparticles the loss of *E. Coli* viability increased sharply from 76.9% after 30 minutes to 98.6% after 1 hour incubation, and increased to 99.9% after 2 and 3 hours incubation. Again, the change after 30 minutes incubation is due to the fact that the loss of cell viability has approached complete inactivation (99.99%). Figure 6.10 (e) illustrates the inactivation rate of *E. coli* with and without Ag nanoparticles. 20% wt.% PEO/1% wt.% chitosan with 1% wt.% Ag blended fibres showed a higher rate of inactivation during the first hour of incubation and this was strikingly decreased in the second hour of incubation, while in the third hour the inactivation rate is nearly constant, indicating it has approached complete inactivation (99.99%).



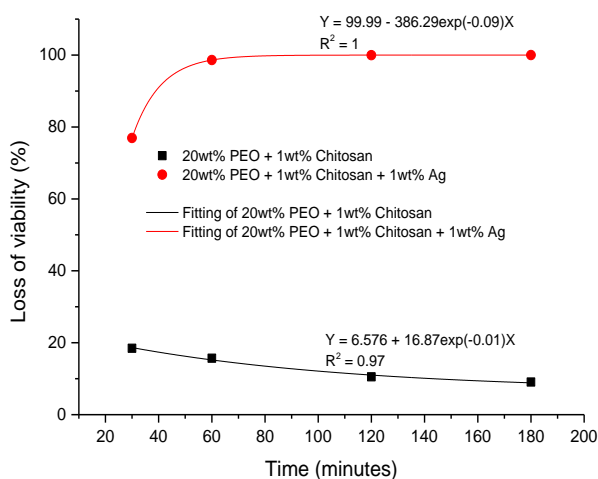
(a)



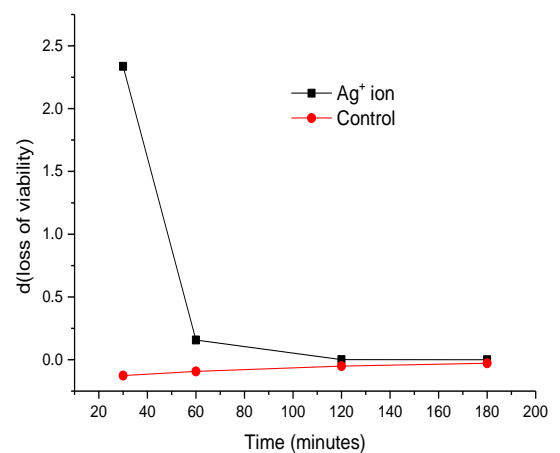
(b)



(c)



(d)

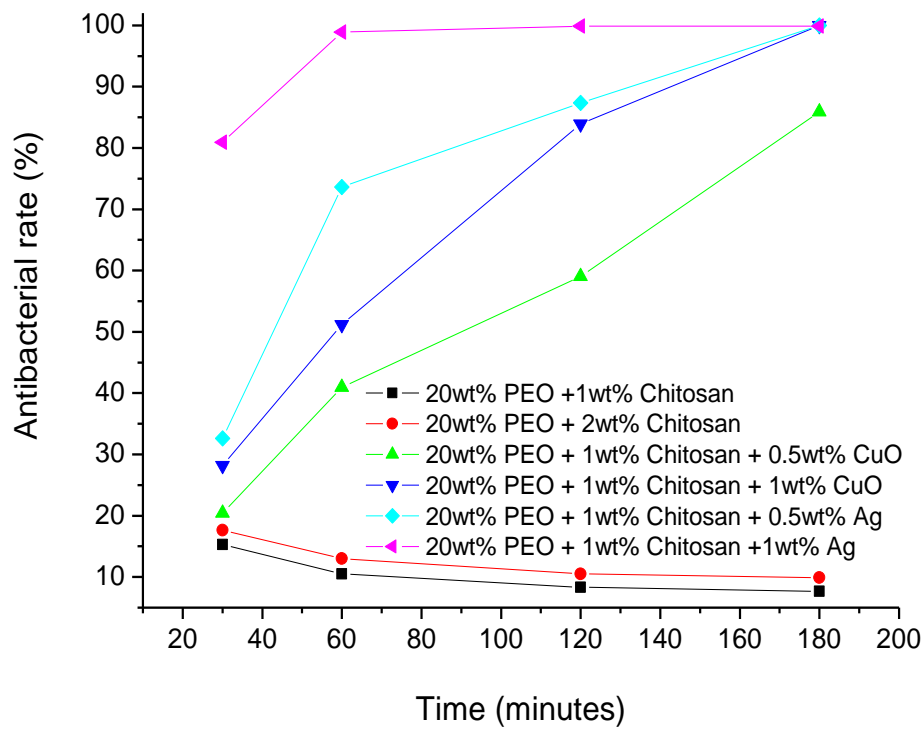


(e)

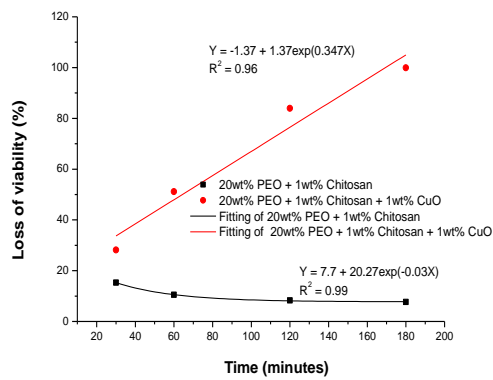
Figure 6.10: Time dependent antibacterial activity against *E.coli* (a) Time-dependent antibacterial activity of PEO/chitosan, PEO/chitosan/CuO and PEO/chitosan/Ag nanofibre mats after incubating with *E.coli* suspension. (b) Time-dependent antibacterial activity for 20wt.%PEO/1wt.%chitosan and 20wt.%PEO/1wt.%chitosan /1wt.%CuO suspension incubated after 30, 60, 120 and 180 minutes. (c) Time-dependent *E. coli* cell inactivation rates for 20wt.%PEO/1wt.%chitosan and 20wt.%PEO/1wt.%chitosan /1wt.%CuO

suspensions extracted from Figure 6.10 (b) with unit of $d(\%)/d(\text{min})$. (d) Time-dependent antibacterial activity for 20wt.%PEO/1wt.%chitosan and 20wt.%PEO/1wt.%chitosan /1wt.%Ag suspension incubated after 30, 60, 120 and 180 minutes. (e) Time-dependent *E. Coli* cell inactivation rates for 20wt.%PEO/1wt.%chitosan and 20wt.%PEO/1wt.%chitosan /1wt.%Ag suspensions extracted from Figure 6.10 (d) with unit of $d(\%)/d(\text{min})$.

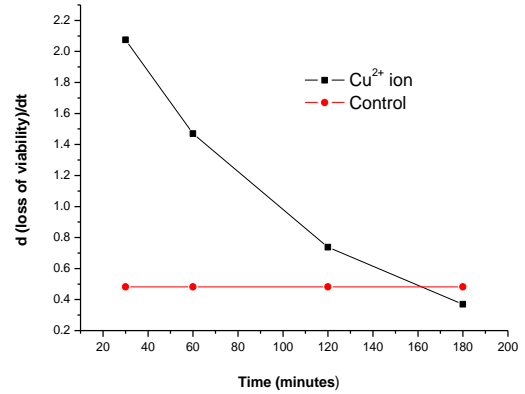
6.4.4 Time-Dependent Antibacterial Activity Against *P. aeruginosa*



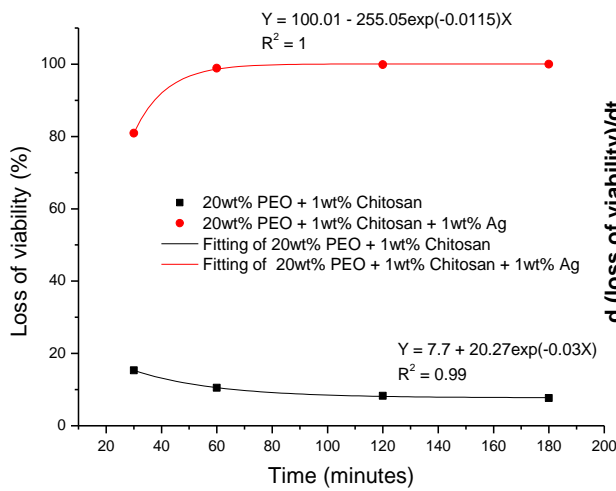
(a)



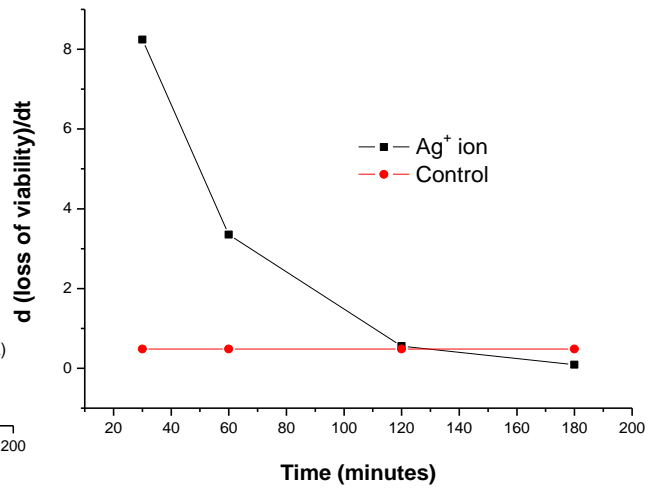
(b)



(c)



(d)



(e)

Figure 6.11: Time dependent antibacterial activity against *P. aeruginosa* (a) Time-dependent antibacterial activity of PEO/chitosan, PEO/chitosan/CuO and PEO/chitosan/Ag nanofibre mats after incubating with *P. aeruginosa* suspension. (b) Time-dependent antibacterial activity for 20wt.%PEO/1wt.%chitosan and 20wt.%PEO/1wt.%chitosan /1wt.%CuO suspension incubated after 30, 60, 120 and 180 minutes. (c) Time-dependent *P. aeruginosa* cell inactivation rates for 20wt.%PEO/1wt.%chitosan and 20wt.%PEO/1wt.%chitosan/1wt.%CuO

suspensions extracted from Figure 6.11 (b) with unit of d(%) / d(min). (d) Time-dependent antibacterial activity for 20wt.%PEO/1wt.%chitosan and 20wt.%PEO/1wt.%chitosan /1wt.%Ag suspension incubated after 30, 60, 120 and 180 minutes. (e) Time-dependent *P. aeruginosa* cell inactivation rates for 20wt.%PEO/1wt.%chitosan and 20wt.%PEO/1wt.%chitosan/1wt.%Ag suspensions extracted from Figure 6.11 (d) with unit of d(%) / d(min).

The time-dependent antibacterial properties of PEO/chitosan, PEO/chitosan/CuO and PEO/chitosan/Ag were assessed using *P. aeruginosa* cells. A bacterial inhibition growth curve was used to study the dynamics of bacterial growth and to evaluate the antibacterial properties of all the samples at different incubation times and is shown in Figure 6.11 (a). Generally, increasing the incubation time increased the antibacterial activity, although for the PEO/chitosan control samples increasing the incubation time decreased antibacterial activity. Ag nanoparticles incorporated into the polymer blends showed better antibacterial activity than their CuO counterparts in PEO/chitosan blended fibres. The loss of viability for 20wt.%PEO/1wt.%chitosan and 20wt.%PEO/1wt.%chitosan/1wt.%CuO blended fibres is shown in Figure 6.11 (b). For blended fibres with CuO nanoparticles the loss of *P. aeruginosa* viability increased gradually from 28.2% after 30 minutes to 51.2% after 1 hour of incubation, and further increased to 83.9% after 2 hours incubation and 99.9% after 3 hours incubation. In contrast, the antibacterial activity of 20wt.%PEO/1wt.%chitosan blended fibres decreased gradually from 15.3% after 30 minutes to 10.5% , 8.3%, and 7.6% after 1, 2, and 3 hours of incubation, respectively. Figure 6.11 (c) illustrates the inactivation rate of *P. aeruginosa* for PEO/chitosan and PEO/chitosan/CuO blended fibres. 20wt.%PEO/1wt.%chitosan/1wt.%CuO blended fibres showed a higher rate of

inactivation in the first hour which sharply decreased in the second and third hour of incubation. However, the rate of inactivation was nearly constant for the control sample 20wt.%PEO/1wt.%chitosan blended fibres in the time period 1 to 3 hours.

The loss of *P. aeruginosa* viability in 20wt.%PEO/1wt.%chitosan and 20wt.%PEO/1wt.%chitosan/1wt.%Ag blended fibres is shown in Figure 6.11 (d). For blended fibres with Ag nanoparticles the loss of *P. aeruginosa* viability increased sharply from 80.9% after 30 minutes to 98.9% after 1 hour of incubation but only increased slightly to 99.9% after 2 and 3 hours of incubation. Again, the change after 30 minutes of incubation is due to the fact that the loss of cell viability has approached complete inactivation (99.99%). Figure 6.11 (e) illustrates the inactivation rate of *P. aeruginosa* cells for both samples with and without Ag nanoparticles. 20wt.%PEO/1wt.%chitosan/1wt.%Ag blended fibres showed a higher rate of inactivation in the first hour of incubation which gradually decreased in the second and third hour.

6.5 Discussion

There are various factors which affect the antimicrobial activity of materials, including adsorption and binding to the bacterial cell surface, diffusion through the cell wall, and permeability through the cytoplasmic membrane, followed by disruption of the cytoplasmic membrane, leakage of the cytoplasmic constituents and death of the microbes (Kangwansupamonkon et al., 2014). It has been shown that chitosan inhibits Gram-negative bacterial growth in polyethylene blends (Mural et al., 2016). An increase in the chitosan concentration increases the antibacterial activity against *E. coli* cells (Mural et al., 2016). Chitosan shows increase antibacterial activity efficiency when

blended with linear polymer chains, such as PEO compared to) than polyvinylpyrrolidone (PVP), where the pyrrolidone rings around PVP may obstruct interactions with bacteria cells (Li et al., 2010). It has been proposed that inhibition of bacterial growth is due to the interaction of the $-NH_2$ group of chitosan with the phospholipids present on the bacterial cell membrane (Kumar et al., 2014; Singh et al., 2012). Another possibility is that protonated NH_3^+ groups in the chitosan can form complex ions with the phosphate groups present in the phospholipid bilayer of the bacterial cell membrane, resulting in the disruption of the osmotic balance which leads to the release of potassium ions, glucose and nucleic acids, thus causing in cell death.

A relevant factor in the evaluation of biocide action on materials is the type of cells involved. Bacteria are generally classified into Gram-negative and Gram-positive depending on the characteristics of their cell wall. Gram-positive cells have an extra thick peptidoglycan layer present on the outer surface, whereas Gram-negative bacteria possess only a thin peptidoglycan layer (Gangadharn et al., 2010). Bacteria, like most other microbes and cells, are negatively charged. However, the magnitude of this charge is dependent on bacterial surface structures and is related to a cell's ability to attach to various substrates (van Loosdrecht et al., 1987). Thus changes to such structures have a huge influence on the antibacterial rate of tested samples. *E. coli* and *P. aeruginosa* cells are $\sim 200 \mu m$ in size, and although within the micrometre range, the membranes of these cells contain pores in the nanometre scale. These nanopores are able to accommodate the nanoparticles, which are smaller than the size of the pores and can cross the membrane. Cell damage can occur due to the formation of reactive oxygen species (ROS), such as superoxide (O_2^-) or hydroxyl (OH^\cdot) radicals. The double bonds in phospholipids are oxidised by ROS and this elevates the fluidity within the membrane and results in increased cellular osmotic stress (Khashan et al., 2016). Even at lower

CuO nanoparticle concentrations, hydroxyl ions could be generated through the catalytic conversion of intracellular hydrogen peroxide (H_2O_2) via Fenton-like reactions (Meghana et al., 2015). Here the electron donating function of nanocrystalline CuO arises from inherent surface defects. Thus Cu^{2+} ions are reduced to the Cu^+ state by cell components and are majorly responsible for the inactivation of bacteria (Meghana et al., 2015). The release of Cu^{2+} ions is considerably greater in nutrient media compared to water, possibly due to the interaction of the media chloride ions with the oxide layer of CuO nanoparticles (Azam et al., 2012). This will increase the concentration of Cu^{2+} ions in the nutrient media available to form ROS which lead to inactivation of bacteria cells.

Our recent work showed that silver nanoparticles are effective antimicrobial agents (Illangakoon et al., 2016). The mechanism relating to the inactivation of bacterial cells can either be through direct contact of nanoparticles with the membrane which causes damage (Smetana et al., 2008) or Ag^+ ions can destroy the cell membrane and DNA replication ability (Feng et al., 2000). It also has been demonstrated that Ag nanoparticles can interact with sulphur-containing proteins present in the cell wall and phosphorous containing compounds present in the cytoplasm, which affects cell respiration and cell division, leading to bacterial death (Yamanaka et al., 2005). It is postulated that the direct contact of Ag nanoparticles with the same number of bacteria and the release of Ag ions is higher in nutrient media than for CuO nanoparticles, which is the reason for the increased antimicrobial activity of Ag observed in this study.

6.6 Summary

A series of PEO, PEO-chitosan blended nanofibres were fabricated with the addition of CuO and Ag nanoparticles using pressurised gyration. Dispersion of nanoparticles was clearly demonstrated from scanning electron micrographs and energy-dispersive x-ray analysis. Antibacterial activity was evaluated using two types of contrasting bacteria. PEO-chitosan blended nanofibres showed a reasonable level of antimicrobial activity. The concentration of the chitosan increased antimicrobial activity. The activity is decreased with incubation time against both *E. Coli* and *P. aeruginosa* microorganisms for the blended fibres without nanoparticles. Ag nanoparticle incorporated blended fibres showed much better antibacterial activity compared with CuO nanoparticle incorporated blended fibres. The antimicrobial activity is increased with incubation time for both types of nanoparticles separately incorporated in the blended fibres. The antibacterial activity is different for the two bacteria tested under the same conditions. More inactivation of cells is observed in *E. Coli* than the in *P. aeruginosa* suspension. The rate of inactivation of bacteria cell is higher in the first hour compared to later times.

Chapter 7 - Conclusions and Future Work

7.1 Conclusions

Pressurised gyration which involves rotating a perforated pot containing a polymer solution or melt at high speed is a promising alternative method for spinning polymer fibres and polymer fibrous structures. The central focus was the direct preparation of ultrafine hybrid fibres with consistent micro and nano scale diameters using the pressurised gyration method. The fundamental objective of this work was to investigate the potential antibacterial activity of hybrid polymer fibres for use in biomedical applications.

This objective was accomplished in three phases: first, the polymer selection process was important due to their unique mechanical, physical and chemical properties; second, pressurised gyration and pressurised melt gyration processes were used to obtain metallic nanoparticles incorporated into polymer fibres and polymer fibrous structures; and finally, the antibacterial activities of hybrid polymer fibres and polymer fibrous structures were observed against the Gram-negative bacteria *E. coli* and *P. aeruginosa*.

7.1.1 Material Selection

Nylon polymer nanofibres exhibit excellent mechanical properties, while PCL, a linear aliphatic biodegradable and biocompatible polyester used in biological applications, has a low melting point and a glass transition temperature. PEO, a biodegradable, biocompatible, non-toxic synthetic polymer, has high solubility in both water and organic solvents and is widely used in foods and cosmetics. Chitosan, a special biocompatible and biodegradable biopolymer is derived from chitin, and is usually blended with other polymers, such as PEO, in order to prepare chitosan based nanofibres and nanofibrous structures due to its low formability and spinnability into nanofibres and nanofibrous structures.

7.1.2 Influence of Process Parameters

Typical pressurised gyration consists of simultaneous centrifugal spinning and solution blowing, where the combination of centrifugal and dynamic fluid flow forces act against the surface tension force to generate fibres. An advancement of this technology resulted is pressurised melt gyration, which does not require solvents as a polymer melt is formed in a gyrating pot containing orifices present on its surface.

In this work, pressurised gyration was used to form nylon nanofibres, PEO nanofibres and PEO/chitosan nanofibres. Key parameters, such as vessel rotating speed, working pressure and polymer concentration, had a significant effect on nanofibre diameter and morphology. The fibre diameter increased when increasing the weight percentage of the polymer, and reduced with increasing vessel rotating speed and the process working pressure.

Using pressurised melt gyration, PCL based fibre non-woven scaffolds were prepared for the first time by melting PCL pellets in a perforated vessel. The rotation speed, working pressure and temperature was very effectively used to vary the diameter, surface morphology and the topography of the fabricated fibrous scaffolds. During the processing, pressure blowing accelerated solution evaporation and solidification. Thus, the working pressure cannot be too high in order to avoid solidification of the PCL pellets. The temperature significantly influenced PCL crystallinity, bonding characteristics, and Ag ion release. The pot temperature could be controlled and micrometre size fibres whose surface roughness could be tailored which could be used in architecture tissue engineering bio-constructs and antimicrobial mats.

7.1.3 Antibacterial Activities

Ag ion release after repeated washing cycles of the nanofibrous mats in de-ionised water was detected by ICP-MS, which indicated the Ag ion concentration and the existence of nanofibrous mats which might also influence the Ag ion release profile. Strong antibacterial activity of Ag-loaded nylon was clearly demonstrated, with bacterial killing rates >99.95%. The antibacterial activity of Ag-loaded nanofibres showed higher efficacy than nylon nanofibres for the Gram-negatives *E. coli* and *P. aeruginosa*, and both Ag nanoparticles and Ag ions were found to enhance cell death.

Antibacterial activity of the scaffolds as prepared was nearly 100% and was constant for all PCL-Ag coated fibrous scaffolds against *E. coli*. However, antibacterial activity gradually decreased with increasing spinning temperature against *P. aeruginosa*.

PEO-chitosan blended nanofibres showed a reasonable degree of antimicrobial activity, and increasing the concentration of chitosan increased the antimicrobial activity. Activity was decreased over time against both *E. coli* and *P. aeruginosa* for the blended fibres without any nanoparticles. Ag incorporated blended fibres showed better antibacterial activity than CuO incorporated blended fibres. Antimicrobial activity was increased with incubation time for both nanoparticle incorporated blended fibres. Antibacterial activity was different for the different bacteria tested under the same conditions, as greater inactivation was observed for *E. coli* compared to *P. aeruginosa*. The rate of inactivation of bacteria was higher in the first hour compared to second and third hours.

7.2 Future Work

As previously stated, the structure of this PhD research has two main parts. The first is using polymer solutions or melts and the pressurised gyration process to produce controllable size hybrid polymer fibres. Antibacterial activity was then investigated and demonstrated the successful incorporation of metallic nanoparticles within polymer fibres/polymer fibrous scaffolds. Metallic nanoparticles showed high levels of antibacterial activity against Gram-negative microorganisms. However, there are several avenues available for future work:

1. Solvent selection is an important parameter for pressurised gyration. According to the experimental studies in this thesis, a very low polymer solution concentration can only form beads, while a high polymer percentage solution results in thicker fibres. Further studies are needed to determine the ration between polymer and solvent to form finer polymer fibres. In addition, the toxicity of solvents is also a considerable factor for

fibre spinning in biomedical applications.

2. The gyration pot used in this work only fixed dimensions. A different sized vessel and different diameter of the orifices should have an influence on the rate of production of polymer fibres.

3. In the pressurised melt gyration process a heating gun was used to melt the solid polymer, but this is not convenient during spinning. It may be better to design a heating element (same diameter as the vessel and hollow in the middle) that can be built to go under or in the rotary vessel to melt the polymer more effectively. Currently, the heating temperature cannot be stably maintained for long, which affects the production rate of fibres; therefore, a thermal insulation material may be useful as a coating surface for the heating element.

4. There has been some reports of producing polymer fibres using infusion gyration based on pressurised gyration. The flow rate of infusion gyration also was found to have a significant influence on fibre size and morphology, and may also affect the incorporation of metallic or non-metallic nanoparticles within polymer fibres.

5. Further work is required to reduce the diameter of the polymer fibres produced by pressurised melt gyration which are not of the micrometre scale. The working pressure involved during the spinning cannot be too high in order to avoid solidification of the polymer. To achieve smaller fibres, a low molecular weight polymer and high heating temperature could be considered.

6. In this work, the fibre length has not been considered, and this should be investigated. Spinning parameters, such as polymer solution concentration, rotation

speed, and working pressure should also cause differences in fibre length. According to reports of electrospinning studies, the polymer solvent system and polymer molecular weight directly influence fibre length, and increasing the solution concentration to the semi-concentrated region allowed the formation of shorter fibres. Different molecular weights of a polymer could be utilised to determine the most efficient parameters for the pressurised gyration process or pressurised melt gyration process.

7. Assessment of antibacterial activities could be extended through an examination of different weight percentages of metallic or non-metallic nanoparticles in order to identify the minimum amount required to be in order to reduce potential toxicity in biomedical engineering applications.

8. So date, the amount of Ag nanoparticles and CuO nanoparticles incorporated into polymer fibres has been recorded as the percentage within a polymer solution, and the EDX analysis demonstrated the location of the nanoparticles within the fibres. Further analysis may be required to determine the distribution of the nanoparticles within each hybrid polymer fibre in order to investigate the most effective combination of polymer and nanoparticle solution.

9. Spinning conditions, like rotation speed and working pressure, influence the fibre diameter. A high rotating speed and high working pressure cause thinner fibres to be produced. Only one spinning condition (36,000 rpm, no working pressure) was used to form the hybrid polymer fibres for the antibacterial activity analysis. Therefore, further study is required to compare the antibacterial rate of different spinning conditions with the same weight percentages of gyration solutions in order to investigate the influence of different surface to volume ratios of hybrid polymer fibres on antibacterial activity

against Gram-negative microorganisms.

10. The high production rate, ease of production, and highly controlled fibre morphology of the gyration spinning process, enables polymer mats to be easily formed for biomedical applications. The metallic nanoparticles embedded within polymer fibres/mats can kill microorganisms present in the air and therefore these could be used as masks or fibrous filters. However, it would be necessary to modify the processing and forming to obtain mats or masks rather than fibres.

References

- Abdelgawad, A.M., Hudson, S.M., & Rojas, O.J. (2014) Antimicrobial wound dressing nanofibre mats from multicomponent (chitosan/silver-NPs/polyvinyl alcohol) systems. *Carbohydrate Polymers*, 100:166-78.
- Alissawi, N., Zaporojtchenko, V., Strunskus, T., Hrkac, T., Kocabas, I., Erkartal, B., et al. (2012) Tuning of the ion release properties of silver nanoparticles buried under a hydrophobic polymer barrier. *Journal of Nanoparticle Research*, 14:928.
- Amir, A., Mahalingam, S., Wu, X., Porwal, H., Colombo, P., Reece, M.J., & Edirisinghe, M. (2016) Graphene nanoplatelets loaded polyurethane and phenolic resin fibres by combination of pressure and gyration. *Comp Sci Technol*, 129: 173-182.
- Amna, T., Hassan, M.S., Barakat, N.A.M., Pandeya, D.R., Hong, S.T., Khil, M.S., et al. (2012) Antibacterial activity and interaction mechanism of electrospun zinc-doped titania nanofibres. *Applied Microbiology and Biotechnology*, 93:743-51.
- Amna, T., Hassan, M.S., Pandurangan, M., Khil, M.S., Lee, H.K., & Hwang, I.H. (2013) Characterization and potent bactericidal effect of Cobalt doped Titanium dioxide nanofibres. *Ceramics International*, 39:3189-93.
- An, J., Zhang, H., Zhang, J.T., Zhao, Y.H., & Yuan, X.Y. (2009) Preparation and antibacterial activity of electrospun chitosan/poly(ethylene oxide) membranes containing silver nanoparticles. *Colloid and Polymer Science*, 287:1425-34.
- Ananth, A., Dharaneedharan, S., Heo, M.S., & Mok, Y.S. (2015) Copper oxide nanomaterials: Synthesis, characterization and astructure-specific antibacterial performance. *Chemical Engineering Journal*, 262:179-188.
- Andrady, A. L. (2008) Science and technology of polymer nanofibers. USA: John Wiley & Sons, Inc.
- Angelova, N., Manolova, N., Rashkov, I., Maximova, V., Bogdanova, S., & Domard, A. (1995) Preparation and properties of modified chitosan films for drug release *Journal of Bioactive and Compatible Polymers*, 10: 285–298.
- Augustine, R., Malik, H.N., Singhal, D.K., Mukherjee, A., Malakar, D., Kalarikkal, N., & Thomas, S. (2014) Electrospun polycaprolactone/ZnO nanocomposite

- membranes as biomaterials with antibacterial and cell adhesion properties. *J Polym Res*, 21:347.
- Azam, A., Ahmed, A.S., Oves, M., Khan, M.S., & Memic, A. (2012) Size dependent antimicrobial properties of CuO nanoparticles against gram -positive and – negative bacterial strains. *Int J Nanomed*, 7: 3527-3535.
- Baba, R. & Jayaram, S.H. (2010) An IGBT-Based pulsed power supply in the fabrication of non-contiguous nanofibres using electrospinning. *IEEE*.
- Badrossamay, M.R., Balachandran, K., Capulli, A.K., Golecki, H.M., Agarwal, A., Goss, J.A., et al. (2014) Engineering hybrid polymer-protein super-aligned nanofibres via rotary jet spinning. *Biomaterials*, 35:3188-97.
- Badrossamay, M.R., McIlwee, H.A., Goss, J.A., Parker, K.K. (2010) Nanofibre assembly by rotary jet-spinning. *Nano Lett*, 10:1157-61.
- Bazbouz, M.B., & Stylios, G.K. (2010) The Tensile Properties of Electrospun Nylon 6 Single Nanofibres. *Journal of Polymer Science: Part B: Polymer Physics*, 48:1719-31.
- Berger, T.J., Spadaro, J.A., Chapin, S.E., & Becher, R.O. (1976) Electrically generated silver ions - quantitative effects on bacterial and mammalian-cells. *Antimicrobial Agents and Chemotherapy*, 9:357-58.
- Blades, H., J. R. White, W. R. White and C. Ford. (1962) Fibrillated strand. *United States Patent 3081519*.
- Blaszczyk-Lezak, I., Hernandez, M., & Mijangos, C. (2013) One Dimensional PMMA Nanofibres from AAO Templates. Evidence of Confinement Effects by Dielectric and Raman Analysis. *Macromolecules*, 46:4995-02.
- Bognitzki, M., Becker, M., Graeser, M., Massa, W., Wendorff, J.H., Schaper, A., et al. (2006) Preparation of sub-micrometer copper fibres via electrospinning. *Advanced Materials*, 18:2384-86.
- Borkar, S., Gu, B., Dirmyer, M., Delicado, R., Sen, A., Jackson, B.R., et al. (2006) Polytetrafluoroethylene nano/microfibers by jet blowing. *Polymer*, 47:8337-43.

- Bosworth, L.A., Turner, L.A., & Cartmell, S.H. (2013) State of the art composites comprising electrospun fibres coupled with hydrogels: a review. *Nanomed-Nanotechnol*, 9:322-35.
- Brayner, R., Ferrari-Iliou, R., Brivois, N., Djediat, S., Benedetti, M.F., & Fievet, F. (2006) Toxicological impact studies based on Escherichia coli bacteria in ultrafine ZnO nanoparticles colloidal medium. *Nano Letters*, 6:866-70.
- Brown, T.D., Edin, F., Detta, N., Skelton, A.D., Hutmacher, D.W., & Dalton, P.D. (2014) Melt electrospinning of poly(ϵ -caprolactone) scaffolds: phenomenological observations associated with collection and direct writing. *Mater Sci Eng C*, 45:698-708.
- Buraidah, M.H., Teo, L.P., Au Yong, C.M., Shah, S., & Arof, A.K. Performance of polymer electrolyte based on chitosan blended with poly(ethylene oxide) for plasmonic dye-sensitised solar cell. *Optical Materials*, 57, 202-211.
- Cao, H.L., Qiao, Y.Q., Liu, X.Y., Lu, T., Cui, T., Meng, F.H., et al. (2013) Electron storage mediated dark antibacterial action of bound silver nanoparticles: Smaller is not always better. *Acta Biomaterialia*, 9:5100-10.
- Capadona, J.R., Van Den Berg, O., Capadona, L.A., Schroeter, M., Rowan, S.J., Tyler, D.J., et al. (2007) A versatile approach for the processing of polymer nanocomposites with self-assembled nanofibre templates. *Nature Nanotechnology*, 2:765-69.
- Carothers, W. H. (1935) Alkylene carbonate and process of making it." United States Patent 1995291: DuPont.
- Catanzano, O., Acierno, S., Russo, P., Cervasio, M., De Caro, M.D.B., Bolognese, A., Sammartino, G., Califano, L., Marenzi, G., Calignano, A., Acierno, D., & Quanglia, F. (2014) Melt-spun bioactive sutures containing nanohybrids for local delivery of anti-inflammatory drugs. *Mater Sci Eng C* 43:300-309.
- Cengiz, F., Krucinska, I., Gliscinska, E., Chrzanowski, M., & Goktepe, F. (2009) Comparative Analysis of Various Electrospinning Methods of Nanofibre Formation. *Fibres & Textiles in Eastern Europe*, 17:13-19
- Chen, S.L., Hou, H.Q., Harnisch, F., Patil, S.A., Carmona-Martinez, A.A., Agarwal, S., et al. (2011) Electrospun and solution blown three-dimensional carbon fibre

- nonwovens for application as electrodes in microbial fuel cells. *Energy Environ. Sci*, 4:1417-21.
- Chik, H. and J. M. Xu. (2004) Nanometric superlattices: non-lithographic fabrication, materials, and prospects *Materials Science & Engineering R-Reports* 43:103-138.
- Cho, K., Park, J., Osaka, T., & Park, S. (2005) The study of antimicrobial activity and preservative effects of nanosilver ingredient. *Electrochimica Acta*, 51:956-60.
- Cho, L.L. (2007) Identification of textile fibre by Raman microspectroscopy. *Forensic Sci J*, 6:55-62.
- Chuang, W.Y., Young, T.H., Yao, C.H., & Chiu, W.Y. (1999) Properties of the poly(vinyl alcohol)/chitosan blend and its effect on the culture of fibroblast in vitro. *Biomaterials*, 20:1479-1487.
- Cloupeau, M. and B. Prunetfoch. (1989) Electrostatic spraying of liquids in cone-jet mode. *Journal of Electrostatics* 22:135-159.
- Cloupeau, M. and B. Prunetfoch. (1990) Electrostatic spraying of liquids - main functioning modes. *Journal of Electrostatics* 25:165-184.
- Colby, R.H., Fetters, L.J., Funk, W.G., & Graessley, W.W. (1991) Effects of concentration and thermodynamic interaction on the viscoelastic properties of polymer-solutions. *Macromolecules*, 24:3873-82.
- Croisier, F. & Jerome, C. (2013) Chitosan based Biomaterials for Tissue Engineering. *Eur Polym J*, 49:780-792.
- Croisier, F., Atanasova, G., Poumay, Y., & Jerome, C. (2014) Polysaccharides-coated PCL nanofibers for wound dressing applications. *Adv Healthcare Mater*, 3:2032-
- Damm, C. & Munstedt, H. (2008) Kinetic aspects of the silver ion release from antimicrobial polyamide/ silver nanocomposites. *Applied Physics A*, 91:479-86.
- Deitzel, J.M., Kleinmeyer, J.D., Harris, D., & Tan, N.C.B. (2001) The effect of processing variables on the morphology of electrospun nanofibres and textiles. *Polymer*, 42:261-72
- Deitzel, J.M., Kleinmeyer, D., Hirvonen, J.K., & Tan, N.C.B. (2001) Controlled deposition of electrospun poly(ethylene oxide) fibers. *Polymer*, 42:8163-70.

- Demir, M. M., I. Yilgor, E. Yilgor and B. Erman. (2002) Electrospinning of polyurethane fibers. *Polymer* 43:3303-3309.
- Desai, K., Kit, K., Li, J., & Zivanovic, S. (2008) Morphological and surface properties of electrospun chitosan nanofibers. *Biomacromolecules*, 9:1000-1006.
- Duesberg, G.S., Loa, I., Burghard, M., Syassen, K., & Roth, S. (2000) Polarized Raman spectroscopy on isolated single-wall carbon nanotubes. *Physical Review Letters*, 85:5436-39
- Ellison, C.J., Phatak, A., & Giles, D.W. (2007) Meltblown nanofibres: Fibre diameter distributions and onset of fibre breakup. *Polymer*, 48:3306-16.
- Elsabee, M.Z. & Abdou, E.S. (2013) Chitosan based edible films and coatings: A review. *Materials Science and Engineering C*, 33:1819-1841.
- Eriskin, C., Kalyon, D.M., & Wang, H.J. (2008) A hybrid twin screw extrusion/electrospinning method to process nanoparticle-incorporated electrospun nanofibres. *Nanotechnology*, 19:165302.
- Feng, B., Tu, H.B., Yuan, H.H., Peng, H.J., Zhang, Y.Z. (2012) Acetic-Acid-Mediated Miscibility toward Electrospinning Homogeneous Composite Nanofibres of GT/PCL. *Biomacromolecules*, 13:3917-25.
- Feng, Q.L., Wu, J., Chen, G.Q., Cui, F.Z., Kim, T.N., & Kim, J.O. (2000) A mechanistic study of the antibacterial effect of silver ions on *Escherichia coli* and *Staphylococcus aureus*. *J Biomed Mater Res*, 52:662-668.
- Ferrari, A.C. (2007) Raman spectroscopy of grapheme and graphite: Disorder, electron-phonon coupling, doping and nonadiabatic effects. *Solid State Communications*, 143:47-57.
- Fong, H., Chun, I., & Reneker, D.H. (1999) Beaded nanofibres formed during electrospinning. *Polymer*, 40:4585-92.
- Fong, H., Liu, W., Wang, C.S., & Vaia, R.A. (2002) Generation of electrospun fibers of nylon 6 and nylon 6-montmorillonite nanocomposite. *Polymer*, 43:775–80.
- Formhals, A. *Process and apparatus for preparing artificial threads*. US Patent Specification 1975504

- Fouda, M.G., & El-Aassar, M.R. Antimicrobial activity of carboxymethyl chitosan/polyethylene oxide nanofibres embedded silver nanoparticles
- Fridrikh, S. V., J. H. Yu, M. P. Brenner and G. C. Rutledge. (2003) Controlling the fiber diameter during electrospinning. *Physical Review Letters* 90:144502.
- Gangadharan, D., Harshvardan, K., Gnanasekar. G., Dixit, D., Popat, K.M., & Anand, P.S. (2010) Polymeric microspheres containing silver nanoparticles as a bactericidal agent for water disinfection. *Water Res*, 44:5481-5487.
- Gea, S., Reynolds, C.T., Roohpur, N., Soykeabkaew, N., Wirjosentono, B., & Bilotti, E., Peijs, T. (2010) Biodegradable composites based on poly(epsilon-caprolactone) and bacterial cellulose as a reinforcing agent. *J Biobased Mater Bio*, 4:384-390.
- Ghule, K., Ghule, A.V., Chen, B.J., & Ling, Y.C. (2006) Preparation and characterization of ZnO nanoparticles coated paper and its antibacterial activity study. *Green Chemistry*, 8:1034-41.
- Gupta, B., Revagade, N., & Hilborn, J. (2007) Poly(lactic acid) fiber: An overview. *Progress in Polymer Science*, 32:455-482.
- Gupta, V. B., & Kothari, V. K. (1997) Manufactured fibre technology. *London: Chapman & Hall.*
- Gupta, K.K., Kundan, A., Mishra, P.K., Srivastava, P., Mohanty, S., Singh, N.K., Mishra, A. & Maiti, P. (2012) Polycaprolactone composites with TiO₂ for potential nanobiomaterials: tunable properties using different phases. *Phys Chem Chem Phys*, 14:12844-12853.
- Hartman, O., Zhang, C., Adams, E.L., Farach-Carson, M.C., Petrelli, N.J., Chase, B.D., & Rabolt, J.F. (2010) Biofunctionalization of electrospun PCL-based scaffolds with perlecan domain IV peptide to create a 3-D pharmacokinetic cancer model. *Biomaterials*, 31:5700-5718.
- Hartman, R. P. A., J. P. Borra, D. J. Brunner, J. C. M. Marijnissen and B. Scarlett. (1999) The evolution of electrohydrodynamic sprays produced in the cone-jet mode, a physical model. *Journal of Electrostatics* 47:143-170.

- Hassan, M.S., Amna, T., Sheikh, F.A., Al-Deyab, S.S., Choi, K.E., Hwang, I.H., et al. (2013) Bimetallic Zn/Ag doped polyurethane spider net composite nanofibres: A novel multipurpose electrospun mat. *Ceramics International*, 39:2503-10.
- Huang, C.B., Chen, S.L., Lai, C.L., Reneker, D.H., Qiu, H., Ye, Y., et al. (2006) Electrospun polymer nanofibres with small diameter. *Nanotechnology*, 17:1558-63.
- Huang, C., S. J. Soenen, J. Rejman, B. Lucas, K. Braeckmans, J. Demeester and S. C. De Smedt. (2011) Stimuli-responsive electrospun fibers and their applications. *Chemical Society Reviews* 40:2417-2434.
- Huang, T., L. R. Marshall, J. E. Armantrout, S. Yembrick, W. H. Dunn, J. M. Oconnor, T. Avgousti Mueller, M. and M. D. Wetzel. (2008) Production of nanofibers by melt spinning. *United States Patent Application 20080242171*, *International Patent Number WO2008121338*.
- Huang, Z.M., Zhang, Y.Z., Kotaki, M., & Ramakrishna, S. (2003) A review on polymer nanofibers by electrospinning and their applications in nanocomposites. *Composites Science and Technology*, 63:2223-53.
- Illangakoon, U.E., Mahalingam, S., Wang, K., Cheong, Y.K., Canales, E., Ren, G.G., Cloutman-Green, E., Ciric, L., & Edirisinghe, M. (2016) Gyrospun antimicrobial nanoparticle loaded fibrous polymeric filters. DOI 10.1016/j.msec.2016.12.001
- Ivask, A., ElBadawy, A., Kaweeteerawat, C., Boren, D., Fischer, H., Ji, Z.X., et al. (2014) Toxicity Mechanisms in Escherichia coli Vary for Silver Nanoparticles and Differ from Ionic Silver. *ACS Nano*, 8:374-86.
- Jalili, R., S. A. Hosseini and M. Morshed. (2005) The effects of operating parameters on the morphology of electrospun polyacrylonitrile nanofibres. *Iranian Polymer Journal* 14:1074-1081.
- Jana, S., Leung, M., Chang, J., & Zhang, M. (2014) Effect of nano- and micro-scale topological features on alignment of muscle cells and commitment of myogenic differentiation. *Biofabrication*, 6:035012.
- Jayasinghe, S. N. and M. J. Edirisinghe. (2002) Effect of viscosity on the size of relics produced by electrostatic atomization. *Journal of Aerosol Science* 33:1379-1388.

- Jenner, G.A., Longerich, H.P., Jackson, S.E., & Fryer, B.J. (1990) ICP-MS – A powerful tool for high-precision trace-element analysis in Earth sciences: Evidence from analysis of selected U.S.G.S. reference samples. *Chemical Geology*, 83:133-48.
- Jiang, S.H., Hou, H.Q., Greiner, A., & Agarwal, S. (2012) Tough and Transparent Nylon-6 Electrospun Nanofibre Reinforced Melamine-Formaldehyde Composites. *ACS Applied Materials & Interface*, 4:2597-03.
- Jirsak, O. (2003) A Method of Nanofibres Production From a Polymer Solution Using Electrostatic Spinning and a Device for Carrying Out The Method. Cz. Patent; 2414(2,994,274).
- Jung, W.K., Koo, H.C., Kim, K.W., Shin, S., Kim, S.H., & Park, Y.H. (2008) Antibacterial activity and mechanism of action of the silver ion in *Staphylococcus aureus* and *Escherichia coli*. *Applied and Environmental Microbiology*, 74:2171-78.
- Kangwansupamonkon, W., Tiewtrakoonwat, W., Supaphol, P., & Kiatkamjornwong, S. (2014) Surface modification of electrospun chitosan nanofibrous mats for antibacterial activity. *J Appl Polm Sci*, 131:40981.
- Kenawy, R., Bowlin, G.L., Mansfield, K., Layman, J., Simpson, D.G., Sanders, E.H., et al., (2002) Release of tetracycline hydrochloride from electrospun poly(ethylene-co-vinylacetate), poly(lactic acid), and a blend. *Journal of Controlled Release*, 81:57–64.
- Khashan, K.S., Sulaiman, G.M., & Abdulameer, F.A. (2016) Synthesis and antibacterial activity of CuO nanoparticles suspension induced by laser ablation in liquid. *Arabian Journal of Science & Engineering*, 41:301-310.
- Khlystalova, T.K., Kuraganova, M.N., Demina, A.I., Petova, M.B., & Tatalannov, O.G. (1986) Hydrolytic stability of polyurethanes in model biological media. *Mechanics of Composite Materials*, 21:763-67.
- Kidoaki, S., Kwon, I.K., & Matsuda, T. (2006) Structural features and mechanical properties of in situ-bonded meshes of segmented polyurethane electrospun from mixed solvents. *Journal of Biomedical Materials Research Part B: Applied Biomaterials*, 76B:219-29.

- Kim, J.S., Kuk, E., Yu, K.N., Kim, J.H., Park, S.J., Lee, H.J., et al. (2007) Antimicrobial effects of silver nanoparticles. *Nanomedicine*, 3:95-01.
- Kim, F.S., Ren, G.Q., Jenekhe, S.A. (2011) One-Dimensional Nanostructures of pi-Conjugated Molecular Systems: Assembly, Properties, and Applications from Photovoltaics, Sensors, and Nanophotonics to Nanoelectromics. *Chemistry of Materials*, 23:682-32.
- Kister, G., Cassanas, G., Bergounhon, M., Hoarau, D., & Vert, M. (2000) Structural characterization and hydrolytic degradation of solid copolymers of D, L- lactide-co- ϵ -caprolactone by Raman spectroscopy. *Polymer*, 41:925-932.
- Ko, J., Mohtaram, N. K., Ahmad, F., Montgomery, A., Carlson, M., Lee, P. C. D., Willerth, S. M., & Jun, M. B. G. (2014) Fabrication of poly(ϵ -caprolactone) microfiber scaffolds with varying topography and mechanical properties for stem cell-based tissue engineering applications, *J. Biomater. Sci.* 25: 1-17.
- Kong, H. & Jang, J. (2008) Synthesis and Antimicrobial Properties of Novel Silver/Polyrhodanine Nanofibre. *Biomacromolecules*, 9:2677-81.
- Kumar, B., Bose, S., & Chatterjee, K. (2014) Amine- functionalised multiwall carbon nanotubes impart osteoinductive and bactericidal properties in poly (ϵ -caprolactone) composites. *RSC Adv*, 4:19086-19098.
- Kumar, R., Howdle, S., & Munstedt, H. (2005) Polyamide/silver antimicrobials: Effect of filler types on the silver ion release. *Journal of Biomedical Materials Research Part B-Applied Biomaterials*, 75B:311-19.
- Kumar, R. & Munstedt, H. (2005) Silver ion release from antimicrobial polyamide/silver composites. *Biomaterials*, 26:2081-88.
- Kundan, A., Mishra, P.K., Srivastava, P., Mohanty, S., Singh, N.K., Mishra, A. & Maiti, P. (2012) Polycaprolactone composites with TiO₂ for potential nanobiomaterials: tunable properties using different phases. *Phys Chem Chem Phys*, 14:12844-12853.
- Lahiri, D., Rouzaud, F., Richard, T., Keshri, A.K., Bakshi, S.R., Kos, L., & Agarwal, A. (2010) Boron nitride nanotubes reinforced polylactide-polycaprolactone copolymer composite: Mechanical properties and cytocompatibility with osteoblasts and macrophages in vitro. *Acta Biomaterialia*, 9:3524-3533.

- Larrondo, L. and R. S. J. Manley. (1981a) Electrostatic fiber spinning from polymer melts. I. Experimental observations on fiber formation and properties. *Journal of Polymer Science Part B-Polymer Physics* 19:909-920.
- Larrondo, L. and R. S. J. Manley. (1981b) Electrostatic fiber spinning from polymer melts. II. Examination of the flow field in an electrically driven jet. *Journal of Polymer Science Part B-Polymer Physics* 19:921-932.
- Larrondo, L. and R. S. J. Manley. (1981c) Electrostatic fiber spinning from polymer melts. III. Electrostatic deformation of a pendant drop of polymer melt. *Journal of Polymer Science Part B-Polymer Physics* 19:933-940.
- Li, D., Wu, T., He, N., Wang, J., Chen, W., He, L., Huang, C., El-Hamshary, H. A., Al-Deyab, S. S., & Ke, Q. (2014) Three dimensional polycaprolactone scaffold via needleless electrospinning promotes cell proliferation and infiltration, *Colloid. Surface B* 121: 432-443.
- Li, M., Zhang, J., Zhang, H., Liu, Y., Wang, C., Xu, X., et al. (2007) Electrospinning: A facile method to disperse fluorescent quantum dots in nanofibres without Forster resonance energy transfer. *Advanced Functional Materials*, 17:3650-56.
- Li, J., Zivanovic, S., Davidson, P.M., & Kit, K. (2010) Characterisation and comparison of chitosan/PVP and chitosan/PEO blend films. *Carbohydrate Polymer*, 79:786-791.
- Li, T., Wu, N., He, J., Wang, W., Chen, L., He, C., Huang, H, Al-Hamshary, S.S., & Al-Deyab, Q. (2014) Three dimensional polycaprolactone scaffold via needleless electrospinning promotes cell proliferation and infiltration. *Colloid Surface B*, 121:432-443.
- Liao, K.H., Ou, K.L., Cheng, H.C., Lin, C.T., & Peng, P.W. (2010) Effect of silver on antibacterial properties of stainless steel. *Applied Surface Science*, 256:4364-46.
- Lieshout, G., Peters, M., & Rutten, F. (2006) A knitted fibrin-covered polycaprolactone scaffold for tissue engineering of the aortic valve. *Tissue Eng Part A*, 12:481-487.
- Liu, H.Q., Edel, J.B., Bellan, L.M., & Craighead, H.G. (2006) Electrospun polymer nanofibres as subwavelength optical waveguides incorporating quantum dots. *Small*, 2:495-99.

- Liu, Y. & He, J.H. (2007) Bubble electrospinning for mass production of nanofibres. *Int J Nonlinear Sci*, 8:393-96.
- Liu, Y., He, J.H., Xu, L., & Yu, J.Y. (2008) The principle of bubble electrospinning and its experimental verification. *J Polym Eng*, 28:55-66
- Liu, Y., Ren, Z.F., & He, J.H. (2010) Bubble electrospinning method for preparation of aligned nanofibre mat. *Materials Science and Technology*, 26:1309-12.
- Liu, R.F., Xu, X.L., Zhuang, X.P., & Cheng, B. (2014) Solution blowing of chitosan/PVA hydrogel nanofibre mats. *Carbohydrate Polymers*, 101:1116-21
- Liu, Z., Zhang, T., Ren, G., & Yang, Z. (2012) Nano-Ag inhibiting action potential independent glutamatergic synaptic transmission but increasing excitability in rat CA1 pyramidal neurons. *Nanotoxicology*, 6:414-23
- Lopez-Haro, M., Jiu, T.G., Bayle-Guillemaud, P., Jouneau, P.H., & Chandezon, F. (2013) Multiscale tomographic analysis of polymer-nanoparticle hybrid materials for solar cells. *Nanoscale*, 5:10945-55.
- Luo, C.J., Nangrejo, M., Edirisinghe, M. (2010) A novel method of selecting solvents for polymer electrospinning. *Polymer*, 51:1654-62.
- Luo, C.J., Stoyanov, S.D., Stride, E., Pelan, E., & Edirisinghe, M. (2012) Electrospinning versus fibre production methods: from specifics to technological convergence. *Chemical Society Review*, 41:4708-35.
- Lyons, J., C. Li and F. Ko. (2004) Melt-electrospinning part I: processing parameters and geometric properties. *Polymer* 45(22):7597-7603.
- Madhally, S.V. & Matthew, H.W.T. (1999) Porous chitosan scaffolds for tissue engineering. *Biomaterials*, 20:1133-42.
- Mahalingam, S. & Edirisinghe, M. (2013) Forming of Polymer Nanofibres by a Pressurised Gyration Process. *Macromolecular Rapid Communications*, 34:1134-39.
- Mahalingam, S., Raimi-Abraham, B.T., Craig, D.Q.M., & Edirisinghe M., (2015) Formation of Protein and Protein-Gold Nanoparticle Stabilized Microbubbles by Pressurized Gyration. *Langmuir*, 31: 659-666.

- Mahalingam, S., Raimi-Abraham, B. T., Craig, D. Q. M., Edirisinghe, M. (2015) Solubility-spinnability map and model for the preparation of fibres of polyethylene (terephthalate) using gyration and pressure. *Chemical Engineering Journal*, 280: 344-353.
- Mahalingam, S., Pierin, G., Colombo, P., Edirisinghe, M. (2015) Facile one-pot formation of ceramic fibres from preceramic polymers by pressurised gyration. *Ceramics International*, 41: 6067-6073.
- Mahalingam, S., Ren, G. G., Edirisinghe, M. (2014) Rheology and pressurised gyration of starch and starch-loaded poly(ethylene oxide). *Carbohydrate Polymer*, 114: 279-287.
- Marchessault, R.H., Morehead, F.F., & Walter, N.M. (1959) Liquid crystal systems from fibrillar polysaccharides. *Nature*, 184:632-33.
- Mahalingam, S., Xu, Z., & Edirisinghe, M. (2015) Antibacterial Activity and Biosensing of PVA-Lysozyme Microbubbles Formed by Pressurized Gyration. *Langmuir*, 31:9771-9780.
- Mary, L.A., Senthilram, T., Suganya, S., Nagarajan, L., Venugopal, J., Ramakrishna, S., et al. (2013) Centrifugal spun ultrafine fibrous web as a potential drug delivery vehicle. *eXPRESS Polymer Letters*, 7:238-48.
- Matsumura, Y., Yoshikata, K., Kunisaki, S., & Tsuchido, T. (2003) Mode of Bactericidal Action of Silver Zeolite and Its Comparison with That of Silver Nitrate. *Applied and Environmental Microbiology*, 69:4278-81.
- McKee, M.G., Elkins, C.L., & Long, T.E. (2004) Influence of self-complementary hydrogen bonding on solution rheology/electrospinning relationships. *Polymer*, 45:8705-15.
- Medeiros, E.S., Glenn, G.M., Klamczynski, A.P., Orts, W.J., & Mattoso, L.H.C. (2009) Solution blow spinning: A new method to produce micro- and nanofibers from polymer solutions. *Journal of Applied Polymer Science*, 113:2322–30.
- Megelski, Silke, Jean S. Stephens, D. Bruce Chase and John F. Rabolt. (2002) Micro- and Nanostructured Surface Morphology on Electrospun Polymer Fibers. *Macromolecules* 35:8456–8466.

- Meghana, S., Kabra, P., Chakraborty, S., & Padmavathy, N. (2015) Understanding the pathway of antibacterial activity of copper oxide nanoparticles. *RSC Advances*, 5:12293.
- Mellado, P., McIlwee, H.A., Badrossamay, M.R., Goss, J.A., Mahadevan, L., & Parker, K.K. (2011) A simple model for nanofibre formation by rotary jet-spinning. *Applied Physics Letters*, 99:203107.
- Messmore, B.W., Hilvat, J.F., Sone, E.D., & Stupp, S.I. (2004) Synthesis, self-assembly, and characterization of supramolecular polymer from electroactive Dendron rodcoil molecules. *J Am Chem Soc*, 126:14452-58.
- Mi, H.Y., Jing, X., Peng, J., Salick, M.R., Peng, X.F., & Turng, L.S. (2014) Poly(ϵ -caprolactone) (PCL) /cellulose nano-crystal (CNC) nanocomposites and foams. *Cellulose*, 21:2727-2741.
- Mitchell, S. B. and J. E. Sanders. (2006) A unique device for controlled electrospinning. *Journal of Biomedical Materials Research Part A* 78A:110-120.
- Mody, V.V., Siwale, R., Singh, A., & Mody, H.R. (2010) Introduction to metallic nanoparticles. *J Pharm Bioallied Sci*, 2:282-289.
- Mohtaram, N.K, Ko, J., King, C., Sun, L., Muller, N., Jun, M. B., & Willerth, S. M. Electrospun biomaterial scaffolds with varied topographies for neural differentiation of human-induced pluripotent stem cells. *J Biomed Mater Res Part A*, DOI: 10.1002/jbm.a.35392.
- Montazer, M. & Malekzadeh, S.B. (2012) Electrospun antibacterial nylon nanofibres through in situ synthesis of nanosilver: preparation and characteristic. *Journal of Polymer Research*, 19:9980.
- Morones, J.R., Elechiguerra, J.L., Camacho, A., Holt, K., Kouri, J.B., Ramirez, J.T., et al. (2005) The bactericidal effect of silver nanoparticles. *Nanotechnology*, 16:2346-53.
- Morris, P. J. T. (2005) Polymer pioneers: a popular history of the science and technology of large molecules (Center for History of Chemistry, No 5). p56: Chemical Heritage Foundation, Philadelphia, PA, USA.

- Mural, P.K.S., Kumar, B., Madras, G., & Bose, S. (2016) Chitosan immobilised porous polyolefin as sustainable and efficient antibacterial membranes. *ACS Sustainable Chem Eng*, 4:862-870.
- Narayanan, G., Gupta, B.S., & Gupta A.E. (2014) Poly(ϵ -caprolactone) nanowebs functionalized with α - and γ -cyclodextrins. *Biomacromolecules*, 15:4122-4133.
- Nayak, R., Padhye, R., Kyratzis, I.L., Truong, Y.B., & Arnold, L. (2011) Recent advances in nanofibre fabrication techniques. *Textile Research Journal*, 82:129-47.
- Nijst, C.L., Bruggeman, J.P., Karp, J.M., Ferreira, L., Zumbuehl, A., Bettinger, C.J., et al. (2007) Synthesis and characterization of photocurable elastomers from poly(-glycerol-co-sebacate). *Biomacromolecules*, 8:3067-73.
- Ohkawa, K., Minato, K.I., Kumagai, G., Hayashi, S., Yamamoto, H. (2006) Chitosan Nanofiber. *Biomacromolecules*, 7:3291-3294.
- Ojha, S.S, Stevens, D.R., Hoffman, T.J., Stano, K., Klossner, R., Scott, M.C., Krause, W., Clarke, L.I. & Gorga, R.E. (2008) Fabrication and Characterization of Electrospun Chitosan Nanofibers Formed via Templating with Polyethylene Oxide. *Biomacromolecules*, 9:2523-2529.
- Oku, T., Motoyoshi, R., Fujimoto, K., Akiyama, T., Jeyadevan, B., Cuya, (2011) J. Structures and photovoltaic properties of copper oxide/fullerene solar cells. *Journal of Physics & Chemistry of Solids*, 72: 1206-1211.
- Oliveira, J.T., Crawford, A., Mundy, J.M., Moreira, A.R., Gomes, M.E., Hatton, P.V., & Reis, R. (2007) A cartilage tissue engineering approach combining starch-polycaprolactone fibre mesh scaffolds with bovine articular chondrocytes. *J Mater Sci: Mater Med*, 18:295-302.
- O'Riordan, A., Iacopino, D., Lovera, P., Floyd, L., Reynolds, K., & Redmond, G. (2011) dielectrophoretic self-assembly of polarized light emitting poly(9,9-dioctylfluorene) nanofibre arrays. *Nanotechnology*, 22:105602.
- Pal, S., Tak, Y.K., & Song, J.M. (2007) Does the antibacterial activity of silver nanoparticles depend on shape of the nanoparticle? A study of the Gram-negative bacterium *Escherichia coli*. *Appl Environ Microbiol*, 2:1712-1720.

- Palza, H. (2015) Antimicrobial Polymers with Metal Nanoparticles. *Int J Mol Sci*, 16: 2099-2116.
- Pant, H.R., Kim, C.S. (2013) Electrospun gelatin/nylon-6 composite nanofibres for biomedical applications. *Polymer International*, 62:1008-13.
- Pant, H.R., Pandeya, D.R., Nam, K.T., Baek, W.I., Hong, S.T., & Kim, H.Y. (2011) Photocatalytic and antibacterial properties of a TiO₂/nylon-6 electrospun nanocomposite mat containing silver nanoparticles. *Journal of Hazardous Materials*, 189:465-71.
- Park, S.J., Lee, B-K., Na, M. H., & Kim, D. S. (2013) Melt-spun shaped fibers with enhanced surface effects: Fiber fabrication, characterization and application to woven scaffolds, *Acta Biomaterialia*, 9:7719-7726.
- Patel, P.A., Eckart, J., Advincula, M.C., Goldberg, A.J., & Mather, P.T. (2009) Rapid synthesis of polymer-silica hybrid nanofibres by biomimetic mineralization. *Polymer*, 50:1214-22.
- Patra, S.N., Easteal, A.J., & Bhattacharyya, D. (2009) Parametric study of manufacturing poly (lactic acid) nanofibrous mat by electrospinning. *Journal of Materials Science*, 44:647-54.
- Pham, Q.P., Sharma, U., & Mikos, A. G. (2006) Electrospun poly(ϵ -caprolactone) microfiber and multilayer nanofiber/microfiber scaffolds: characterization of scaffolds and measurement of cellular infiltration. *Biomacromolecules*, 7:2796-2805.
- Pham, Q.P., Sharma, U., & Mikos, A. G. (2006a) Electrospinning of polymeric nanofibers for tissue engineering applications: A review. *Tissue Engineering* 12:1197-1211.
- Pillai, C.K.S. & Sharma, C.P. (2009) Electrospinning of Chitin and Chitosan nanofibers. *Trends Biomater Artif Organs*, 22:179-201.
- Radheshkumar, C. & Munstedt, H. (2006) Antimicrobial polymers from polypropylene/silver composites-Ag⁺ release measured by anode stripping voltammetry. *Reactive and Functional Polymers*, 66:780-88.

- Raimi-Abraham, B.T., Mahalingam, S., Edirisinghe, M., & Craig, D.Q.M. (2014) Generation of poly (N-vinylpyrrolidone) nanofibres using pressurised gyration. *Materials Science and Engineering: C*, 39:168-176.
- Rasekh, M., Ahmad, Z., Frangos, C. C., Bozec, L., Edirisinghe, M., & Day, R. M. (2013) Spatial and temporal evaluation of cell attachment of printed polycaprolactone microfibers. *Acta Biomaterialia*, 9:5052-5062.
- Ren, G., Hu, D., Cheng, E.W.C, Vargas-Reus, M.A., Reip, P., & Allaker, R.P. (2009) Characterisation of copper oxide nanoparticles for antimicrobial applications. *International Journal of Antimicrobial Agents*, 33:587–90.
- Ren, J., Blackwood, K. A., Doustgani, A., Poh, P. P., Steck, R., Stevens, M. M., & Woodruff, M. A. Melt electrospun polycaprolactone strontium-substituted bioactive glass scaffolds for bone regeneration, *J. Biomed. Mater. Res. Part A*, 102: 3140-3153.
- Reneker, D.H. & Yarin, A.L. (2008) Electrospinning jets and polymer nanofibres. *Polymer*, 49:2387-25.
- Ren, J., Blackwood, K.A., Doustgani, A., Poh, P.P., Steck, R., Stevens, M.M., & Woodruff, M.A. Melt electrospun polycaprolactone strontium-substituted bioactive glass scaffolds for bone regeneration, *J Biomed Mater Res Part A*, 102:3140-3153.
- Rey, Alejandro D. (2007) Capillary models for liquid crystal fibers, membranes, films, and drops. *Soft Matter* 3:1349-1368.
- Ruparelia, J.P., Chatterjee, A.K., Duttgupta, S.P., & Mukherji, S. (2008) Strain specificity in antimicrobial activity of silver and copper nanoparticles. *Acta Biomaterialia*, 4:707-16.
- Rupprecht, A. (1966)Preparation of oriented DNA by wet spinning. *Acta Chemica Scandinavica* 20:494-504.
- Salata, O. (2004) Applications of nanoparticles in biology and medicine. *J Nanobiotechnol* 2:3
- Sankar, D., Shalumon, K. T., Chennazhi, K. P., Menon, D., & Jayakumar, R. (2014) Surface plasma treatment of poly(caprolactone) micro, nano, and multiscale

- fibrous scaffolds for enhanced osteoconductivity. *Tissue Eng Part A*, 20:1689-1702.
- Samir, M.A.S.A., Alloin, F., & Dufresne, A. (2005) Review of recent research into cellulosic whiskers, their properties and their application in nanocomposite field. *Biomacromolecules*, 6:612-26.
- Samitsu, S., Shimomura, T., Heike, S., Hashizume, T., & Ito, K. (2008) Effective Production of Poly(3-alkylthiophene) Nanofibres by means of Whisker Method using Anisole Solvent: Structural, Optical, and Electrical Properties. *Macromolecules*, 41:8000-10.
- Sangsanoh, P. & Supaphol, P. (2006) Stability improvement of electrospun Chitosan Nanofibrous membranes in neutral or weak basic aqueous solutions. *Biomacromolecules*, 7:2710-2714.
- Sarasam, A. & Madihally, S.V. (2005) Characterization of chitosan-polycaprolactone blends for tissue engineering applications. *Biomaterials*, 26:5000-5006.
- Schiffman, J. D. & Schauer, C.L. (2007) Cross-linking Chitosan Nanofiber. *Biomacromolecules*, 8:594–601.
- Schwarz, K.N., Kee, T.W., & Huang, D.M. (2013) Coarse-grained simulations of the solution-phase self-assembly of poly(3-hexylthiophene) nanostructures. *Nanoscale*, 5:2017-27.
- Schiffman, J.D. & Schauer, C.L. (2007) Cross-linking Chitosan Nanofiber. *Biomacromolecules*, 8:594–601.
- Selmer-Olsen E., Ratnaweera H.C., Pehrson R. (1996) A novel treatment process for dairy wastewater with chitosan produced from shrimp-shell waste. *Water Science and Technology*, 34:33–40.
- Senthilram, T., Mary, L.A., Venugopal, J.R., Nagarajan, L., Ramakrishna, S., & Dev VRG. (2011) Self crimped and aligned fibres. *Materials Today*, 14:226-29.
- Shenoy, S.L., Bates, W.D., Frisch, H.L., & Wenk, G.E. (2005) Role of chain entanglements on fibre formation during electrospinning of polymer solutions: good solvent, non-specific polymer-polymer interaction limit. *Polymer*, 46:3372-84.

- Shi, Q., Vitchuli, N., Nowak, J., Noar, J., Caldwell, J.M., Breidt, F., et al. (2011) One-step synthesis of silver nanoparticle-filled nylon 6 nanofibres and their antibacterial properties. *Journal of Materials Chemistry*, 21:10330-35.
- Shin, H. and S. L. Samuels. (1992) Flash-spinning polymeric plexifilaments. *United States Patent 5147586*.
- Sinha-Ray, S., Zhang, Y., Yarin, A.L., Davis, S.C., & Pourdeyhimi, B. (2011) Solution Blowing of Soy Protein Fibres. *Biomacromolecules*, 12:2357-63.
- Singh, S.K., Singh, M.K., Kulkarni, P.P., Sonkar, V.K., Gracio, J.J.A., & Dash, D. (2012) Amine-modified graphene: Thermo-protective safer alternative to graphene oxide for biomedical applications. *ACS Nano*, 6:2731-2740.
- Smetana, A.B., Klabunde, K.J., Marchin, G.R., & Sorensen, C.M. (2008) Biocidal activity of nanocrystalline silver powders and particles. *Langmuir*, 24:7457-7464.
- Sondi, I. & Salopek-Sondi, B. (2004) Silver nanoparticles as antimicrobial agent: a case study on E-coli as a model for Gram-negative bacteria. *Journal of Colloid and Interface Science*, 275:177-82.
- Sukigara, S., M. Gandhi, J. Ayutsede, M. Micklus and F. Ko. (2003) Regeneration of Bombyx mori silk by electrospinning – part 1: processing parameters and geometric properties. *Polymer* 44:5721–5727.
- Sun, K. & Li, Z.H. (2011) Preparations, properties and applications of chitosan based nanofibers fabricated by electrospinning. *Express Polym Lett*, 4:342-361.
- Tang, S. & Mukhopadhyay, S.K. (2006) Melt-blown lyocell: Influence of solution characteristics on fibre properties. *Journal of the Textile Institute*, 97:39-47.
- Teo, W.E. & Ramakrishna. S. (2006) A review on electrospinning design and nanofibre assemblies. *Nanotechnology*, 17:R89-06
- Theron, A., Zussman, E., & Yarin, A.L. (2001) Electrostatic field-assisted alignment of electrospun nanofibres. *Nanotechnology*, 12:384-90.
- Tienen, R.G., Heijkants, P., Buma, J.H., Pennings, R.P. (2002) Tissue ingrowth and degradation of two biodegradable porous polymers with different porosities and pore sizes. *Biomaterials*, 23:1731-1738.

- Tseng, R.J., Baker, C.O., Shedd, B., Huang, J., Kaner, R.B., Ouyang, J.Y., et al. (2007) Charge transfer effect in the polyaniline-gold nanoparticle memory system. *Applied Physics Letters*, 90:053101.
- Tranquada, J.M., Sternlieb, B.J., Axe, J.D., Nakamura, Y., & Uchida, S. (1995) Evidence for stripe correlations of spins and holes in copper oxide superconductors. *Nature*, 375:561
- Van Lieshout, M., Peters, G., Rutten, M., & Baaijens, F. (2006) A knitted fibrin-covered polycaprolactone scaffold for tissue engineering of the aortic valve, *Tissue. Eng. Part A* 12: 481-487.
- Van Loosdrecht, M.C.M., Lyklema, J., Norde, W., Schraa, G., & Zehnder, A.J.B. (1987) Electrophoretic mobility and hydrophobicity as a measure to predict the initial steps of bacterial suspension. *Appl Environ Microbiol*, 53:1898-1901.
- Van Tienen, T. G., Heijkants, R. G., Buma, P., de Groot, J. H., Pennings, A. J., & Veth, R. P. (2002) Tissue ingrowth and degradation of two biodegradable porous polymers with different porosities and pore sizes, *Biomaterials*, 23: 1731-1738.
- Vargas-Reus, M.A., Memarzadeh, K., Huang, J., Ren, G.G., & Allaker, R.P. (2012) Antimicrobial activity of nanoparticulate metal oxides against peri-implantitis pathogens. *International Journal of Antimicrobial Agents*.
- Vera-Sorroche, J., Kelly, A.L., Brown, E.C., Gough, T., Abeykoon, C., Coates, P. D., Deng, J., Li, K., Harkin-Jones E., & Price, M. (2014) The effect of melt viscosity on thermal efficiency for single screw extrusion of HDPE. *Chem Eng Res Des*, 92:2404-2412.
- Vitchuli, N., Shi, Q., Nowak, J., Kay, K., Caldwell, J.M., Breidt, F., et al. (2011) Multifunctional ZnO/Nylon 6 nanofibre mats by an electrospinning-electrospraying hybrid process for use in protective applications. *Science and Technology of Advanced Materials*, 12:055004.
- Wang, Z., Cui, Y., Wang, J., Yang, X., Wu, Y., Wang, K., Gao, X., Li, D., Li, Y., Zheng, X-L., Zhu, Y., & Kong, D. (2014) The effect of thick fibers and large pores of electrospun poly(ϵ -caprolactone) vascular grafts on macrophage polarization and aerial regeneration. *Biomaterials*, 35:5700-5710.

- Wang, Y.Z., Li, Y.X., Yang, S.T., Zhang, G.L., An, D.M., Wang, C., et al. (2006) A convenient route to polyvinyl pyrrolidone/silver nanocomposite by electrospinning. *Nanotechnology*, 17:3304-07.
- Wang, H.N., Li, Y.B., Zuo, Y., Li, J.H., Ma, S.S., & Cheng, L. (2007) Biocompatibility and osteogenesis of biomimetic nano-hydroxyapatite/polyamide composite scaffolds for bone tissue engineering. *Biomaterials*, 28:3338-48.
- Wei, Q.F., Ye, H., Hou, D.Y., Wang, H.B., & Gao, W.D. (2006) Surface functionalization of polymer nanofibres by silver sputter coating. *Journal of Applied Polymer Science*, 99:2384-88.
- Weitz, R.T., Harnau, L., Rauschenbach, S., Burghard, M., & Kern, K. (2008) Polymer nanofibers via nozzle-free centrifugal spinning. *Nano Lett*, 8:1187-91.
- Williams, R.L., Doherty, P.J., Vince, D.G., Grashoff, G.J., & Williams, D.F. (1989) The biocompatibility of silver. *Critical Reviews in Biocompatibility*, 5:221-43.
- Woodings, K. (2001) *Regenerated Cellulose Fibres*. CRC Press LLC, Woodhead Publishing's Ltd, Cambridge, UK (Chapter 1).
- Wu, H., Zhang, R., Liu, X., Lin, D., & Pan, W. (2007) Electrospinning of Fe, Co, and Ni nanofibres: synthesis, assembly, and magnetic properties. *Chemistry of Materials*, 19:3506-11.
- Wu, J., Zheng, Y., Song, J., Luan, X., Wen, Z., Wu, X., Chen, Q., & Wan, S. (2014) In situ synthesis of silver-nanoparticles/bacterial cellulose composites for slow-released antimicrobial wound dressing. *Carbohydr Polym*, 102:762-771.
- Wu, X., Li, J.D., Wang, L., Huang, D., Zuo, Y., & Li, Y.B. (2010) The release properties of silver ions from Ag-nHA/TiO₂/PA66 antimicrobial composite scaffolds. *Biomedical Materials*, 5:044105.
- Xiu, Z.M., Zhang, Q.B., Puppala, H.L., Colvin, V.L., & Alvarez, P.J.J. (2012) Negligible Particle-Specific Antibacterial Activity of silver Nanoparticles. *Nano Letters*, 12:4271-75.
- Xu, S.Y., Shi, Y., & Kim, S.G. (2006) Fabrication and mechanical property of nano piezoelectric fibres. *Nanotechnology*, 17:4497-01.

- Xu, W., Yang, W., & Yang, Y. (2009) Electrospun starch acetate nanofibers: development, properties, and potential application in drug delivery. *Biotechnology Progress*, 25:1788-1795.
- Xu, X. L., L. X. Yang, X. Y. Xu, X. Wang, X. S. Chen, Q. Z. Liang, J. Zeng and X. B. Jing. (2005) Ultrafine medicated fibers electrospun from W/O emulsions. *Journal of Controlled Release* 108:33-42.
- Xu, Z., Mahalingam, S., Basnett. P., Raimi-Abraham, B. T., Roy, I., Craig, D. Q. M., Edirisinghe, M. (2016) Making Nonwoven Fibrous Poly(epsilon-caprolactone) Constructs for Antimicrobial and Tissue Engineering Applications by Pressurized Melt Gyration. *Macromolecular Materials & Engineering*, 301: 922-934.
- Yamanaka, M., Hara, K., & Kudo, J. (2005) Bactericidal actions of a silver ion solution on Escherichia coli, studied by energy-filtering transmission microscopy and proteomic analysis. *Appl Environ Microbiol*, 71:7589-7593.
- Yan, G.L., Zhuang, X.P., Tao, X.X., & Cheng, B.W. (2013) Solution blowing of silicon carbide nanofibre and its thermal stability. *Science of Advanced Materials*, 5:209-15.
- Yang, Y., X. Li, M. Qi, S. Zhou and J. Weng. (2008) Release pattern and structural integrity of lysozyme encapsulated in core-sheath structured poly(DL-lactide) ultrafine fibers prepared by emulsion electrospinning. *European Journal of Pharmaceutics and Biopharmaceutics* 69:106-116.
- Yang, Z., Liu, Z.W., Allaker, R.P., Reip, P., Oxford, J., Ahmad, Z. & Ren, G. (2010) A review of nanoparticle functionality and toxicity on the central nervous system. *Journal of The Royal Society Interface*, S411-22.
- Yi, F. & LaVan, D.A. (2008) Poly(glycerol sebacate) nanofiber scaffolds by core/shell electrospinning. *Macromol Biosci*, 8:803-06.
- Yoo, H.S., Kim, T.G., & Park, T.G. (2009) Surface-functionalized electrospun nanofibres for tissue engineering and drug delivery. *Advanced Drug Delivery Reviews*, 61:1033-42.

- Yoshio, M., Shoji, Y., Tochigi, Y., Nishikawa, Y., & Kato, T. (2009) Electric field assisted alignment of self-assembled fibres composed of hydrogen-bonded molecules having laterally fluorinated mesogens. *J Am Chem Soc*, 131:6763-67.
- Zeleny, J. (1914) The electrical discharge from liquid points, and a hydrostatic method of measuring the electric intensity at their surfaces. *Physical Review*, 3:69- 91.
- Zeleny, J. (1915) On the conditions of instability of electrified drops with applications to the electrical discharge from liquid points. *The Proceedings of the Cambridge Philosophy Society*, 18:71-83.
- Zhang, L.F., Koppersta, P., West, M., Hedin, N., & Fong, H. (2009) Generation of polymer ultrafine fibres through solution (air-) blowing. *Journal of Applied Polymer Science*, 114:3479-86.
- Zhang, J.H., Markiewicz, M.J., Mowery, B.P., Weisblum, B., Stahl, S.S., & Gellman, S.H. (2012) C-Terminal Functionalization of Nylon-3 Polymers: Effects of C-Terminal Groups on Antibacterial and Hemolytic Activities. *Biomacromolecules*, 13:323-31.
- Zhang, S. Q., Karaca, B. T., Van Oosten, S. K., Yuca, E., Mahalingam, S., Edirisinghe, M., Tamerler, C. (2015) Coupling Infusion and Gyration for the Nanoscale Assembly of Functional Polymer Nanofibers Integrated with Genetically Engineered Proteins. *Macromolecular Rapid Communications*, 36: 1322-1328.
- Zhou, Y.Z., Yang, J., He, T.T., Shi, H.F., Cheng, X.N., & Lu, Y.X. (2013) Highly Stable and Dispersive Silver Nanoparticle-Graphene Composites by a Simple and Low-Energy-Consuming Approach and Their Antimicrobial Activity. *Small*, 9:3445-54.